Synthesis and Characterization of Polymeric Gas Sensing Materials for Detection of Agriculture Lagoon Off-Gas

by

Kayoung (Gina) Kim

A thesis
presented to the University of Waterloo
in fulfillment of the
thesis requirement for the degree of
Master of Applied Science
in
Chemical Engineering

Waterloo, Ontario, Canada, 2023

Author's Declaration

I hereby declare that I am the sole author of this thesis. This is a true copy of the thesis, including any required final revisions, as accepted by my examiners.

I understand that my thesis may be made electronically available to the public.

Abstract

With increasing food demand, agriculture and farming industry have grown. This led to an increase in production of agricultural waste. The waste is converted into manure via anaerobic fermentation which continuously produces biogas. Every year, a large volume of biogas-containing pollutants, including greenhouse gases (GHG), are released from manure fermentation.

To monitor the progress of manure fermentation and control gas pollutants released into the atmosphere, a sensor that can detect components of biogas in a continuous and reliable manner is necessary. For a more economic system, the sensor should be able to operate at room temperature (roughly, 22-25℃ range) and specifically detect certain gas analytes.

Methane and ammonia are selected as the target gases for detection because of their significance. Methane is a small molecule hydrocarbon and very potent greenhouse gas. At high concentrations, there is a possibility of combustion and asphyxiation, thus monitoring its presence and concentration is essential. Ammonia is the main source of odor from manure fermentation and can be toxic at a low concentration. As both target gases are toxic and reactive, formaldehyde was used as a "simulant" or "surrogate" gas (a less hazardous gas) for preliminary in-lab testing of sensing material sensitivity with the gas chromatography (GC) set-up.

Any sensor requires a sensing material that responds to one specific gas analyte. Polyaniline (PANI), polypyrrole (PPy), and polydimethylsiloxane (PDMS) have been indicated in the literature to exhibit affinity for ammonia and/or methane. They were tested first with gas chromatography (GC) using formaldehyde. Out of the three, PANI showed better sensing capabilities.

Tin (IV) oxide, zinc oxide, sodium dodecyl sulphate, titanium (IV) oxide and hydrochloric acid were selected as the top 5 dopants for polyaniline. PANI was synthesized in the lab with varying dopant levels for GC testing. Scanning electron microscopy (SEM), energy-dispersive X-ray spectroscopy (EDX), X-ray diffraction (XRD), and ultraviolet-visible (UV-Vis) spectroscopy were used to further characterize the synthesized materials for their physical and chemical properties.

PANI doped with 2.5% ZnO-sodium dodecyl sulfate (SDS) showed higher sensitivity for sensing formaldehyde as it had the greatest response (sorption) at a low concentration. ZnO incorporation into PANI was poor. When SDS was added, ZnO incorporation improved, which led to higher gas sorption. The notable interaction of SDS and ZnO could be scrutinized further if the formulation needs to be optimized for best ZnO incorporation without sacrificing the PANI structure.

When tested with the actual micro-electrical-mechanical system (MEMS) sensor at 50 ppm methane source (test chamber in System Design Engineering), both PANI with 5% SnO_2 and 5% ZnO sorbed methane at room temperature. PANI-5% ZnO was proven to be the most suitable sensing material for methane detection, showing the highest signal at 50 ppm methane levels.

Acknowledgements

I would like to express my sincere gratitude and appreciation to Professor Penlidis for his invaluable guidance and unwavering support throughout my M.A.Sc. degree. His dedication to mentoring and his profound knowledge in the field were instrumental in writing this thesis. I am truly fortunate to have had the privilege of learning under his mentorship.

I extend my sincerest gratitude to Ph.D. candidate Bhoomi Mavani for her unwavering support, her expertise, and her friendship throughout my research endeavor. Bhoomi's methodical training helped me gain confidence working in lab and thoughtful discussions with her have brought new perspectives to my research, helping me refine my ideas.

I also want to thank Ph.D. candidate Yassar Shama and Prof. Eihab Abdel-Rahman (and his research group in Systems Design Engineering) for research collaboration with the MEMS sensor and testing. I also thank Prof. Mekonnen for allowing use of UV-Vis spectrophotometer.

Lastly, I owe deepest gratitude to my parents for all the trust and support they provided during my studies.

Table of Contents

List of Figures

List of Tables

Chapter 1 Motivation, Objectives and Outline

1.1 Research Motivation and Objectives

In the agricultural industry, the nutrition balance of the soil is controlled by manure. The manure is prepared in a pit or lagoon until the chemical composition is suitable for application. To measure the composition of the manure, a sample is taken for testing at a separate facility, which may take up to 3 weeks (or an infrared scanning of manure can be done when manure is spread). For more economical quality control, continuous monitoring of the biogas emitted from the manure was suggested. In addition, there are various gaseous pollutants in this biogas, including greenhouse gases (CO_2, CH_4) and toxic gases (NH_3, H_2S). While the concentrations of these compounds are low (ppm level), biogas is continuously released, which leads to significant amount of cumulative pollution. Thus, reliably measuring concentration is essential for monitoring air pollution caused by agricultural lagoons.

The sensor would be installed at the top of the manure pits to detect the composition and concentration of rising gases. The sensor must be able to detect gases with a short response and recovery time to allow continuous monitoring of manure conditions. The sensor system needs to be lightweight, semi-permanent and it should require low energy. This would imply ambient operating temperature as heating would add extra parts and energy requirements to the sensor system. Hence, this thesis focuses on investigating sensing materials that can detect methane and ammonia with operation temperature of 22-25°C, which would be more economical than existing sensors (see section 2.4, describing metal oxide sensors operating at elevated temperatures, above 300°C).

The gases in question have widely different properties, thus different sensing materials for each gas can be considered. A good candidate would have a reasonable sensitivity for the application, selectivity against other interferents, short response and recovery time, and good stability (ability to be regenerated and used for a long time).

This thesis focuses on developing polymeric materials as sensing materials for ammonia and methane detection at the 10-50 ppm range. Since one deals with a mixture of gases with many interferents, polymeric materials are advantageous for detecting a specific gas analyte.

1.2 Thesis Outline

Chapter 2 describes the background knowledge of agricultural lagoons and the target analytes: methane, ammonia, carbon dioxide and nitrogen oxides. It also explains the three main criteria of sensor technology and what can be done to modify typical sensing materials.

Chapter 3 describes the experimental setup for sensing material synthesis and for testing the sensing capabilities of the materials. Characterization techniques for these materials are also discussed.

Chapter 4 discusses sorption experiment data and characterization of synthesized polymeric materials. The selected gas sensing materials are tested for sorption with a 10 ppm formaldehyde source to determine the optimal material and dopant for maximized gas sorption. This gives a good indication of which material to test with the actual micro-electrical-mechanical system (MEMS) sensor. The polyaniline (PANI) based materials are characterized by various techniques for crystallinity, surface

morphology, dopant incorporation and oxidation states in an effort to explain and corroborate the gas sorption results.

The findings are summarized in Chapter 5, main contributions are emphasized, and recommendations are made for further investigations.

At the end of the document, six appendices (A to F) are included, which show summaries of the literature search, experimental data and related calculations, along with statistical analysis completed for this thesis. The last appendix (G) contains copyright permissions acquired for figures borrowed from the literature.

Chapter 2 Literature Background

2.1 Manure Lagoon

With the increased food demand worldwide, animal husbandry had to deal with increasing quantities of cattle waste as a result. Typically, these wastes are removed from animal pens with water. The waste generated in this manner still contains nutrients undigested by the animals, so it is treated further into manure. A common method of producing manure is fermentation of the liquid waste in a manure lagoon (see Figure 1). Manure lagoons are also called anaerobic lagoons because they use anaerobic bacteria for digestion of remnant nutrients. The manure is produced in an open outdoor basin with a volume typically ranging from 100k to 1200k ft^3 [1]. As the waste settles, it separates into three layers: solid, slurry, and liquid. The solid layer is denser than other components and sinks to the bottom to be removed batch-wise. The slurry layer contains most of the nutrients in liquid form, making them easy to transport via pumping. The liquid layer is mostly water containing some manure.

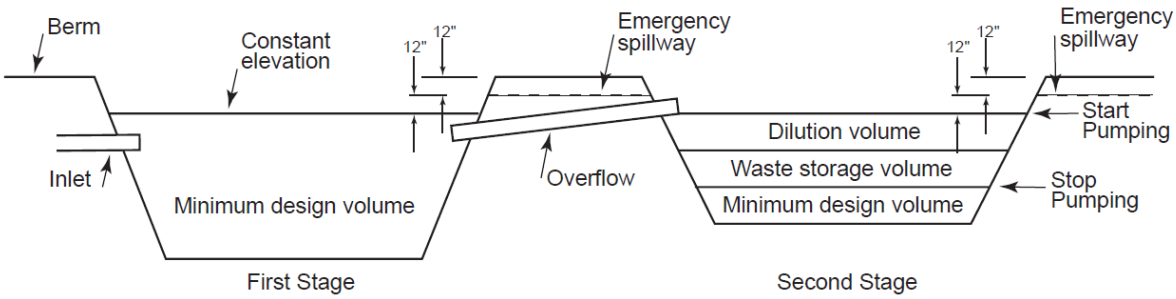

Figure 1. A two-stage anaerobic lagoon designed for the treatment of livestock manure (reproduced with permission from [1])

2.2 Off-Gas Composition

Manure is prepared via anaerobic digestion of the waste slurry. Anaerobic digestion involves reactions in three stages: hydrolysis of macromolecules, followed by generation of organic acids, and finally decomposition of acids into lighter gases [2]. During this process, the residual nutrients such as nitrogen are converted into useable form and off-gas is released. Theoretically, $1.9m^3$ of off-gas is generated from 54kg of cow feces each day [2]. The actual composition of biogas differs based on the type of raw material used for manure production, with CH_4 and CO_2 as the major components (approx. 60% v/v and 40% v/v, respectively) and trace amounts of H_2S and NH_3 [3]. The digestion reactions occur sequentially with the product of a prior reaction used as a reactant in the next one. Because of this, the composition of off-gas changes as the fermentation progresses. The analysis of its composition can be an indicator of the progress of manure preparation.

2.2.1 Methane

Methane is a simple hydrocarbon that is naturally generated from biological processes. It is highly flammable with lower flammability level of 5.3% v/v [4], so it is being considered as a potential fuel to replace non-regenerative crude oil. However, due to its symmetrical molecular structure, it is non-polar and relatively non-reactive compared to other hydrocarbons, making it hard to detect or isolate at

ambient temperature. In addition, methane is the most abundant greenhouse gas after carbon dioxide but with 30 times greater greenhouse effect than CO_2 [5]. Thus, it is of high interest to detect and monitor methane release for both safety and sustainability.

2.2.2 Ammonia

Ammonia (NH_3) is a common product of biological reactions and can be toxic at low concentrations. Assuming an 8-hour shift, a worker could have adverse health effects if exposed to concentration greater than 50 part-per-million (ppm) of ammonia (8-hour total weight average (TWA) permissible exposure limit (PEL) set by Occupational Safety and Health Administration) [6]. It has a distinct odour that is detectable at 2.6 ppm by the human nose and becomes unbearable at 60.9 ppm [7]. NH_3 is a weak base, water soluble and a reactive compound. Due to these properties, its gaseous state is short-lived; it exhibits a steep gradient with a high concentration near the source, which then quickly decreases with distance [8]. Depending on the location of the sensor, the typical range would differ, but 50 ppm or lower could be reasonable target concentration based on toxicity.

2.2.3 Hydrogen Sulphide

Commonly known for the source of "rotten egg" smell, hydrogen sulphide (H_2S) is a strong odour inducing component of biogas. While H_2S is present in the manure off-gas at a low concentration (~1000ppm) [3], it is flammable and toxic (8-hour TWA PEL of 10 ppm) [9]. For H_2S, there is already a sensing material researched by Arabi et al. [10] that utilizes gas sorption properties of polymeric materials, thus H_2S was not included in the scope of this research.

2.2.4 Nitrogen Oxides

Manure is a way to add nitrogen into the soil to promote plant growth. There are three types of nitrogen oxides produced from fermentation of manure: NO, NO_2 and N_2O [11].

N_2O is a relatively stable nitrogen oxide that is commonly produced from biological processes. The term "NO_X" is designated to indicate NO and NO_2 for their reactivity and prevalence in air pollution and greenhouse effect. When manure is added to the soil, the excess nitrogen undergoes nitrogen fixation by microorganisms. It has been observed that the NO_X emissions from soil increased when manure was added [12]. While the amount of nitrogen oxides is not significant in the vicinity of manure lagoons [13], because of the impact NO_X has on air pollution and safety, current sensors will be explored for context (see section 2.4.4).

2.2.5 Humidity

Water is always present as gaseous state (vapour) in varying proportions in ambient air. Depending on the environment temperature and pressure, the concentration of water can differ typically over the range of 30%-70% relative humidity (RH). RH denotes the ratio of absolute humidity to the maximum possible humidity at given conditions. As the manure lagoon contains a large volume mixture of water and manure, humidity will have a greater effect on the sensor operation than in typical ambient conditions. As water takes up ~3% v/v of ambient air [14], which is much larger than the concentration range of other target gases, it is more practical to treat it as an interferent gas for sensor applications. In general, interactions between water vapour (humidity), sensing materials and gas analytes can be a complex issue, largely unstudied in the literature.

2.3 Sensing Criteria

Regardless of sensor mechanics, all sensing materials and sensors share the core characteristics of sensitivity, selectivity, stability, operating temperature, response time and recovery time [15] [16].

2.3.1 Sensitivity

This is a measure of the minimum concentration of target gas a sensor can detect. The difference in the sensor response at baseline (no gas exposure) and upon target gas exposure is considered and if there is significant change, it is defined as successful gas detection by the sensor. A sensor is more sensitive if it shows greater change in response at as low a gas concentration as possible.

For this thesis, the sensitivity of sensing material is calculated based on the amount of target gas sorbed into the material (see equation 1), since the change in response is typically proportional to the amount of gas sorbed. For this application, the desired gas concentration is in the part per million (ppm) range.

$$\boldsymbol{Sensivity} = \frac{\boldsymbol{Target\ gas\ sorbed\ concentration}}{\boldsymbol{Total\ target\ gas\ concentration}} \qquad 1$$

2.3.2 Selectivity

In a real system, the analyte is a mixture of gases that could interfere with detection of the target gas. A sensor should only produce a signal for the desired gas species. Selectivity is defined as a sensing material's affinity towards one gas over the other species (interferents). Typically, this is measured as the ratio of amounts of gases sorbed or appropriate detection signals between two gases (see equation 2).

$$\boldsymbol{Selectivity} = \frac{\boldsymbol{R_g}}{\boldsymbol{R_i}} = \frac{\boldsymbol{S_g}}{\boldsymbol{S_i}} \qquad 2$$

where R is some detection signal, S is sorption of gas, g stands for target gas, and i for interferent.

The greater the sorption concentration or signal of the target gas to that of the interferent gas, the higher the selectivity. It is important to investigate selectivity of sensors to minimize error in the practical application of the sensor. In general and in the long term, for applications to lagoon off-gas, the interaction of sensing material with other gases should be studied to minimize possible errors in the analysis. Off-gas contains gases with higher reactivity than methane and ammonia that could interfere with sensor performance (e.g. hydrogen sulphide, NO_x).

2.3.3 Stability

For practical applications, the stability of the sensing material is essential. There are many categories of stability including but not limited to: reversibility of gas sorption, mechanical integrity, and resistance to change in sensor performance with ageing or repeated use. When designing a sensor, the stability of the sensing material is necessary to get reliable results while monitoring gas concentrations.

2.4 Gas Sensing Techniques

There are numerous methods for detecting gas species at low concentrations. In this section, different sensors and methods are discussed for each gas of interest.

2.4.1 Methane (CH_4) Sensors

Typical methane sensors use a semiconductor such as zinc oxide or tin oxide for methane to adsorb and react with the sensing material. An electrical potential is subsequently applied to detect the change in conductivity. The downside of the current methods is that they require high operating temperature (usually 350-450˚C) due to the high stability of methane [17]. Other common methods are combustion and infrared sensing, both requiring more complex and expensive units [18].

Dosi et al. [18] developed a laser-induced graphene sensor doped with palladium nanoparticles. The commercial Kapton film was scribed by laser to form a porous carbonized polymer reminiscent of graphene. This showed an increase in flexibility of the material allowing more freedom of positioning of the material. The sensing material was tested by observing the change in electrical signal upon exposure to an air/methane mixture. The sensor response is typically defined as:

$$\boldsymbol{Response}\ (\%) = \frac{\left(\boldsymbol{R_g} - \boldsymbol{R_a}\right)}{\boldsymbol{R_a}} \times \mathbf{100} \qquad 3$$

where Rg and Ra are the resistances of the sensor in target gas and pure air, respectively.

Applying an optimal voltage of 0.6 V, the sensor was able to detect a minimum of 5 ppm at room temperature within 50 s of exposure. The sensor is responsive only when oxygen (air) is present in the surroundings. Long time use results in formation of a water layer on top on the sensor; this would impede the surface reaction leading to the sensor response weakening over time. At 5 ppm of methane, the signal decayed 16 min after exposure. After each measurement, 12 min of drying time (no methane) was required to achieve 99% of the previous signal strength. The drying time would increase with higher product concentration. The humidity of the air also interferes with this sensor. This response cycle of the material is not very ideal for usage; however, the sensor exhibits good sensitivity.

Bhattacharyya et al. [19] used nanocrystalline zinc oxide thin film as sensing material for methane detection. The ZnO film was not doped and deposited onto a SiO_2-based plate as shown in Figure 2. Gold and palladium-silver electrode contacts were tested for performance with ZnO film and Pd-Ag contact was found to be more efficient as it performed better at lower operating temperature levels. For detection of 0.1% methane, the optimal operating temperature is 250˚C with response and recovery times of 22 s and 28 s, respectively. This is better performance than a typical SnO_2-based sensor, but more study into the dopant for ZnO would be beneficial for the manure sensor.

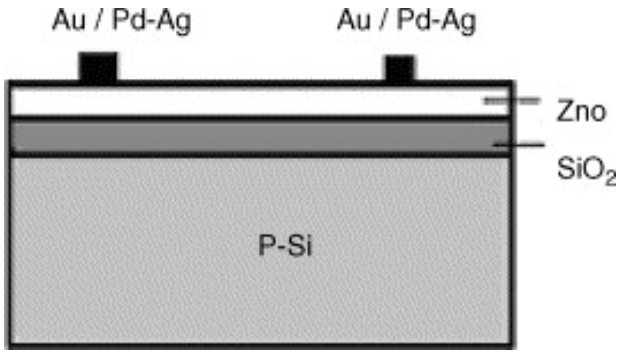

Figure 2. Schematic of the sensor structure with an Au or Pd-Ag (26%) contact (reproduced with permission from [19])

Quaranta et al. [20] used osmium for improvement of tin oxide sensor performance. While having sensitivity to different gases and inexpensive production, metal oxide semiconductors lack selectivity and tend to be poor in sensitivity without an appropriate catalyst. The addition of 5% osmium into tin oxide reduced the optimal operating temperature to 250-300˚C from that of pure SnO_2 (350-400˚C). The doped SnO_2 can detect down to 200 ppm and had response and recovery times of approximately 2 min and 6 min at 1000 ppm methane. The downside is the deterioration of sensor over time due to ageing.

Navazani et al. [21] utilized SnO_2 with reduced graphene oxide (rGO) and polyaniline (PANI) to achieve room temperature methane sensing. In this experiment, pure PANI and PANI with 10wt.% SnO_2@rGO hybrid added were compared. See Figure 3 for the suggested mechanism for formation of SnO_2@rGO-PANI.

The hybrid material can detect down to 100 ppm, which is much better sensitivity compared to pure PANI and SnO_2@rGO which cannot detect such low concentration of methane at room temperature. At 1000 ppm, the response and recovery time was 360 s and 1150 s, respectively, which did not change significantly from that of pure PANI with 320 s and 1100 s. As shown in Figure 4, pure PANI has low methane selectivity against ammonia but SnO_2@rGO-PANI showed a significant improvement in selectivity.

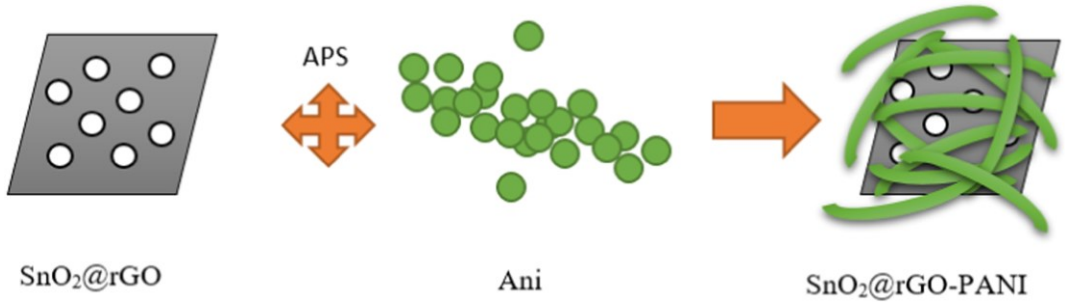

Figure 3. The formation mechanism for SnO_2@rGO-PANI ternary nanohybrid (reproduced with permission from [21])

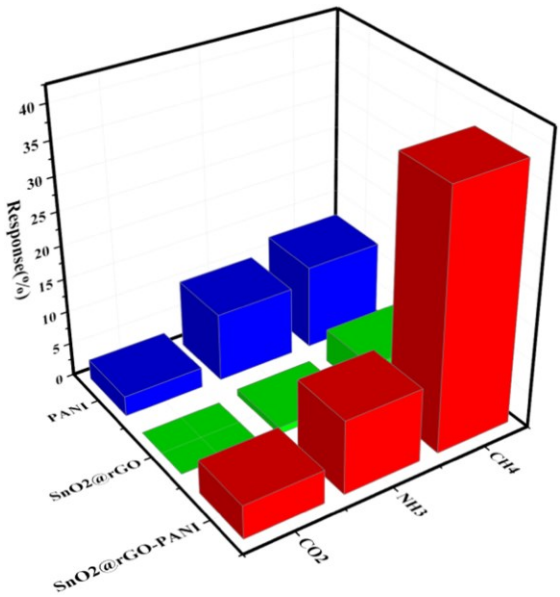

Figure 4. Response of SnO_2 @rGO–PANI hybrid sensor to 1000 ppm methane compared with other analytes at room temperature (reproduced with permission from [21])

Merkel et al. [22] investigated the gas sorption properties of poly(dimethlysiloxane) (PDMS) for pure common diatomic gases (e.g., oxygen gas) and methane at 35˚C with varying pressure. Figure 5 summarizes the obtained sorption isotherms for the gases tested. At the same pressure, the sorption would be favored in the order of CO_2 > CH_4 > diatomic gases (e.g. O_2). While the paper only tested the sorption of individual gas species, PDMS could be tested as a sensing material for sensitivity and selectivity for methane since it does sorb methane.

Khoshaman et al. [23] analyzed two deposition methods of cryptophane A (crypt A) on quartz resonators for gravimetric detection of methane. The research expands upon the fact that crypt A shows an affinity towards methane molecules and that the sensitivity of the sensor made seems to be affected by the deposition method. Testing methane adsorption at room temperature, the crypt A sensor showed sensitivity down to 3 ppm. In addition, the effect of humidity on the sensor was investigated, but the results were not reliable.

Hannon et al. [24] tested various materials typically used. Polyaniline salt was protonated using hydrochloric acid for absorption of methane. The sensor was exposed to CH_4, CO, SO_2, and NH_3 in 1-30 ppm concentration range at room temperature. The sensitivity was tested by measuring the electrical resistance change (response) and polyaniline showed significant response. Sorption was detected down to 2 ppm of methane.

Sen et al. [25] incorporated ZnO nanoparticles into HCl-doped polyaniline to achieve detection of methane at ambient temperature. 3 wt.% ZnO-PANI could detect down to 100 ppm methane. In addition, Sen et al. tested the effect of humidity (~20%-70% RH) on the sensor. Typically, a water layer can form on the sensor surface at a higher humidity level and reduce contact between the sensor and the sample. For ZnO-PANI, humidity had a low impact on the sensitivity of the material which is promising for the target application. This will make the sensor more reliable for analysis of off-gas since it could be high in humidity from evaporation in the lagoon.

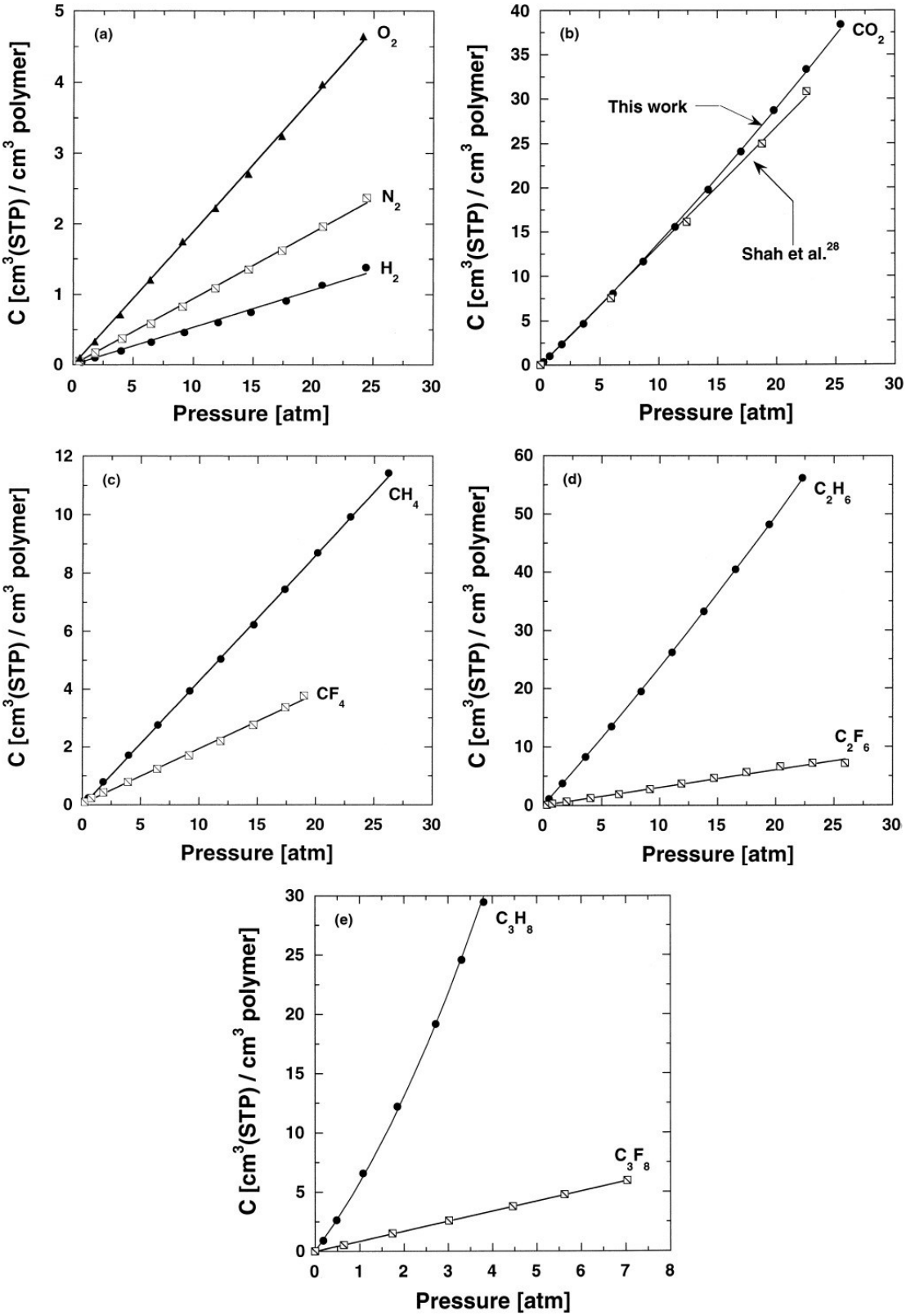

Figure 5. Sorption isotherms in PDMS at 35 °C: (a) H_2, N_2, and O_2; (b) CO_2; (c) CH_4 and CF_4; (d) C_2H_6 and C_2F_6; e) C_3H_8 and C_3F_8 (reproduced with permission from [22])

Assuming 50 ppm is an adequate minimum for the methane detection limit, the SnO_2@rGO-PANI developed by Navazani et al. [21] appears to be a good starting point, considering both sensitivity for methane and selectivity against ammonia. Another possible selection would be ZnO-doped protonated PANI suggested by Sen et al. [25] because its sorption of methane at ambient temperature and low impact of humidity on its performance is desirable for the application.

See also Appendix A.1 for a summary of methane sensing materials and brief comments about their reference sources. Based on the information of this section and Appendix A.1, Table 1 shows the top 4 selected sensing materials to be experimentally evaluated (see Chapter 3).

Table 1. Top 4 most promising materials for methane

Sensing material	Detection Limit	Sensor Type	Operating Temperature	Reference
PANI-SnO_2	100 ppm	Chemiresistor	Room Temperature	[21]
PANI-ZnO (~3wt.%)	100 ppm	Chemiresistor	Room Temperature	[25]
PANI-HCl (Emeraldine Salt)	2 ppm	Chemiresistor	Room Temperature	[24]
PDMS	N/A[1]	Permselectivity[2]	Room Temperature	[26]

[1]Lit. tests for permeability (no data on sorption)

[2]Detection by difference in gas permeation across the material (separation)

2.4.2 Ammonia (NH_3) Sensors

Ammonia odor causes nausea and possible respiratory issues, thus a sensor for detection is necessary for both analysis of manure and safety. There are several sensors available for ammonia with ambient operating temperature.

Kukla et al. [27] developed $HClO_4$ doped polyaniline (PANI) for detection of ammonia at room temperature. The $HClO_4$-PANI was made into a film with thickness of 0.1-0.5 μm to test for conductance as a function of film thickness. The ammonia in the air reacts with PANI to reduce the conductance of the material and the presence of an acid enhances this effect, thus increasing the sensitivity. The $HClO_4$-PANI film was able to detect 5-2000 ppm of ammonia with about 10% error at 20˚C. The response and recovery times are 90 s and 4 min, respectively. The PANI-ammonia reaction is dominated by chemisorption, but physisorption may also occur under certain conditions often at a similar rate. More specifically, the $HClO_4$-PANI-ammonia absorption appears like physisorption. The desorption of ammonia requires activation for the reverse reaction, thus thermal regeneration of the sensor by short-term heating to 104-107˚C was needed. Long-term exposure (more than 1 hour) to high concentration of ammonia makes the adsorption irreversible and renders the sensor unusable.

Wang et al. [28] utilized PANI doped with $CuFe_2O_4$ for improved sensitivity at room temperature. The change in electrical signal was measured upon exposure to ammonia at various concentrations. The sensitivity of $CuFe_2O_4$-PANI was 5 ppm, with response and recovery times of 84 s and 54 s at 20˚C. The short recovery time is advantageous in continuous monitoring of concentration. As shown in Figure

6 and Figure 7, the doped PANI had higher sensitivity/ppm than the pure constituents. The humidity affects the resistance of the sensor, thus careful calibration and/or calculations are recommended if the humidity fluctuates near the pit. The study also tested selectivity against methane and $CuFe_2O_4$-PANI showed good selectivity for ammonia.

Zhang et al. [29] used $SrGe_4O_9$ as dopant for PANI to make an ammonia sensing material with high sensitivity. $SrGe_4O_9$ shows high sensitivity to ammonia; however, the material's initial resistance is very high, making the signal detection very hard. On the other hand, when incorporated into the $SrGe_4O_9$-PANI (PSN) complex, the sensor response was stronger than that of pure PANI as shown in Figure 8. The sensor could detect reliably down to 0.25 ppm at room temperature for response and recovery times of 62 s and 223 s. Overall, the PSN has improved sensitivity and given faster response and recovery times than pure PANI, thus making it ideal for detection of ammonia at lower concentrations.

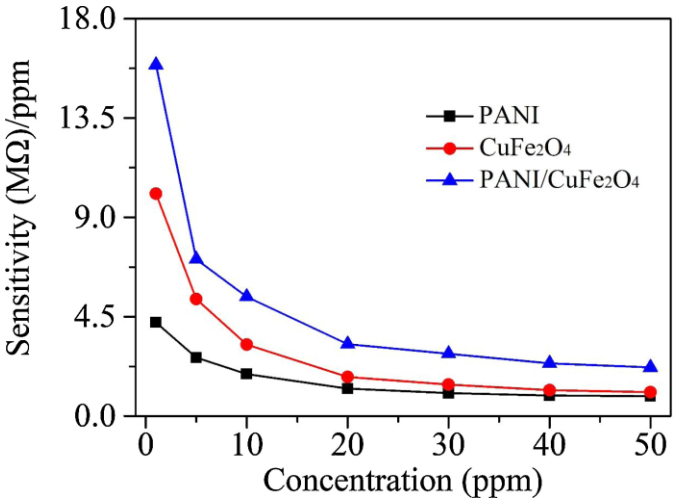

Figure 6. Sensitivity of PANI, $CuFe_2O_4$ and PANI/$CuFe_2O_4$ at different concentrations of ammonia (reproduced with permission from [28])

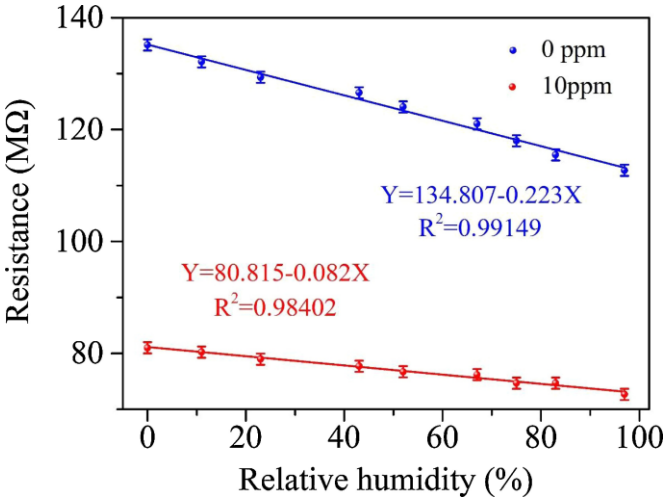

Figure 7. Resistance of the PANI/$CuFe_2O_4$ hybrid film sensor as a function of relative humidity at 0 ppm and 10 ppm ammonia concentration at 20 ℃ (reproduced with permission from [28])

In addition, PSN showed good selectivity to ammonia over other toxic gases (hydrogen sulfide, formaldehyde, carbon monoxide, sulfur dioxide, carbon dioxide, and methane) as the signal response for ammonia was at least 4 times stronger than other gases. As shown in Figure 9, humidity in air reduces the sensor response, thus it is recommended to calibrate or control humidity when using this material.

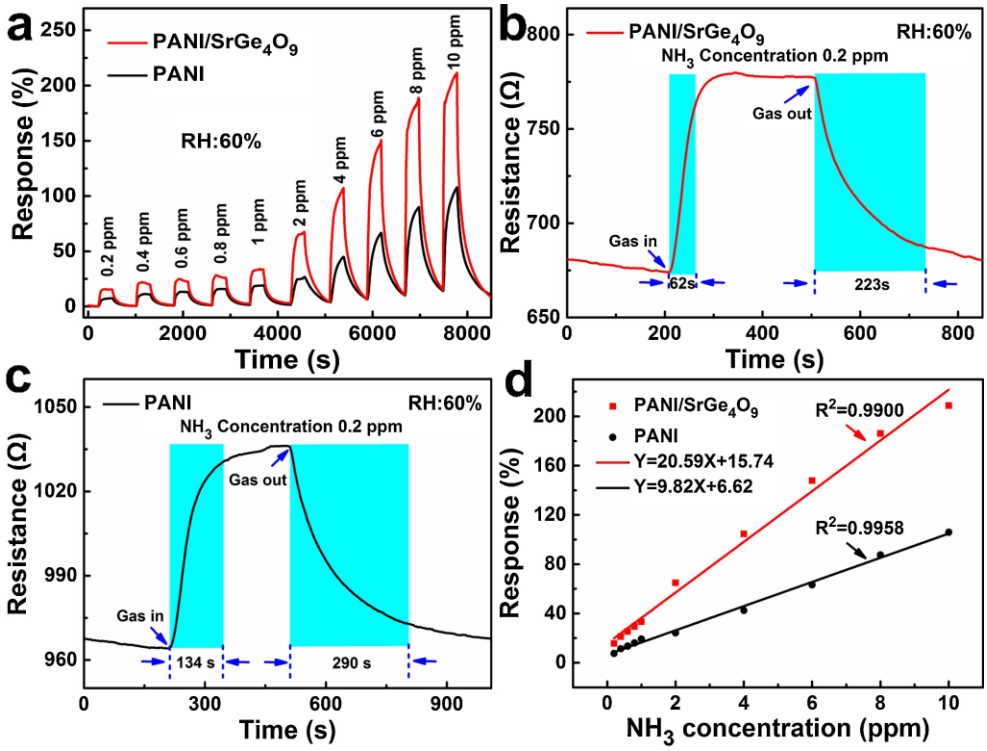

Figure 8. (a) Dynamic response-recovery curves of pure PANI and PSN sensors toward 0.2–10 ppm NH_3 at 25 °C; Real-time resistance changes of the gas sensors towards 0.2 ppm NH_3 at room temperature; (b) PSN gas sensor; and (c) pure PANI sensor; (d) Response-concentration fitting curves of flexible sensors based on pure PANI and PSN toward 0.2–10 ppm NH_3 at 25 °C (reproduced with permission from [29])

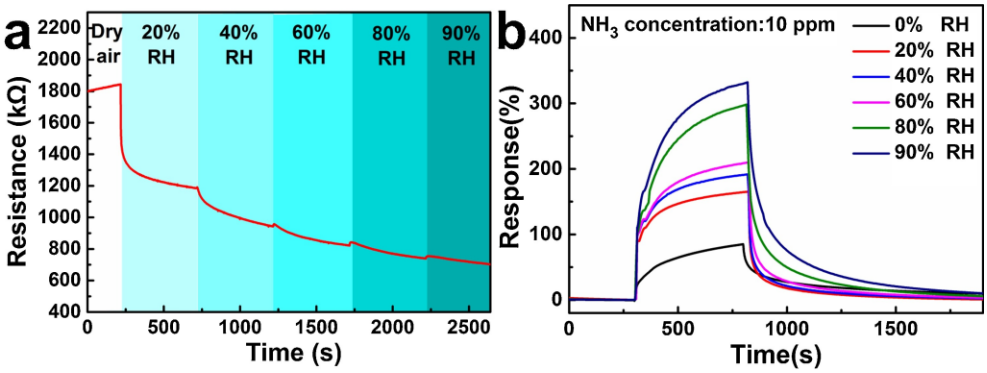

Figure 9. The effect of relative humidity on gas sensing performance of the PSN sensor at room temperature: (a) base resistance of the sensor under 0–90% RH; (b) gas responses toward 10 ppm NH_3 under 0–90% RH (reproduced with permission from [29])

Kulkarni et al. [30] developed a selective ammonia sensor based on PANI doped with tungsten oxide (WO_3-PANI) that can be prepared on a flexible polyethylene terephthalate (PET) surface. The sensor detection limit was 1 ppm at room temperature and increase in ammonia concentration showed corresponding increase in the response magnitude (see Figure 10). Testing at 100 ppm concentration of each gas, the WO_3-PANI showed very small signal response to the test gases (NO_2, H_2S, CH_3OH, and C_2H_5OH) compared to that of ammonia (see Figure 10 (a)). However, humidity reduced the sensor response.

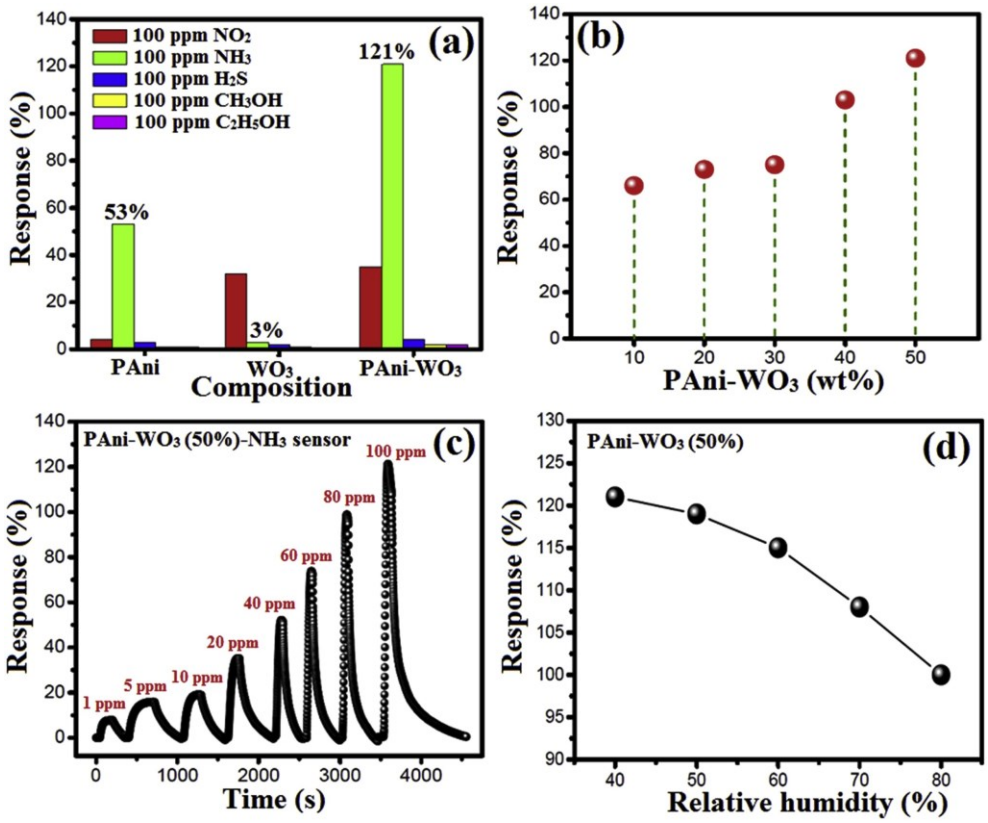

Figure 10. (a) Selectivity study of PANI, WO_3 and flexible PANI-WO_3 sensors towards different test gases, (b) Response study of flexible PANI-WO_3 (50%) hybrid nanocomposites, (c) Response study of flexible PANI-WO_3 (50%) hybrid nanocomposites to 1–100 ppm of NH_3, (d) Humidity study of PANI-WO_3 (50%) hybrid nanocomposites (reproduced with permission from [30])

Nicho et al. [31] constructed a polyaniline-polymethyl methacrylate (PANI-PMMA) composite which is sensitive to low ammonia concentrations (10-4000 ppm at ambient temperature), as its electric and optical properties change in the presence of the analyte. The composite can be recovered by purging it with nitrogen gas for reversing ammonia adsorption.

Jiang et al. [32] found that a thin film of poly(pyrrole) (PPy) that is prepared by electrolytic polymerization changes electrical resistance when exposed to ammonia. The material displayed adequate sensitivity with pure ammonia of 10-4000 ppm (at ambient temperature) and responded in less than 20 s while recovering within 60 s of purging.

Gangopadhyay and De [33] found that a poly(pyrrole)-poly(vinyl alcohol) (PPy-PVA) composite prepared via electropolymerization showed sorption affinity to ammonia. The composite showed a change in electrical resistance when exposed to 1~10% ammonia. However, the exposure to ammonia at higher concentrations, as well as prolonged exposure (24+ hours), caused an irreversible change in resistance. Similar irreversible sorption of NH_3 was observed with poly(pyrrole) coating palladium nanoparticles (PPy-Pd) tested by Hong et al. [34]. PPy-Pd was able to detect down to 50 ppm but sorption of ammonia at high concentration was irreversible, making it non-ideal for agricultural applications.

Similarly, Ahmad et al. [35] synthesized poly(pyrrole)-molybdenum sulfide (PPy-MoS_2) nanocomposite which showed higher sorption of ammonia. PPy was polymerized onto MoS_2 to form a porous structure which increased both electrical conductivity and sorption of PPy. PPy-MoS_2 showed a decrease in electrical conductivity when exposed to ammonia (lowest concentration of detection at 300 ppm). Unlike PPy-PVA, adsorption of NH_3 on PPy-MoS_2 is reversible at the tested concentration range (300-1000 ppm). This composite showed selectivity against VOCs such as ethanol, acetaldehyde, formaldehyde, and diethyl ether.

Chabuksawr et al. [36] synthesized polyaniline doped with acrylic acid (0.03M) (PANI:AA) that can be used for ammonia detection for a concentration range of 1-600 ppm. Interestingly, as the ammonia concentration increased, the response time decreased while the recovery time increased. The minimum response time was 1 min for ammonia concentration higher than 58 ppm, while the maximum was 2.5 min for concentration lower than 2 ppm. The recovery time was 4.5-6 min.

Khun et al. [37] investigated the possibility of using porous nanosized SnO_2 synthesized via a nonaqueous sol-gel method for ammonia gas sensing. The film prepared using SnO_2 was tested at 50 ppm ammonia at different operating temperatures in the 25-200˚C range. Khun et al. state that SnO_2 showed better sensitivity compared to other metal oxides due to its porosity which increased surface area for sorption.

A sensing material could be a foam as it could improve surface area for contact with target analyte. Dacrory et al. [38] developed cellulose-graphene oxide (GO) cryogel (foam) with the polymer functionalized with ethylenediamine for affinity towards ammonia. With GO, the material can be used with a resistive sensor. Cellulose-GO detected ammonia as low as 5 ppm, with the electrical resistance decreasing upon exposure. The lesser ethylenediamine (crosslinker) added, the sensing material performed better, which implies that there is a close relation between polymer structure and sorption.

Matsugushi et al. [39] prepared films from four blends of polymethyl methacrylate-polyaniline copolymers doped with bis2-ethyl hexyl hydrogen phosphate (PMMA-PANI: DiOHP) to test the change in electrical conductivity from exposure to ammonia gas at varying concentrations. Each sample showed a different affinity to ammonia and PMMA-PANI:DiOHP prepared with toluene as the solvent showed the fastest response time (and good reversibility). This was the only blend that showed porosity and Matsugushi et al. state that this structural property made it the optimal sample. However, the response time (11 min at 30˚C for 500 ppm) was not good enough for practical use and further study was recommended.

Gong et al. [40] also utilized TiO_2 for ammonia detection but instead of layered films, the oxide fibres encased polyaniline nanograins to form a titanium oxide-PANI composite. The sensitivity of PANI as ammonia gas detector was greatly improved to a lower detection limit of 50 ppt (part-per-trillion).

While such an ultrasensitive sensor may not be necessary, it is a good example of how PANI can be modified structurally to improve sensor performance.

Tripathi et al. [41] synthesized protonated PANI and mixed it with 2~8 wt.% Al_2O_3 to make a composite pellet. This composite was tested for change in electrical signal with exposure to ammonia at 100-1500 ppm at room and elevated temperature. Tested at room temperature, Al_2O_3-PANI composite with higher metal oxide content showed increased sensitivity at higher NH_4 concentration. The concentration of Al_2O_3 had no significant effect on the sensitivity at 300 ppm. It would be recommended to dope the sensing material with 6~8 wt.% Al_2O_3 if the ammonia concentration is higher than 300 ppm.

Khuspe et al. [42] utilized camphor sulfonic acid (CSA) doped PANI-SnO_2 (50 wt.%) composite. The PANI-SnO_2-CSA (30 wt.%) was the most ideal for detecting NH_3 at 100 ppm (30˚C) with sensitivity of 0.91 (ratio of resistance change as signal before and after exposure). Note that CSA-PANI had the worst performance compared to the individual components due to poor morphology despite the increased conductivity due to protonation of PANI.

Liu et al. [43] found that polyaniline doped with WS_2 (PANI-WS_2) performs well under humid conditions. PANI-WS_2 can detect down to 10 ppm of ammonia and showed faster response and recovery times when the relative humidity (RH) level was between 22% to 68%. WS_2 as a dopant improves the sensor performance of PANI when the analyte has 22% RH or higher, which makes it a promising material for the off-gas NH_3 detection. Similarly, poly(acrylic acid) is found to be more sensitive to ammonia at higher humidity levels [44].

Lee et al. [45] tested the effectiveness of quartz crystal microbalance (QCM) gas sensors with alternating layers of TiO_2 and polyacrylic acid (PAA) to selectively detect amine odors. The TiO_2/PAA had low detection level (0.1ppm) while being stable over a wide range of humidity (30-70% RH) at room temperature. It was found that ambient ammonia concentration of 15 ppm can be sorbed in such a way that the concentration may go up to 20000 ppm inside the film composite. Mirmohseni and Oladegaragoze [46] utilized polyvinylpyrrolidone coated QCM and detected ammonia at low concentrations. However, the polymer showed higher signal (shift in frequency) with water vapour thus, non-ideal for agricultural setting.

See also Appendix A.2 for a summary of ammonia sensing materials and brief comments about their reference sources. Based on the information of this section on ammonia and Appendix A.2, the top 4 materials (Table 2) were synthesized and studied (see Chapter 3).

Table 2. Top 4 most promising materials for ammonia

Sensing material	Detection Limit	Operating Temperature	Reference
PANI-TiO_2	1 ppm	Room Temperature	[47]
PPy	10 ppm	Room Temperature	[32]
PANI-In_2O_3	50 ppm	Room Temperature	[48]
PANI-HCl[1M]	2ppm	Room Temperature	[24]

2.4.3 Humidity

As with any biological processes, the anaerobic lagoon contains a large portion of water. Because of this there would be considerable amount of vapour within the off-gas. A sensor that can either accurately detect water concentration or is selective towards a specific target analyte is necessary for the application. Typically, the sensor is expected to perform at RH 5-50%. Some papers in the literature (e.g. references [28], [29], [30]) have attempted to tackle the humidity issue, but the efforts were far from systematic.

2.4.4 Nitrogen Oxides

The literature studies reviewed herein were based on sensing materials for inorganic gases in fuel exhausts. See Appendix A.3 for a summary. Nitrogen oxides cannot be detected (at least so far) using polymeric materials, thus metal oxides like NiO and/or ZrO_2 are used. Plashnitsa et al. [49] used a NiO-based electrode for detection of NO_2. This sensor was able to detect down to 50 ppm at 800˚C but had poor selectivity as presence of CH_4 produced significant signal response.

Sekhar et al. [50] used $La_{0.8}Sr_{0.2}CrO_3$ as a working electrode in a mixed potential sensor to detect NO_X down to 100 ppm at 600°C. A positive current bias was used to improve selectivity towards NO_X; however, the stability of the sensor was poorer with the positive current bias which caused a baseline drift over time (700 h).

Chen and Xiao [51] synthesized a composite $La_{1.67}Sr_{0.33}NiO_4$ doped with 10 wt. % yttria-stabilized-zirconia (YSZ) potentiometric sensor for NO_X. The sensor was operated between 400 and 550°C, had a poor detection limit of 700 ppm, and moderate response and recovery times of 4 and 6 seconds, respectively.

Yang et al. [52] designed a potentiometric NO_X sensor that used Pt electrodes on an YSZ electrolyte. Pt-loaded zeolite (PtY) was used as a filter to remove interferents such as CO, propane, and NH_3. The sensor was highly selective due to the added filter and had an optimum operating temperature of 500°C. The sensor was sensitive and could detect NO_X down to 1 ppm but lacked stability as there was a baseline drift over time.

Figueroa et al. [53] also used a Pt-loaded zeolite Y as a catalyst with a Pt reference electrode to detect NO_X. A filter was used to catalyze the ionization of NO_X. The sensor was tested over a range of 100-400 ppm at temperatures between 300°C and 500°C. This sensor had high selectivity due to a filter that acted as a separator and catalyst.

Kim et al. [54] developed a NO_X gas sensor for monitoring air quality within a vehicle's interior. In_2O_3 was able to detect down to 0.5 ppm of NO_2 at 300°C with response and recovery times around 1 minute. The sensor was evaluated over the range of 200 - 350°C and was most sensitive between 275-300°C.

Jha et al. [55] created a selective NO_X sensor by functionalizing carbon nanotubes with copper phthalocyanine (CNT-CuPC). Even at low concentrations of NO_X (0.5 ppm), the CNT-CuPC was more than 10 times selective towards NO_X than other interferent gases (CO, SO_2, and NH_3). At room temperature, the sensor had response and recovery times of 3 and 6 minutes, respectively.

See also Appendix A.3 for a summary of ammonia sensing materials and brief comments about their reference sources.

2.5 Dopants for Polymeric Sensing Materials

Many previous works on sensor for methane and ammonia utilized conductivity-altering properties of semi-conductive polymers such as polyaniline (PANI).

PANI is a conductive polymer unique for having different oxidation states. The monomer, aniline, consists of a benzene ring and amine group. This amine group could be either reduced or oxidized, giving polyaniline three forms with distinct properties depending on the ratio of the oxidized amine group in the chain (see Figure 11). In Figure 12, y is the fraction of reduced units and (1-y) represents that of oxidized units. PANI is categorized into three states based on the (1-y) values (see Table 3) [56].

Polyaniline in its leucoemeraldine base state is not conductive. It only becomes conductive when it is moderately oxidized to emeraldine base (EB) and/or protonated to emeraldine salt (ES) [57]. The oxidation causes 'gaps' in the delocalized electron cloud which promotes the charge to be carried along the polymer chain. The protonation with acid introduces an anion to the polymer which allows oxidized EB to achieve charge neutrality for better stability and conductivity [58] [59]. On average, EB has conductivity of 10^{-8} S/cm while ES is conductive like a typical metal with 10^{0} S/cm [60].

Each oxidation state can be in a form of a base (e.g. leucoemeraldine base (LEB)) or a protonated state (e.g. emeraldine salt (ES)), by treating the material with a base or acid. EB is the stable form; thus, it is more commonly used for research. However, the exact oxidation state is unknown as it is dependent on the synthesis conditions. The simplest method of distinguishing the oxidation state of PANI is observing the absorbance peak(s) via ultraviolet/visible (UV/Vis) spectroscopy [61].

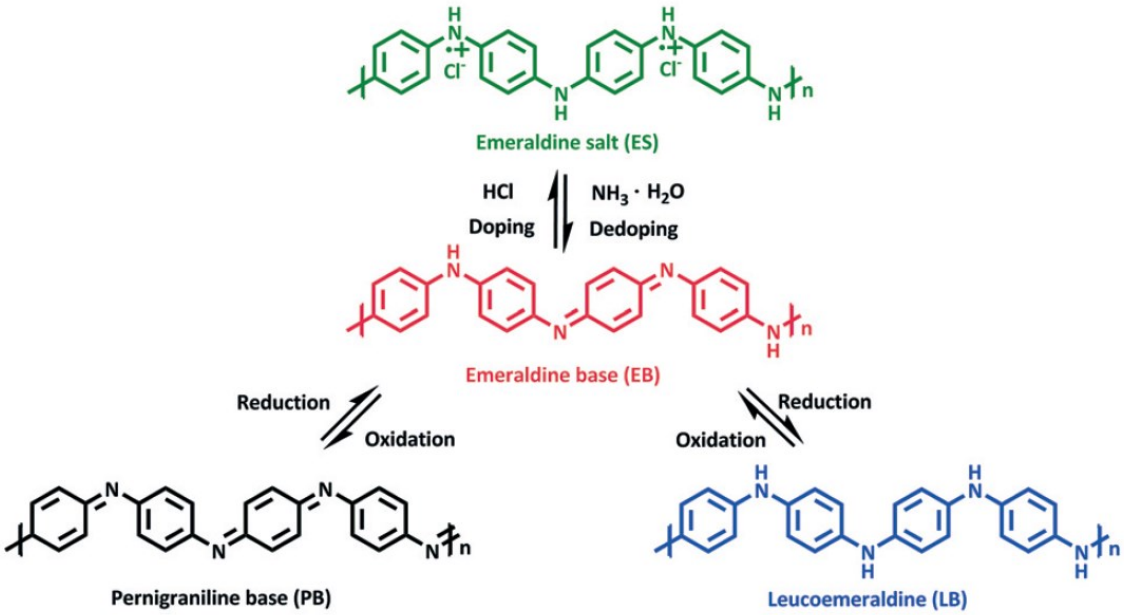

Figure 11. Typical structures of different PANIs (emeraldine salt, emeraldine base, pernigraniline base, leucoemeraldine base) and their interconversion (reproduced with permission from [57])

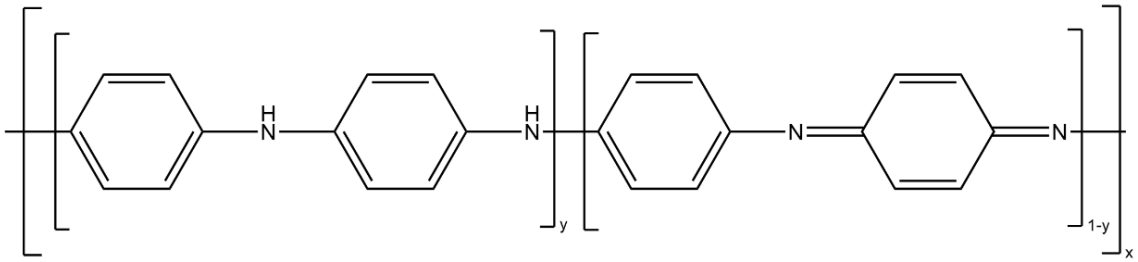

Figure 12. Generalized structure of PANI

Table 3. Oxidation states of PANI

Oxidation State of PANI	REDOX	Oxidation number (1-y)
Leucoemeraldine Base (LEB)	Reduced form	0
Emeraldine Base (EB)	Neutral form	0.5
Pernigraniline Base (PB)	Oxidized from	1

Chapter 3. Experimental

3.1 Polymeric Sensing Material Synthesis

After careful consideration of sensor criteria for the specific application and existing sensing materials from the literature, polyaniline (PANI) was chosen as the candidate for synthesis, doping and characterization. PANI is advantageous in this application for its stability, cost, and ability to operate at ambient conditions. The synthesis was relatively simple with high yield (80-90%), which allows modification with different dopants.

Polypyrrole (PPy) and polydimethylsiloxane (PDMS) were purchased from Sigma-Aldrich and used as received without further purification.

Metal oxide nanoparticles were used for PANI doping. Tin (IV) oxide (SnO_2) (avg. particle size ≤100 nm), zinc oxide (ZnO) (avg. particle size <40 nm, 20 wt.% suspension in H_2O) and titanium (IV) oxide (TiO_2) (particle size ~21 nm, 99.5% concentration) were purchased from Sigma-Aldrich. Deionized (DI) water was used as the reaction medium, and for washing and rinsing, and ethanol (ACS grade) was used as received for additional washing and rinsing of the synthesized polymers.

3.1.1 Synthesis of PANI without dopant

PANI was prepared in the lab by interfacial-dispersion polymerization of aniline with ammonium persulfate (APS) as initiator and deionized (DI) water as the continuous dispersion phase. 1.0 mL of aniline (A.C.S. reagent, Sigma-Aldrich, Oakville, Ontario, Canada) was added to 49 mL of deionized water and then mixed using a sonicator for 30 minutes. This solution was then cooled to -1°C before the addition of a solution containing 1.5 g of APS (ACS reagent, Sigma-Aldrich, Oakville, Ontario, Canada) in 7.5 mL of deionized water. The mixture was swirled manually for one minute to ensure thorough mixing. The mixture was subsequently left to react at -1°C for 6 hours with occasional intermittent stirring [62]. The polymer was filtered out using a funnel and Wattman #5 filter paper and washed with deionized water until the liquid was clear yellow. Then, the polymer was washed with ethanol three times as over-washing could cause some loss of low molecular weight chains (or dopants, if dopants were used). The filtered material was left to dry for about a day and collected into a glass vial for storage under atmospheric conditions. The yield of each sample was also calculated to estimate the loss of material during synthesis. Typical yields obtained with PANI were above 85%.

3.1.2 PANI with Metal Oxide (MO) Dopants

PANI was doped with metal oxide by adding the metal oxide to the aniline and DI water dispersion before sonication. MO was added by weight percentage of total (aniline and dopant) weight:

$$\boldsymbol{dopant\ conc.} = \frac{\boldsymbol{m_{dopant}}}{\boldsymbol{m_{dopant}} + \boldsymbol{m_{aniline}}} \times \mathbf{100\%} \qquad 4$$

PANI with dopant is notated as PANI-(concentration) (dopant). For example, PANI synthesized with 5% zinc oxide is designated as 'PANI-5% ZnO'.

The rest of the procedure was kept identical to the one described in the previous section.

3.1.3 PANI with Sodium Dodecyl Sulphate (SDS)

Based on the process developed by Sen et al. [25], sodium dodecyl sulphate (SDS) 5mM was dissolved into the water/aniline "solution" to compare the incorporation of ZnO into PANI. The reaction mixture was sonicated, and the rest of the procedure was identical to the above section. As SDS is a surfactant (non-reactive) and present in very small relative amounts, any sample with SDS added during synthesis is notated as PANI-(dopant)-SDS.

3.1.4 PANI with Hydrochloric Acid (HCl)

PANI is known to be conductive when doped with acid to change its oxidation state. When synthesized in neutral pH, PANI is in emeraldine base form (PANI-EB). When doped (synthesized) with acid, PANI is in emeraldine salt form (PANI-ES). For the comparison of PANI-EB and PANI-ES gas sorption capability, PANI was also synthesized in acidic conditions. Aniline was added to 1M HCl instead of DI water and the rest of the procedure was kept identical to Section 3.1.1.

3.2 Gas Sensing Setup

The sensing materials were synthesized in the lab with various dopants for evaluating their sorption performance. A schematic of the gas analysis setup is shown in Figure 13. All the gas concentration measurements were done using a Varian 450 gas chromatograph (GC) with a specialized photon discharge helium ionization detector (PDHID) for high accuracy and detection down to ppb range.

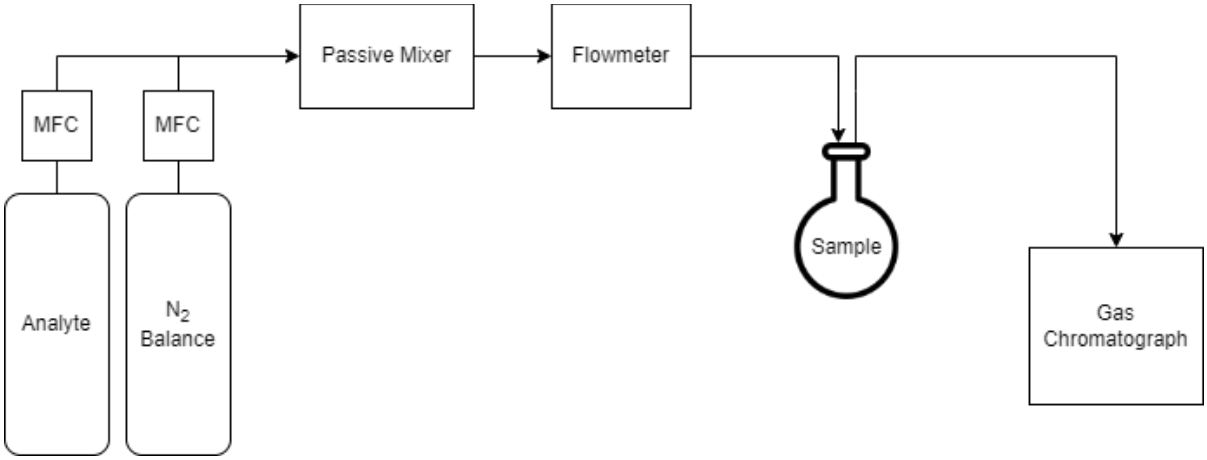

Figure 13. Schematic of the test system, where MFC denotes mass flow controller

Each sensing material was tested by exposing it to a known concentration of analyte (e.g., 5 ppm of a specific gas in a nitrogen balance). Before the sequence of trials, a "blank" run was performed, which measures the concentration of exiting gas of the system without any sensing material inside the testing chamber. This confirms the source concentration of analyte as there is a chance of loss during the gas transport along the system.

After exposure to the sensing material, the gas stream flows into the GC and the concentration of analyte were measured. Then, the concentration of gas analyte was compared before and after passing through the sample chamber. The larger the difference in concentration in a "blank" flask and with the sensing material indicates better sorption and better sensitivity to the analyte. The tests were conducted at room temperature (about 22˚C) and approximately at 15 psi.

Polyaniline (PANI), doped PANI (with metal oxides with or without sodium n-dodecyl sulphate (SDS)), polypyrrole (PPy) and polydimethylsiloxane (PDMS) with different end groups were tested for formaldehyde (F) sorption (formaldehyde source at 10 ppm). The sensing material was deposited into a round-bottom flask via a suspension of the sensing material in ethanol, and then the ethanol was evaporated, leaving only the sensing material in the flask. To note, PDMS was deposited in the round-bottom flask directly as it is in a liquid state at room temperature. All sorption tests were performed with 0.1g of each sample in ambient conditions. Table 4 shows the samples tested and the sequence of tests performed.

Table 4. List of trials with PANI, doped PANI, PDMS, PPy

Sample #	Name	Test	Purpose
1	PANI	F 10 ppm	Sensitivity of F
2	PANI-5% SnO_2	F 10 ppm	Sensitivity of F
3	PANI-10% SnO_2	F 10 ppm	Sensitivity of F
4	PANI-5% ZnO	F 10 ppm	Sensitivity of F
5	PANI-5% ZnO-SDS	F 10 ppm	Sensitivity of F
6	PANI-2.5% ZnO	F 10 ppm	Sensitivity of F
7	PANI-2.5% ZnO-SDS	F 10 ppm	Sensitivity of F
8	PDMS-T (trimethylsilyl terminated)[(1)]	F 10 ppm	Sensitivity of F
9	PDMS-M (monohydroxy terminated)[(2)]	F 10 ppm	Sensitivity of F
10	PANI-HCl	F 10 ppm	Sensitivity of F
11	PANI-SDS	F 10 ppm	Sensitivity of F
12	PANI-HCl-SDS	F 10 ppm	Sensitivity of F
13	PANI-20% ZnO	F 10 ppm	Sensitivity of F
14	PANI-5% TiO_2	F 10 ppm	Sensitivity of F
15	PANI-20% TiO_2	F 10 ppm	Sensitivity of F
16	Polypyrrole[(1)]	F 10 ppm	Sensitivity of F
17	PANI-2.5% ZnO-SDS B[(3)]	F 10 ppm	Sensitivity of F

[(1)] Purchased from Sigma Aldrich
[(2)] Purchased from Alfa Aesar
[(3)] Corresponding sample was synthesized again to eliminate the possibility of material aging as the cause of sorption decreasing over time

3.3 Gas Analytes

The gas analytes of interest can be evaluated in the gas sensing system. The concentrations of each analyte were calculated based on the ideal gas law with the mixture in a balance of nitrogen gas (Praxair, California, USA).

Methane is flammable and explosive, whereas ammonia is toxic and corrosive, hence both present special safety issues and also need special modifications in the GC columns and setup. Due to these concerns, formaldehyde was used as a "simulant" for the GC sorption tests and sensing material evolution (in Chemical Engineering). The final test with the actual MEMS sensor used methane directly in a special chamber enclosure (in collaboration with the Department of Systems Design Engineering, Prof. Eihab Abdel-Rahman group).

3.4 PANI Material Characterization

Several representative sensing materials were selected for characterization. See Table 5 for the selected samples. The tested samples were chosen as representatives for different material types (e.g. dopant, oxidation state, etc.)

Table 5. Table of characterization tests performed on the PANI materials

Material	SEM	EDX	XRD	UV-Vis
PANI	v	v	v	v
PANI 5% SnO_2	v	v		
PANI 10% SnO_2				
PANI 2.5% ZnO	v	v		
PANI 2.5% ZnO-SDS	v	v		
PANI 5% ZnO	v	v		
PANI 5% ZnO-SDS	v	v		
PANI 20% ZnO				
PANI 5% TiO_2	v	v		
PANI 20% TiO_2				
PANI-HCl	v	v	v	v
PANI-HCl-SDS				
PANI-SDS	v	v	v	v

3.4.1 Scanning Electron Microscopy (SEM) and Energy Dispersive X-Ray Analysis (EDX)

Pristine PANI and PANI doped with metal oxide (ZnO) and/or hydrochloric acid (HCl) were synthesized using in-situ polymerization. Scanning electron microscopy (SEM) was performed on the samples using UltraPlus FESEM (University of Waterloo, WATLAB facility). In parallel, energy dispersive X-ray analysis (EDX) was conducted using the same equipment to obtain information of the presence/concentrations of different atomic elements in the polymer.

A square piece of carbon tape was placed on a SEM specimen stub. PANI powder was dispersed in ethanol and the "solution" was dispensed onto the tape. The sample was left at room temperature for the solvent to evaporate and observed using SEM. EDX was conducted on sample surfaces with the most even coverage to obtain the average distribution of elements over the specific area as reliably as possible.

3.4.2 X-Ray Diffraction (XRD)

The crystallinity of pristine PANI, PANI-HCl and PANI-SDS was analyzed using GIXRD (Grazing Incidence X-ray Diffraction). The three samples were chosen (see Table 5) as a representative analysis on crystallinity of PANI without MO dopants. A fine powder of polymeric sample was mounted on a glass slide using a double-sided tape prepared by Dr. Nina Heinig from the University of Waterloo WATLAB facility. A PANalytical X'Pert Pro MPD Powder XRD was used to analyze the prepared sample with X-ray wavelength of Kα 1.54 Å (Cu target) operating at 45 kV and 35 mA with scanning range of 5°-90° with step-size of 0.10°.

3.4.3 Ultraviolet–Visible Spectroscopy (UV-Vis)

Selective PANI samples were analyzed using a Cary 60 UV-Vis spectrophotometer to determine their oxidation state. The UV-Vis spectrophotometer was used courtesy of Prof. T. Mekonnen. Department of Chemical Engineering, University of Waterloo. 1.0 mg of PANI material was suspended in 50 mL of N-methyl-2-pyrrolidone (NMP) for 15 hours prior to analysis. The assay was done under ambient conditions. Scans were done twice for each sample, following the procedure as described in Mavani [63].

3.5 Micro-Electrical-Mechanical System (MEMS) Sensor Test

Micro-electrical-mechanical system or MEMS refers to any electrical device that has any sort of mechanical motion and the whole system has one or more dimensions in the micrometer scale [64]. These are spatially efficient, amenable to handheld devices, and highly sensitive, which is ideal for sensors that are lightweight and wearable.

A MEMS static bifurcation sensor (see Figure 14) has been developed, where a solid sensing material can be loaded to detect a target gas [10]. The main component of the sensor is a 60 μm by 30 μm platform suspended by two cantilevers (125 μm by 5 μm; see Figure 15) that vibrate in a certain frequency when electrical potential difference (pull-in voltage) is applied. This frequency changes when the mass of the platform changes. If a sensing material that sorbs a target gas is loaded, the sensor is referred to as 'functionalized'. When the sensor is exposed to an analyte, the sensing material will sorb the target gas and the overall mass of the platform will increase. This will lead to a shift in frequency which can be detected and translated (if needed) into the concentration of the target gas.

In collaboration with Yasser Shama (Ph.D. candidate, Department of Systems Design Engineering, University of Waterloo), the final gas detection test was performed with methane at 50ppm. The sensing material was loaded onto the sensor by suspending the material powder in ethylene glycol with material concentration of 10-15 wt.% and leaving it to dry, thus allowing for an even coating on the surface.

The MEMS sensor is placed in an enclosed chamber and the enclosure is purged with nitrogen gas. Then, the target gas fills the chamber until the concentration inside stabilizes. The displacement of the sensor platform is continuously monitored when static pull-in voltage is applied. This leads to a sudden increase in frequency (see Figure 16), which can be translated into sensitivity of the sensor. The experimental setup can be seen in Figure 17.

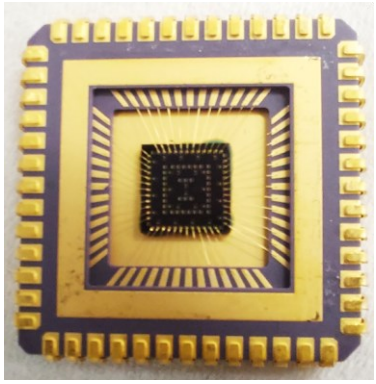

Figure 14. An image of the MEMS sensor (photo taken by the author in Systems Design Engineering lab circa August 2022)

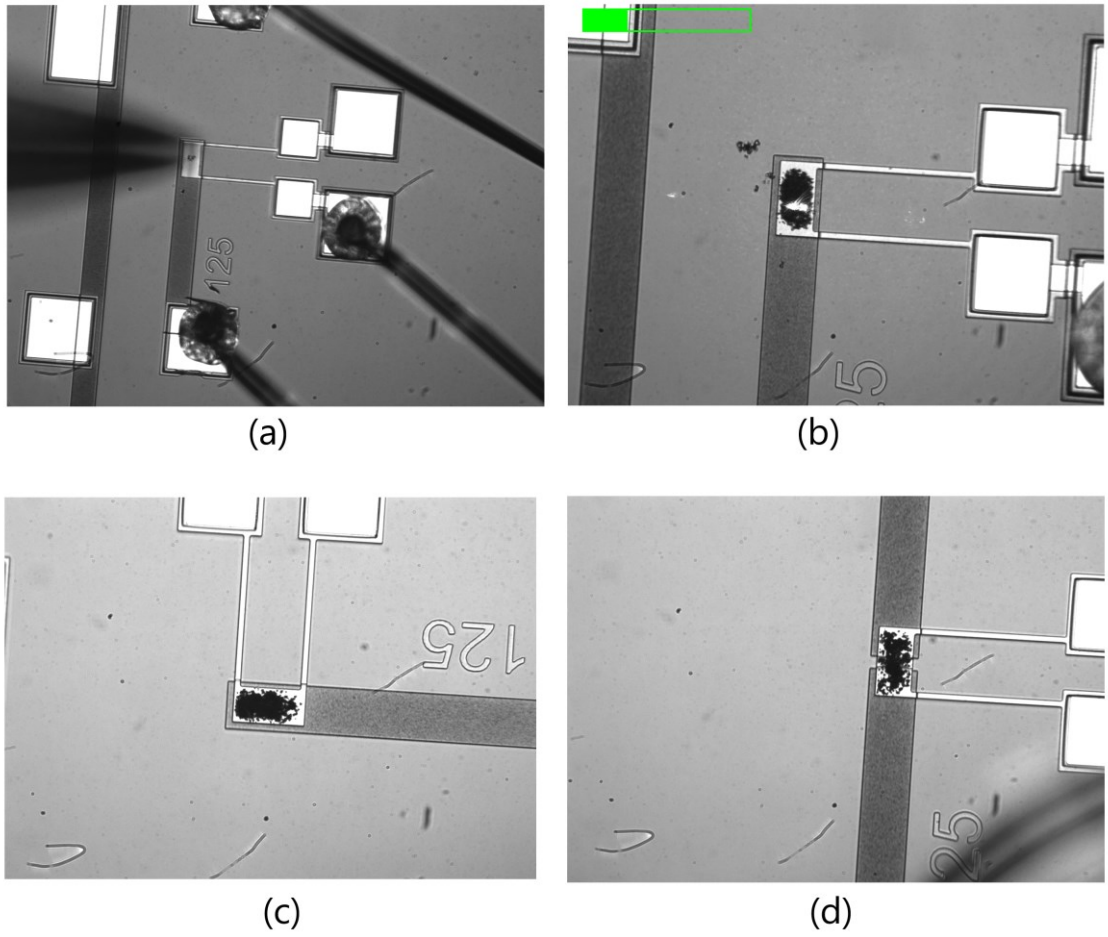

Figure 15. Close up shot of a) sensing material deposition b-d) functionalized sensor (reproduced with permission from [10], open access)

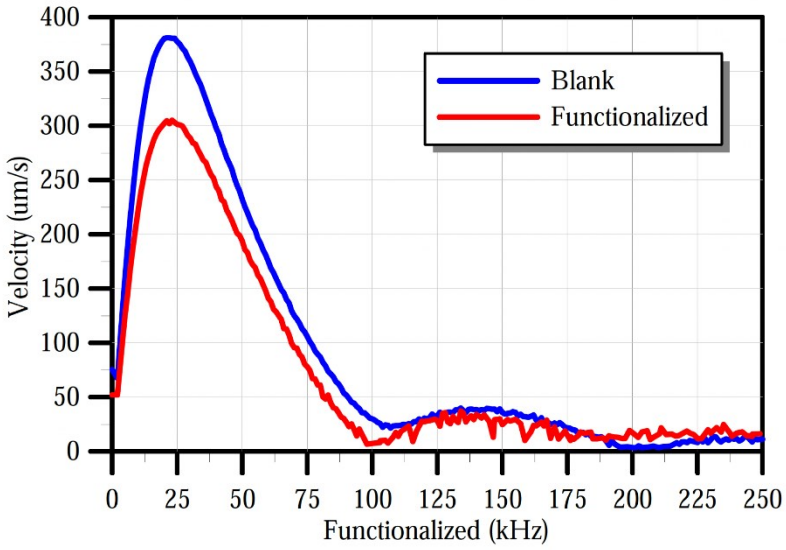

Figure 16. Frequency response of the sensor before and after functionalization with PANI (reproduced with permission from [10], open access)

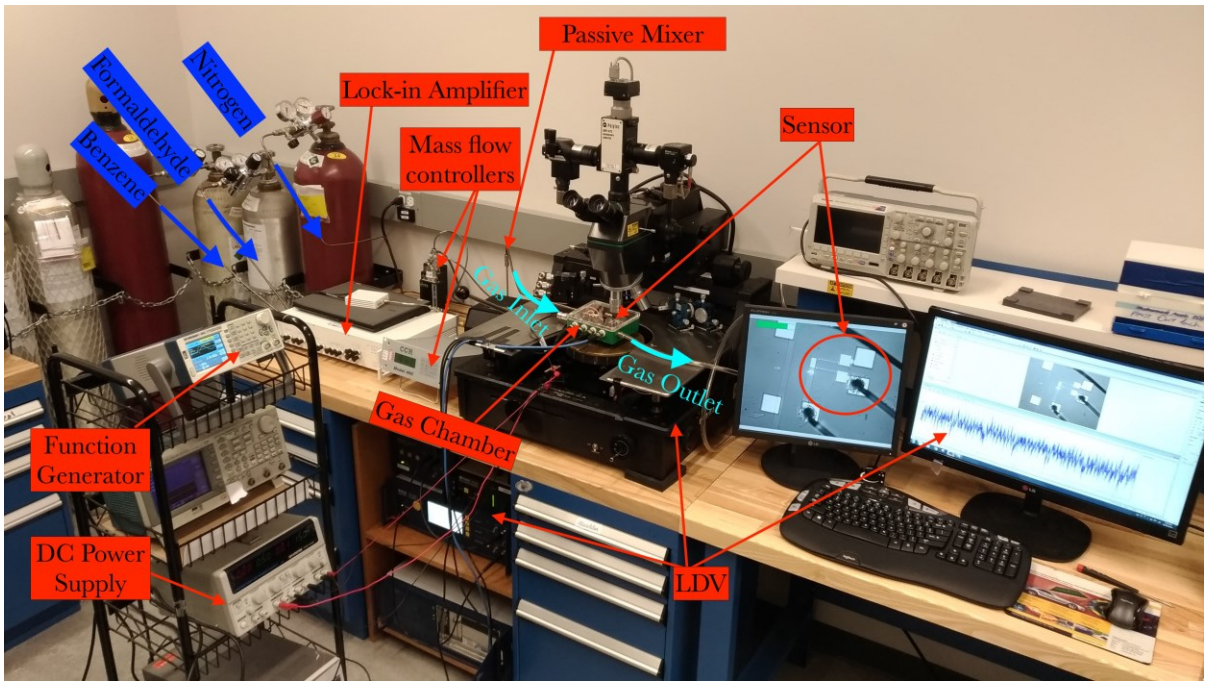

Figure 17. The experimental setup of MEMS sensor testing (reproduced with permission from [10], open access) (the gas cylinder was changed to methane during the testing for this research)

Chapter 4. Results and Discussion

4.1 Gas Sorption

4.1.1 PANI, PPy, and PDMS Formaldehyde Sorption

Formaldehyde (F) sorption (source 10 ppm) of pristine polymers (no dopants) was measured to evaluate the base sorption behaviour of each material. This gives a sense of which polymer should be modified for sorption of the target gas. The experimental procedure has been described in section 3.2.

The measure of sorption will be the difference between the F concentration of the blank runs and the concentration of F after contact with a testing sample. The relative sorption was calculated based on the blank (baseline) value for the corresponding trial. The baseline measurements were analyzed to account for variation experienced between different trial dates. While there were fluctuations between trial dates, the graphical and statistical analysis confirmed relative stability of blank values (see Appendix B for figures and related analysis). The least significant difference (LSD) was used to confirm that blank values were similar enough to ensure the data can be compared between trials (see Appendix C).

As seen in Table 6, Figure 18 and Figure 19, PANI showed the highest sorption out of the four polymers with 2.45 ppm of F sorbed. PPy followed PANI with 0.94 ppm sorption, which is rather low to be considered significant sorption. PDMS, regardless of its end group, showed negligible sorption with 0.58 ppm and 0.24 ppm for PDMS-T and PDMS-M, respectively. This is complete lack of affinity towards F. PDMS in the form of a thin liquid layer probably led to a smaller surface area for gas sorption to occur. Both PANI and PPy are in a powder form, which allows for increased contact with gas as polymer grains have interstitial space between them. Based on the observed trend, a sensing material that is in the solid state (powder or grain particles) is preferred for the ease of loading the material onto a sensor platform. PANI is the best polymer for the sorption of formaldehyde, thus it was modified with a dopant to check whether sorption could be improved.

Table 6. Formaldehyde sorption (ppm) for PANI, PPy, and PDMS (exposed to F=10 ppm)

Material	Average sorption values
PANI	2.45 ppm of F
PPy	0.94 ppm of F
PDMS-T	0.58 ppm of F
PDMS-M	0.24 ppm of F

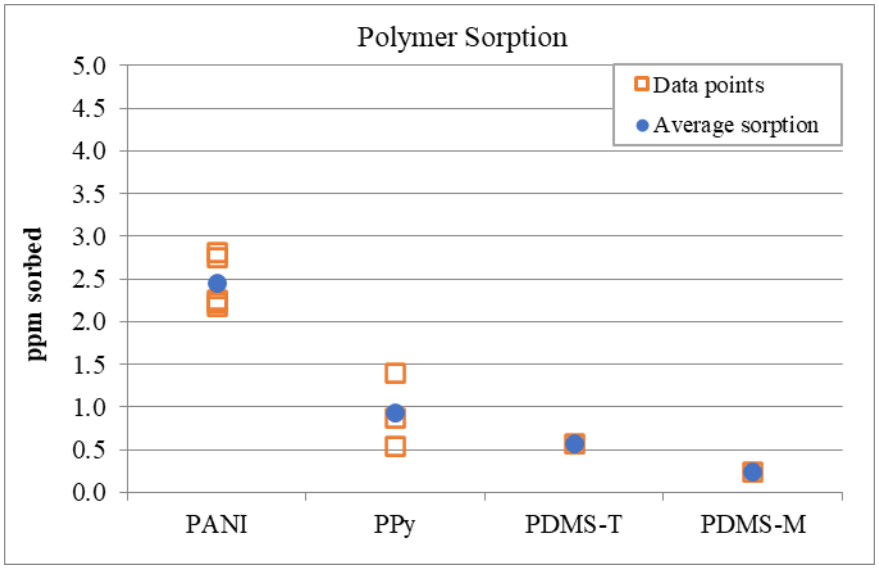

Figure 18. Formaldehyde sorption (ppm) for PANI, PPy, and PDMS (exposed to F=10 ppm)

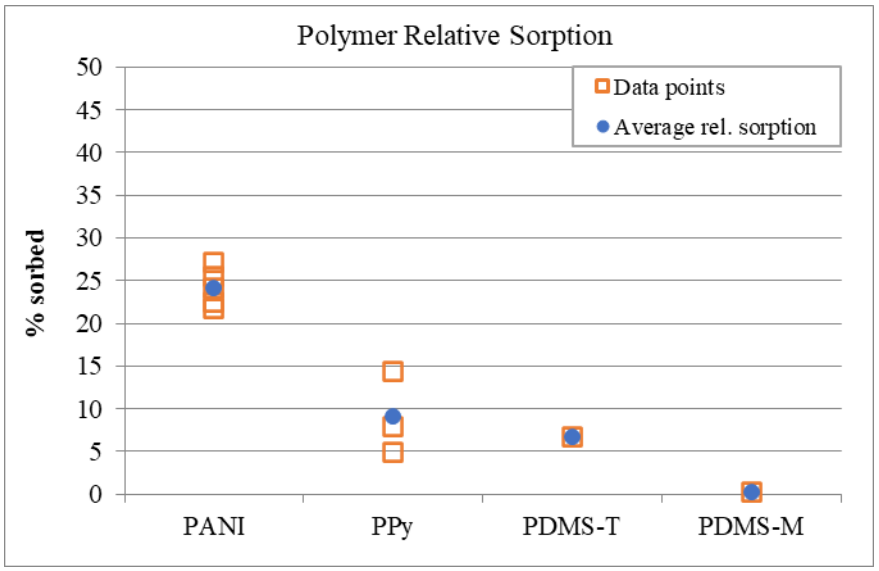

Figure 19. Formaldehyde sorption (relative percentage) for PANI, PPy, and PDMS (exposed to F=10 ppm)

4.1.2 PANI and PANI doped with MO Formaldehyde Sorption

PANI was doped with varying concentrations (weight basis) of metal oxides to investigate whether sorption of the target gas could be enhanced. Note that all sorption tests were independently replicated on different dates.

SnO_2 has been used as a sensing material for methane sensing (see section 2.4.1). As seen in Table 7, PANI 5% SnO_2 had the highest (average) sorption of F out of the three materials. Figure 20 and Figure 21 show the sorption picture for F by PANI and PANI with different SnO_2 concentrations. However, if one calculates 95% confidence intervals (CI) (see Appendix D for calculations), the gas sorption averages are statistically the same (see Table 28 in Appendix E for proof). This means the difference in averages is negligible compared to the error fluctuation of sorption values observed in the sorption test. Based on this observation, 5% was a good SnO_2 concentration to use, if a dopant is to be tested as an alternative sensing material. Between 5% and 10%, the lower MO content is preferred for evident reasons, if the sorption levels are similar.

Table 7. Formaldehyde sorption (ppm) for PANI and PANI doped with SnO_2 (exposed to F=10 ppm)

Material	Average sorption values with SE	95% CI ranges
PANI	2.45 $\pm$ 0.310 ppm of F	2.06, 2.83
PANI 5% SnO_2	2.49 $\pm$ 0.425 ppm of F	1.96, 3.02
PANI 10% SnO_2	2.28 $\pm$ 0.254 ppm of F	1.65, 2.92

Note: The range (denoted as ± (value)) is based on one standard deviation (standard error, SE)

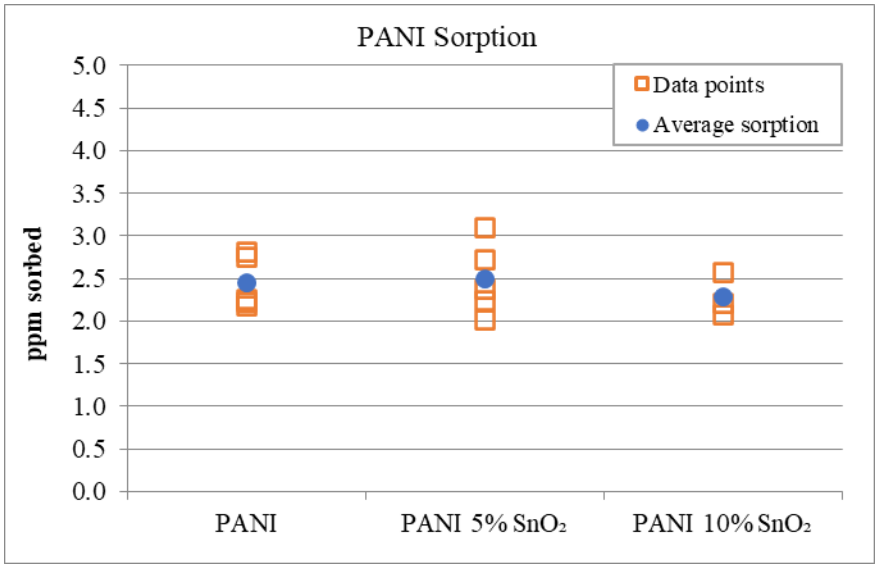

Figure 20. Formaldehyde sorption (ppm) for PANI and PANI doped with SnO_2 (exposed to F=10 ppm)

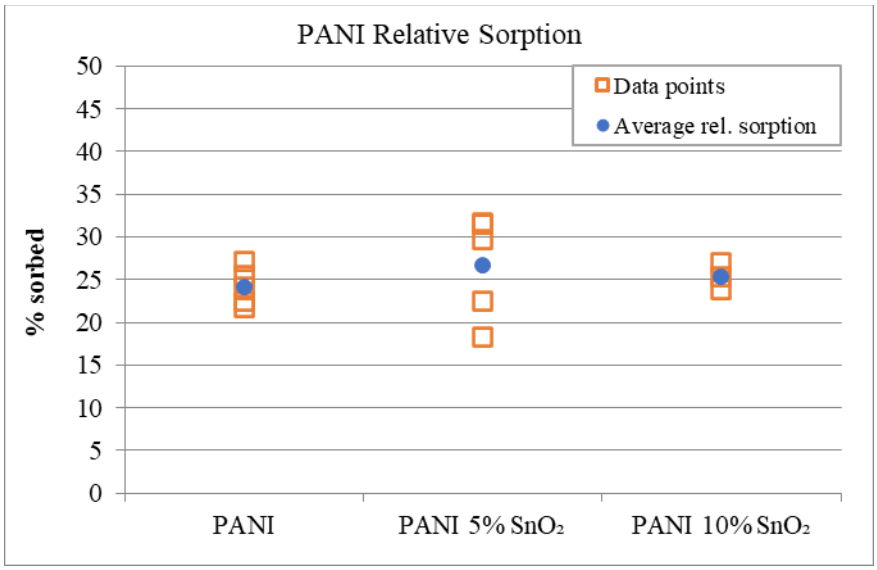

Figure 21. Formaldehyde sorption (relative percentage) for PANI and PANI doped with SnO_2 (exposed to F=10 ppm)

PANI with ZnO was prepared next and tested with F 10ppm source. Table 8, Figure 22 and Figure 23 show the sorption values of PANI and its ZnO-doped variants. PANI-ZnO showed sorption along the same levels as PANI (see Appendix E for statistical analysis). ZnO nanoparticle addition has been observed before to generate "heterogeneities" in the polymer structure at higher concentrations, as it has the tendency to form aggregates [65], hence the poorer sorption of PANI with 5% and 20% ZnO. The interaction between ZnO and PANI will be discussed further in section 4.2.

PANI-2.5% ZnO was the best sensing material in this series with 2.47 ppm sorption from 10 ppm F source. While this is insignificant increase from pristine PANI, the addition of ZnO could make PANI have affinity towards methane. The methane sorption effectiveness of PANI-ZnO was tested in section 4.3.

Table 8. Formaldehyde sorption (ppm) for PANI and PANI doped with ZnO (exposed to F=10 ppm)

Material	Average sorption values with SE	95% CI ranges
PANI	2.45 $\pm$ 0.310 ppm of F	2.06, 2.83
PANI 2.5% ZnO	2.47 $\pm$ 0.199 ppm of F	1.98, 2.97
PANI 5% ZnO	2.02 $\pm$ 0.153 ppm of F	1.64, 2.40
PANI 20% ZnO	2.25 $\pm$ 0.355 ppm of F	1.37, 3.13

Note: The range (denoted as ± (value)) is based on one standard deviation (standard error, SE)

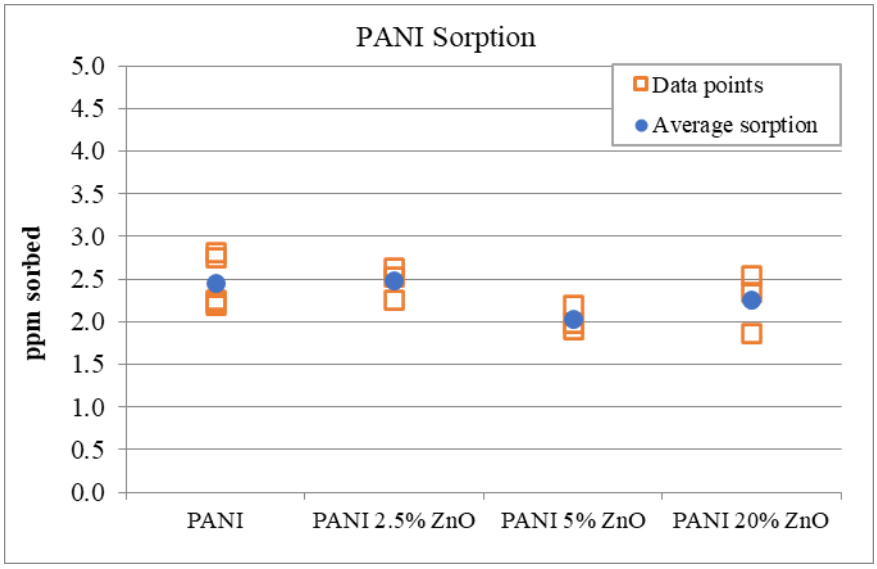

Figure 22. Formaldehyde sorption (ppm) for PANI and PANI doped with ZnO (exposed to F=10ppm)

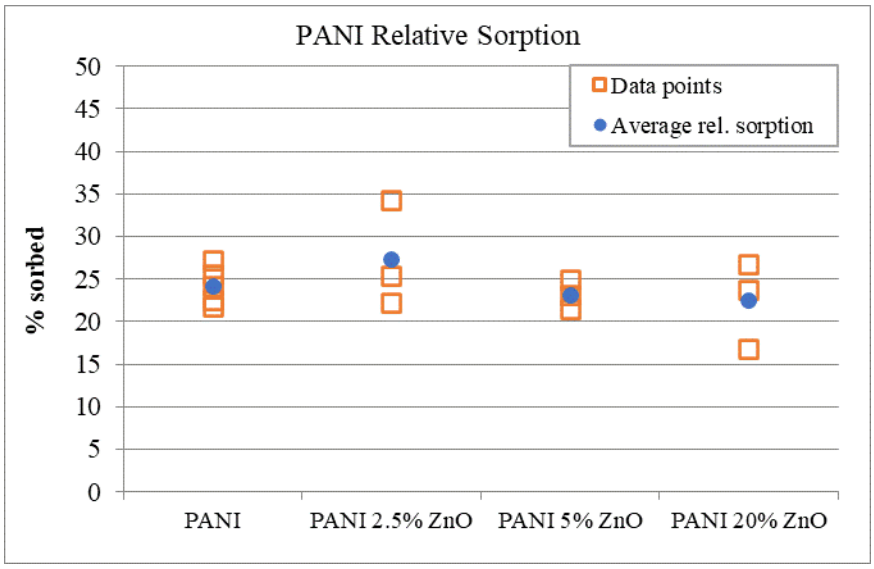

Figure 23. Formaldehyde sorption (relative percentage) for PANI and PANI doped with ZnO (exposed to F=10ppm)

PANI doped with 5% and 20% of titanium oxide (TiO_2) showed reduced sorption of F. As seen in Table 9, the sorption is lower than pristine PANI regardless of the amount of TiO_2 added. While the reduction in sorption is not favorable, it is an indicator that the dopant had a significant effect on changing the properties and morphology of PANI. This is supported by a further reduction in sorption by PANI 20% TiO_2. A more detailed analysis on the effect of TiO_2 on the structure of PANI will be done in section 4.2.

Table 9. Formaldehyde sorption (ppm) for PANI and PANI doped with TiO_2 (exposed to F=10 ppm)

Material	Average sorption values with SE	95% CI ranges
PANI	2.45 $\pm$ 0.310 ppm of F	(2.06, 2.83)
PANI 5% TiO_2	1.84 $\pm$ 0.297 ppm of F	(-0.83, 4.50)
PANI 20% TiO_2	1.76 $\pm$ 0.350 ppm of F	(-1.39, 4.90)

Note: The range (denoted as $\pm$ (value)) is based on one standard deviation (standard error, SE); PANI-TiO_2 includes 0 in the 95% CI range due to a small number of replicated trials

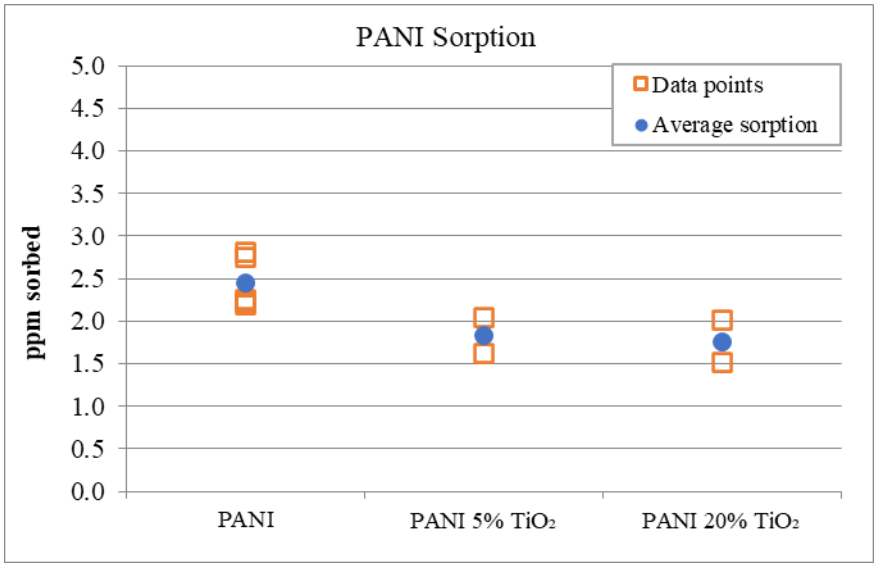

Figure 24. Formaldehyde sorption (ppm) for PANI and PANI doped with TiO_2 (exposed to F=10ppm)

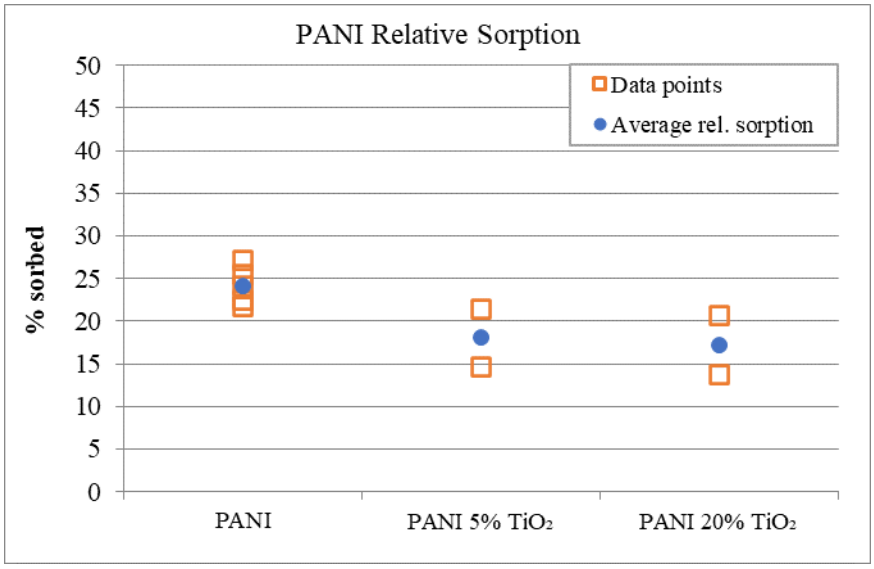

Figure 25. Formaldehyde sorption (relative percentage) for PANI and PANI doped with TiO_2 (exposed to F=10 ppm)

4.1.3 PANI doped with non-MO dopants

Doping PANI with protic acid such as hydrochloric acid (HCl) is known to improve its conductivity by converting it into a PANI salt (see also section 4.2.4). Many literature papers utilize PANI-HCl doped with other materials when testing for resistive gas sensing [24] [25], but they do not test for actual gas sorption. Thus, pristine PANI and PANI-HCl were compared for gas sorption using formaldehyde. In addition, reduction of sorption due to ZnO doping of PANI was theorized to be due to the high surface energy of ZnO nanoparticles [65]. To prevent ZnO aggregation, an emulsifier can be used for better dispersion of the nanoparticles. Therefore, sodium dodecyl sulphate (SDS), a typical emulsifier [25], was tested in parallel.

Figure 26 and Figure 27 along with Table 10 show that no significant improvements were observed during doping PANI with HCl and/or SDS. PANI-HCl had 2.14 ppm sorption, which is a slight decrease in sorption from pristine PANI when it comes to formaldehyde sorption. Although it lacks gas sorption effectiveness, its increased conductivity makes it ideal for resistive sensors. This suggests that PANI can be synthesized using DI water (at neutral pH) to avoid using strong acids during synthesis and reduce production costs, unless conductive PANI is necessary.

PANI-HCl-SDS was also tested for interaction of the two dopants. The sorption of the sample showed negligible difference, which suggests lack of interaction between HCl and SDS. A more significant change can be observed when ZnO and SDS interact below in section 4.1.4.

Table 10. Formaldehyde sorption (ppm) for PANI and PANI with HCl (exposed to F=10 ppm)

Material	Average sorption values with SE	95% CI ranges
PANI	2.45 ± 0.310 ppm of F	2.06, 2.83
PANI-HCl	2.14 ± 0.529 ppm of F	1.30, 2.98
PANI-HCl-SDS	2.11 ± 0.004 ppm of F	2.08, 2.14
PANI-SDS	2.08 ± 0.133 ppm of F	1.75, 2.41

Note: The range (denoted as ± (value)) is based on one standard deviation (standard error, SE)

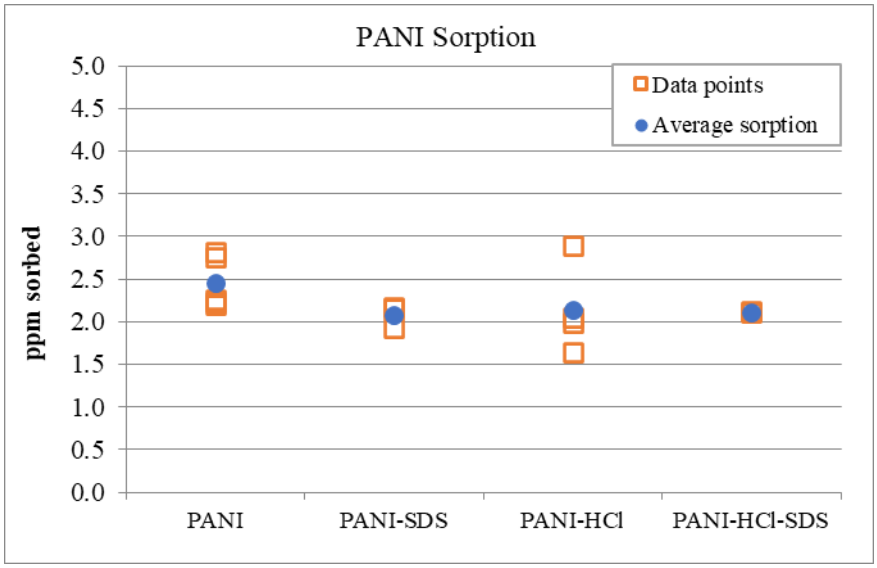

Figure 26. Formaldehyde sorption (ppm) for PANI and PANI doped with SDS (5mM) and HCl (1.1M) (exposed to F=10 ppm)

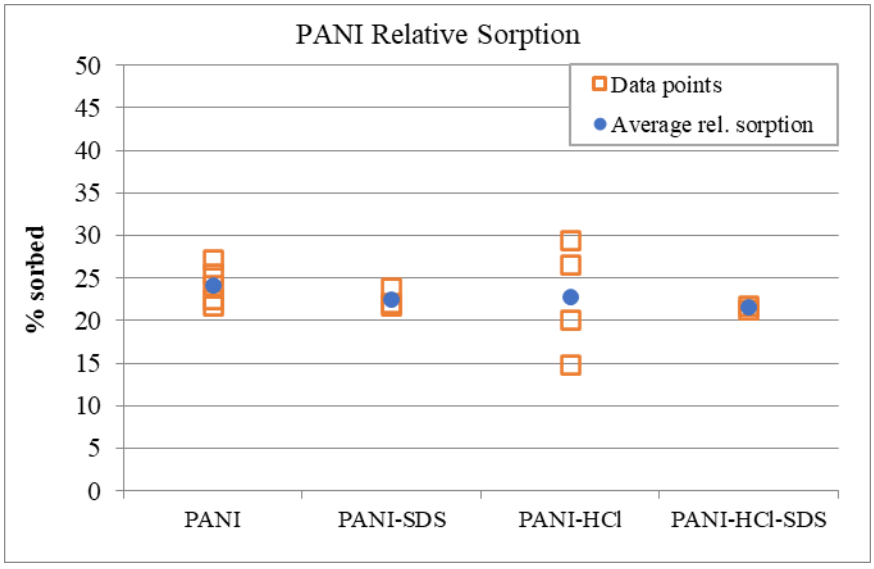

Figure 27. Formaldehyde sorption (relative percentage) for PANI and PANI doped with SDS (5mM) and HCl (1.1M) (exposed to F=10 ppm)

4.1.4 Interaction of MO dopant and non-MO dopant

A separate batch of PANI-ZnO was synthesized with 5mM SDS emulsifier to investigate whether polymerization yield could be improved. Both batches (with and without SDS) were tested for sorption performance.

Table 11 and Figure 28 show results from sorption tests. No considerable enhancements (relative to pristine PANI sorption) were observed. A discussion on morphology of the different materials follows in section 4.2.1.

Table 11. Formaldehyde sorption (ppm) for PANI and PANI doped with ZnO and SDS (exposed to F=10 ppm)

Material	Average sorption values with SE	95% CI ranges
PANI	2.45 ± 0.310 ppm of F	2.06, 2.83
PANI 2.5% ZnO	2.47 ± 0.199 ppm of F	1.98, 2.97
PANI 2.5% ZnO-SDS	2.81 ± 0.791 ppm of F	1.83, 3.79
PANI 5% ZnO	2.02 ± 0.153 ppm of F	1.64, 2.40
PANI 5% ZnO-SDS	2.70 ± 0.639 ppm of F	1.91, 3.50
PANI 20% ZnO	2.25 ± 0.355 ppm of F	1.37, 3.13
PANI-SDS	2.08 ± 0.133 ppm of F	1.75, 2.41

Note: The range (denoted as ± (value)) is based on one standard deviation (standard error, SE)

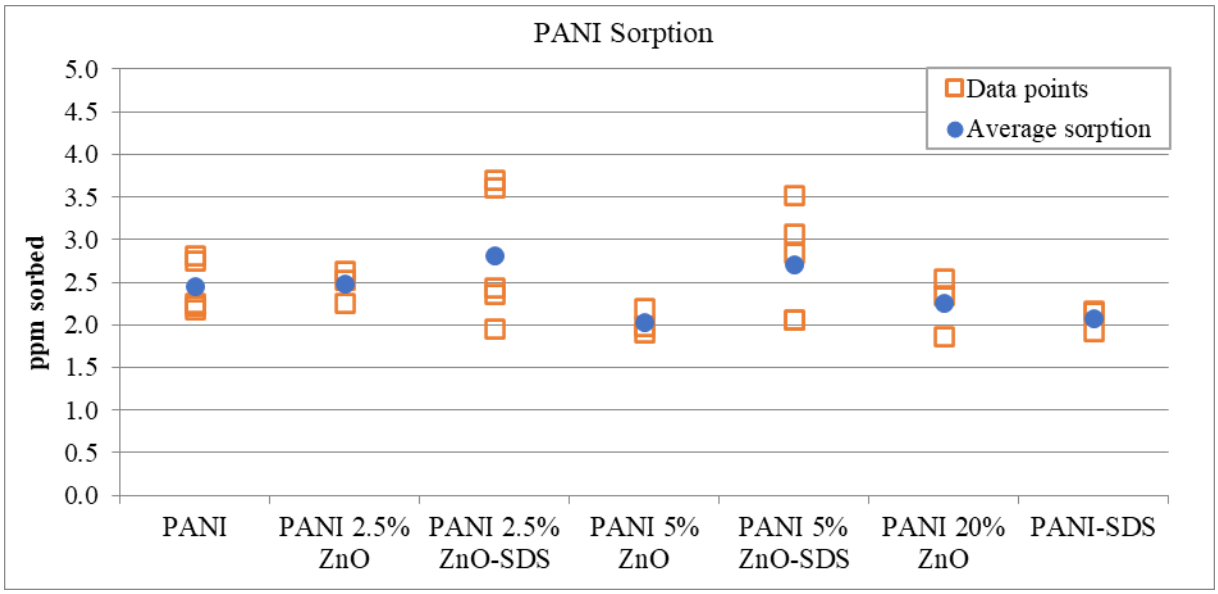

Figure 28. Formaldehyde sorption (ppm) for PANI and PANI-ZnO with SDS (5mM) (exposed to F= 10ppm)

4.2 Material Characterization

4.2.1 Surface Morphology

PANI images were captured using SEM, as seen in Figure 29. The right image (higher magnification) displays the filament-like structures (orange circle) intertwined with amorphous regions (green arrows) filling the space in between. PANI forms nanofibers during polymerization [66]. The non-homogenous structure forms small clusters with high surface area, which is known to improve gas sorption. When PANI is doped with HCl (PANI-HCl) (see Figure 30), the image shows no filaments. It appears as more uniform 'spheres' in clusters and the 'cavities' between successive structures seem more consistent in depth. This could be due to the introduction of an ionic bond between Cl^- and cationic N in the polymer chain. The additional intermolecular attraction force causes closer packing of polymer chains, thus forming a more "repetitive" surface structure. It can be speculated that a cauliflower-like structure will have a larger surface area and improve gas sorption properties than pristine PANI.

When SDS (sodium dodecyl sulfate) was used in the PANI synthesis (hereby called PANI-SDS), the structure of the polymer is almost like that of PANI (see Figure 29 vs Figure 31). PANI-SDS has filaments in clusters like PANI with amorphous patches in between (Figure 31). Under the higher magnification of Figure 32, there is an apparent difference in the thickness of the filaments and length of the clusters. PANI has larger filaments than PANI-SDS, likely due to the emulsification effect of SDS in the water/aniline monomer mixture allowing for participation of more polymer molecules to form in clusters at the same time.

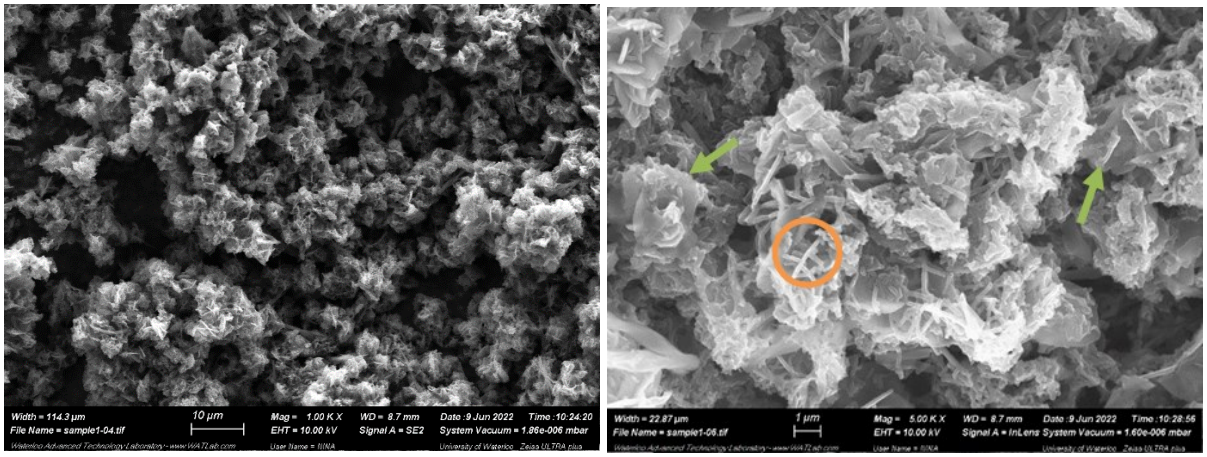

Figure 29. SEM image of PANI at 1000x (left) and 5000x (right) magnification; Filaments (orange circle) and amorphous regions (green arrows)

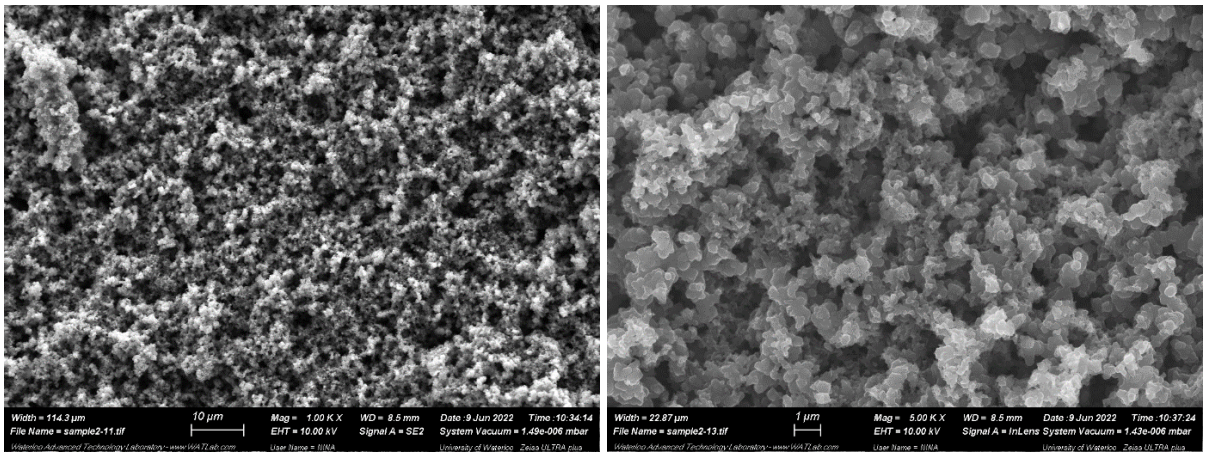

Figure 30. SEM image of PANI-HCl at 1000x (left) and 5000x (right) magnification

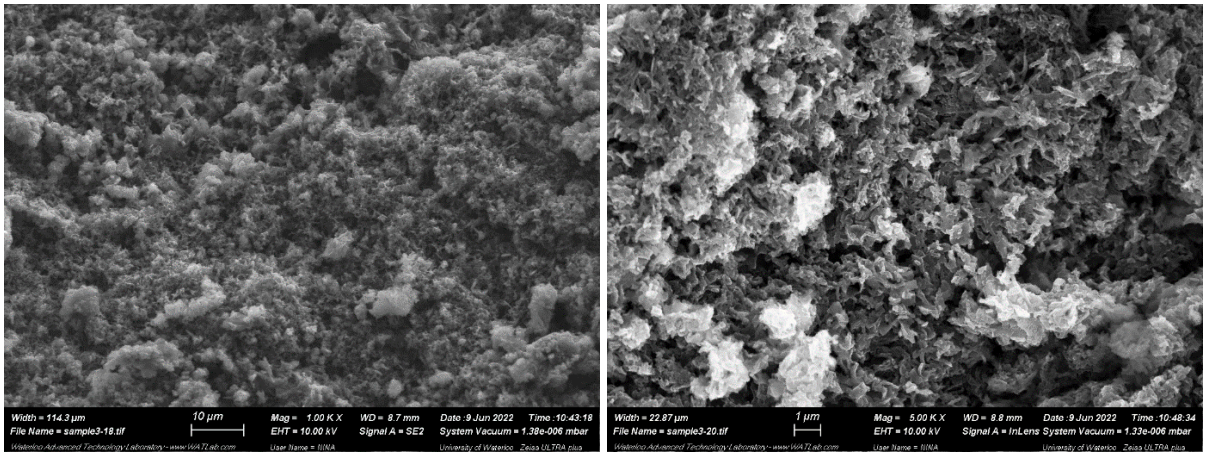

Figure 31. SEM image of PANI-SDS at 1000x (left) and 5000x (right) magnification

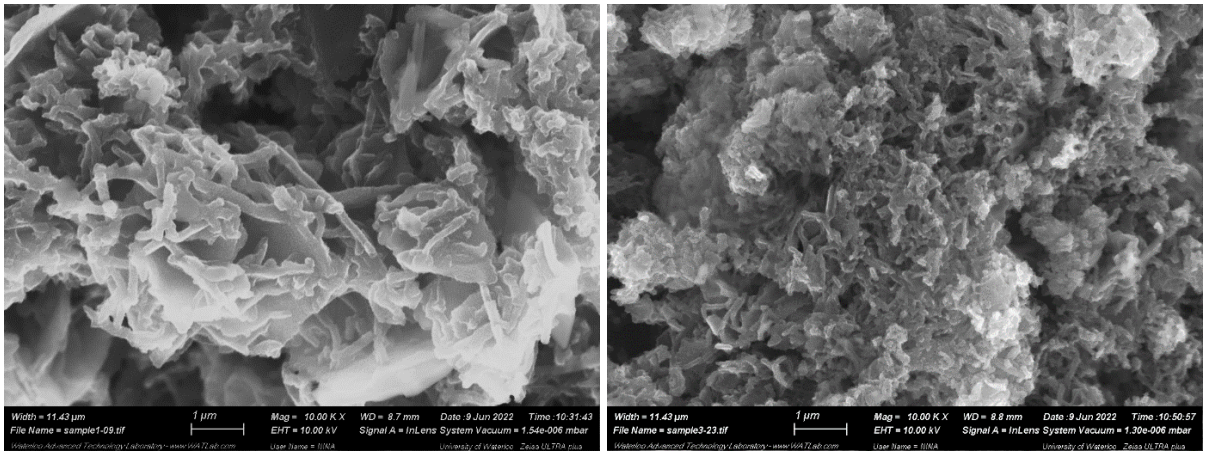

Figure 32. SEM image of PANI (left) and PANI-SDS (right) at 10000x magnification

Figure 33 to Figure 35 show how adding a metal oxide dopant (zinc oxide, ZnO) in the polymer affects its structure. For PANI with 2.5% and 5% ZnO, there are aggregates in spherical 'pockets' that were not observed in other PANI samples. For PANI-ZnO with SDS, the pockets are not found, and the surface looks more homogenous with respect to structural characteristic (see Figure 36). The varying surface structure is evident in Figure 34, which shows different sections of the sample at 10000x magnification. One can see different regions; a structure like undoped PANI (Figure 34, right) and one containing shorter filaments and 'spheres' (Figure 34, left). This could be likely due to incomplete mixing of dopant and monomer as such effect was not found in the sample with SDS and ZnO together (Figure 36 and Figure 37).

As seen in Figure 36, the addition of SDS in the formulation of PANI-5% ZnO improved the uniformity of the structure. There are shorter filaments observed compared to pristine PANI. As observed earlier with PANI-SDS, the presence of SDS affects the formation of PANI filaments and its overall surface structure. This affects the gas sorption property of PANI via increased surface area for PANI-analyte contact. When SDS was added to make PANI with ZnO, the average sorption increased from 2.02 to 2.25 ppm and 2.47~2.80 ppm (see Table 11). This is a notable trend since adding ZnO alone reduced sorption of F. Unfortunately, experimental noise was also higher with the SDS addition, so it is not possible to discriminate different effects reliably.

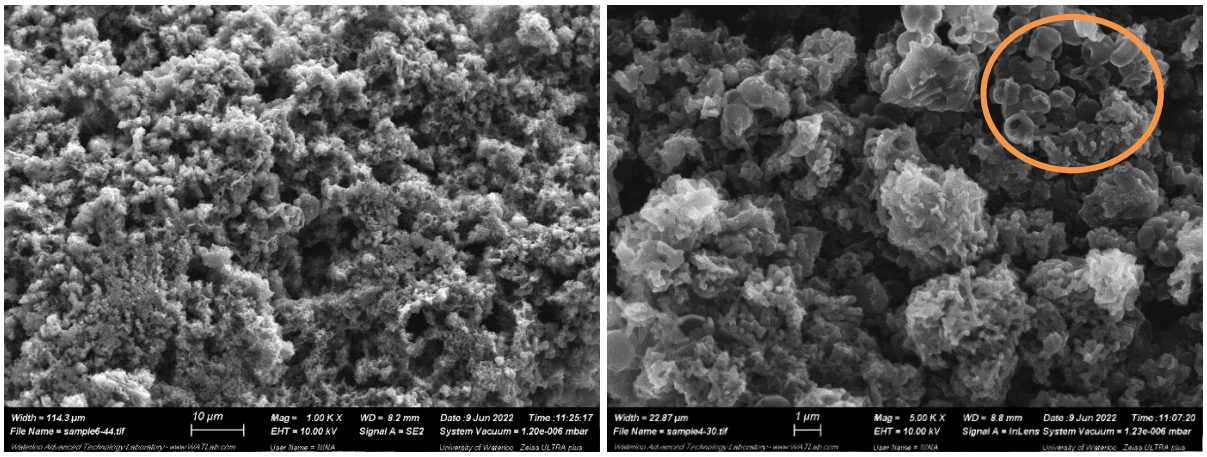

Figure 33. SEM image of PANI-5% ZnO at 1000x (left) and 5000x (right) magnification; orange circle highlights distinct spherical pocket unique to PANI with ZnO.

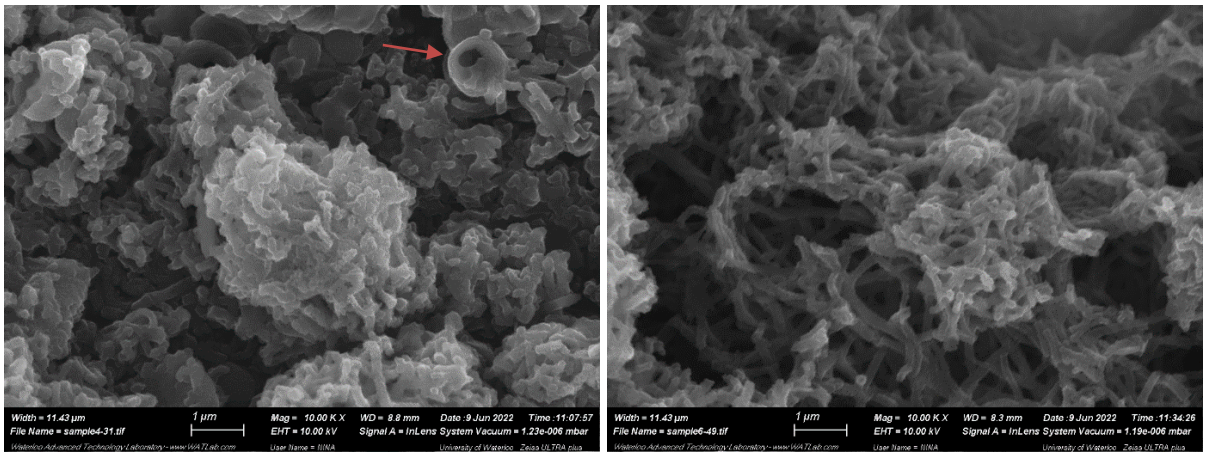

Figure 34. SEM image of PANI-5% ZnO at 10000x magnification of different sections; spherical pockets (red arrow) found in the left picture

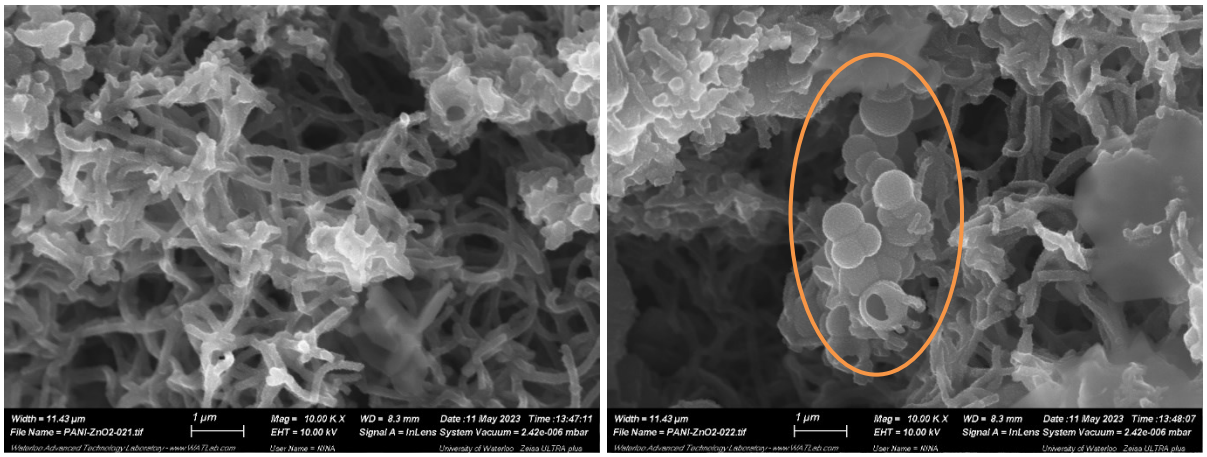

Figure 35. SEM image of PANI-2.5% ZnO at 10000x magnification of different sections; spherical pockets (orange circle) found in the right picture

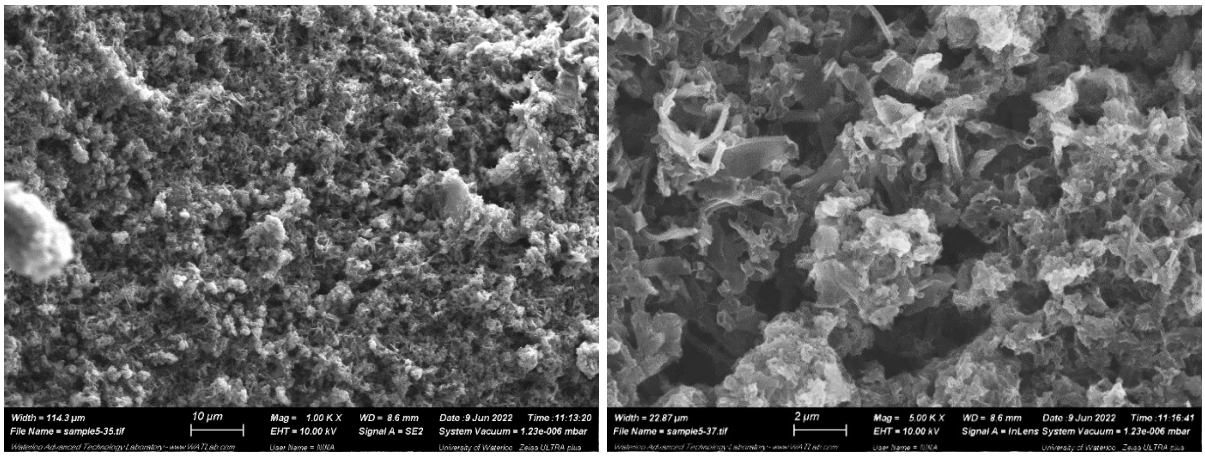

Figure 36. SEM image of PANI-5% ZnO-SDS at 1000x (left) and 5000x (right) magnification

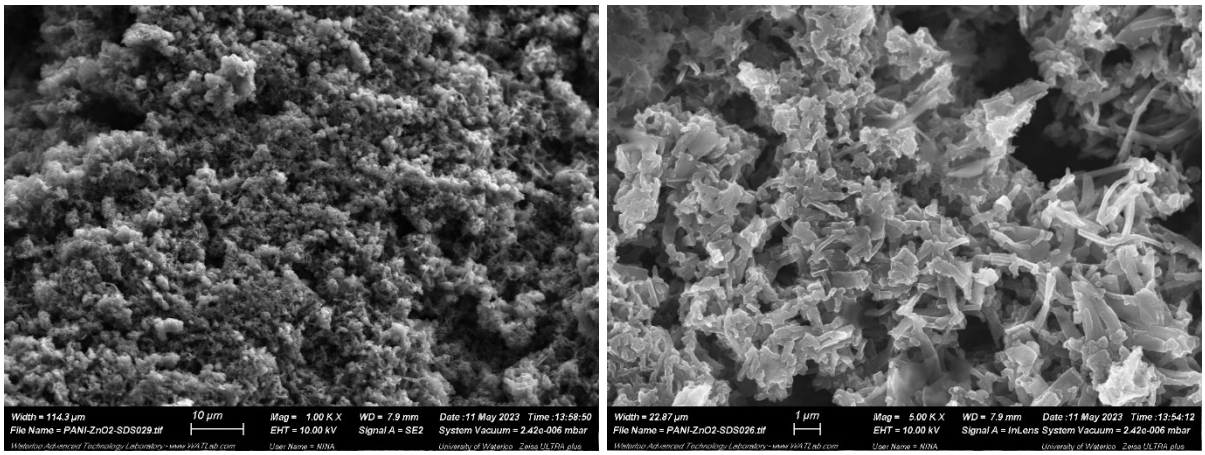

Figure 37. SEM image of PANI-2.5% ZnO-SDS at 1000x (left) and 5000x (right) magnification

PANI-5% SnO_2 had great incorporation of dopant (see Table 7) and the surface imaging shows lighter specks (see Figure 38). These are speculated (since the particle size of SnO_2 is ≤100 nm) as brighter spots indicating either the section having higher atomic number or protruded surface [67]. More on a quantitative measure of dopant incorporation will follow in section 4.2.2. The overall morphology of the material (Figure 38) is reminiscent of pristine PANI with short filaments and amorphous regions.

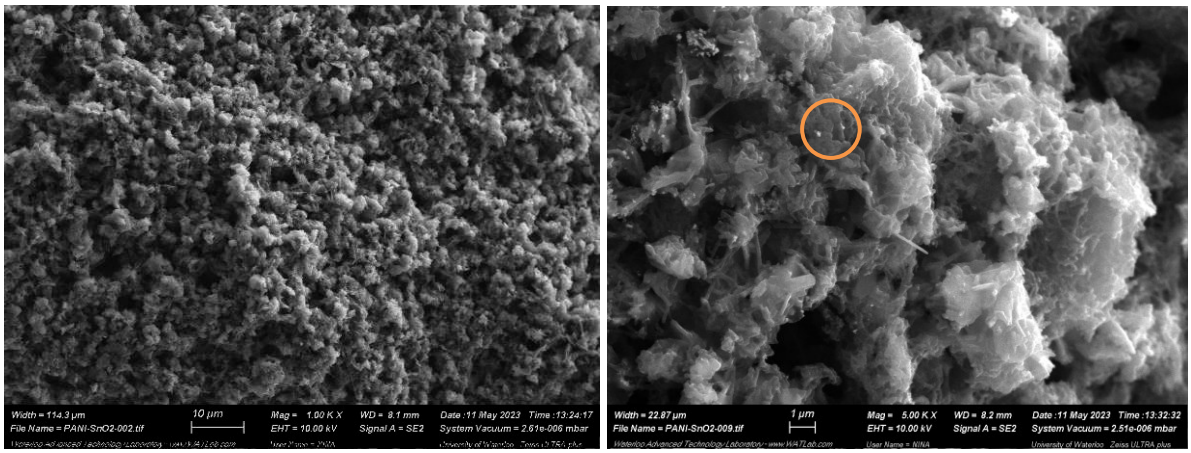

Figure 38. SEM image of PANI-5% SnO_2 at 1000x (left) and 5000x (right) magnification; orange circle highlights SnO_2 embedded in the polymer matrix

When PANI is doped with TiO_2, certain structures were clustered and became less uniform. Two different sections of the sample were analyzed using EDX (see Table 12) and found to contain 2.87% and 4.59% of Ti, proving that there is uneven distribution of TiO_2 dopant. This heterogenous nature can also be observed in the SEM images that follow.

Figure 39 shows distinct rectangular prisms embedded in an amalgam of filaments present in proximity to each other. When one of the prisms was randomly selected and analyzed, it had 3.10% Ti content (measured with EDX) which is higher than the area average of 2.87%, but lower than the expected amount of 5% (amount added during synthesis), so it is speculated that TiO_2 was enclosed in PANI and formed rectangular prisms. In Figure 40, the surface contains a matrix of fibers like that of pristine PANI without distinct prisms, possibly due to a lack of TiO_2 on the surface. This explains the poor gas

sorption (see section 4.1.2) as encased TiO_2 means lack of contact with the analyte, and reduced surface area for sorption.

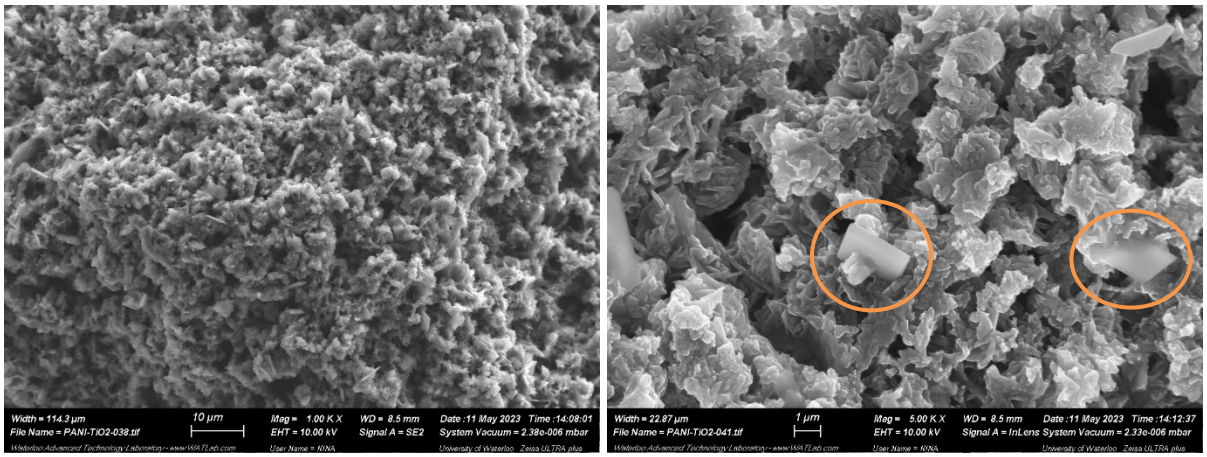

Figure 39. SEM image of PANI-5% TiO_2 at 1000x (left) and 5000x (right) magnification; orange circles highlight square plate-like structure unique to the sample

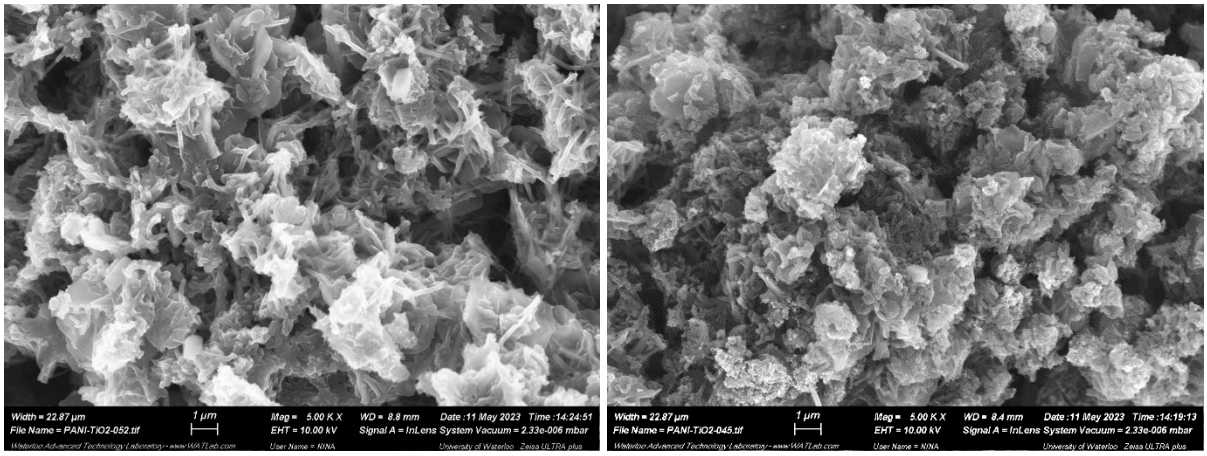

Figure 40. SEM image of PANI-5% TiO_2 at 5000x magnification of different areas

4.2.2 Dopant Incorporation

Table 12 and Table 13 show the summary of EDX analysis of the samples. The compositions of the major elements for the polymer chains (C, N, O, and S) are similar for all the samples, so it can be speculated that PANIs (regardless of addition of dopants) have similar molecular weights. The incorporation of a dopant (basically, the dispersion of MO within the polymer matrix during in-situ polymerization) would be considered successful if a significant fraction of the characteristic element is detected. According to the chemical formula, polyaniline would have a C:N molar ratio of 6:1. The initiator ammonium persulfate (APS) adds sulfate groups at each end of polyaniline, thus the molar ratio of O:S should be 4:1. However, metal oxides (dopants) could also contribute to increased oxygen due to the inherent presence of O atoms.

Table 14 cites the molar ratios based on EDX measurements. The C:N ratios fluctuate around 6:1, with an average value of 6.5:1, which is very close to the theoretical (expected) value. The average O:S ratio is close to 5.8:1, higher than the theoretical one. These values can easily be explained based on the error

inherent in EDX determinations. EDX gives a measure based on the specific (localized) spot of the specimen surface area, not of the whole sample. Therefore, the measurement will be affected by heterogeneities in the distribution of a specific element, especially of a metal oxide (and by how embedded the specific element is in the bulk of the polymer). The solution to this would be multiple measurements per SEM image (at different spots), but this can become time-consuming and eventually rather expensive.

For PANI-HCl, the polymerization was performed in a 1.1M HCl solution (~50 mL) and resulted in 1.69% of Cl element in the sample. Considering the structure of PANI emeraldine salt (PANI-ES), the theoretical ratio of Cl/N is 1.00 at maximum incorporation of Cl ion (see Figure 11). However, the literature shows that the typical ratio is 0.440 or even lower [68]. Comparing this to the experimental Cl/N ratio of 0.13, the incorporation of Cl^- has low efficiency despite having an excess amount of HCl in the reaction. While the ratio is not optimal, it is sufficient to make a significant difference in the structure and composition of the synthesized PANI, as observed in Section 4.2.1.

Both PANI-5% SnO_2 and PANI-5% TiO_2 had good incorporation of dopants with % loss of only 0.14% and 0.41%, respectively. These samples showed high stability in synthesis. It is notable that TiO_2 showed fluctuations of Ti content between 2.87 wt.%~4.59 wt.%

For PANI-5% ZnO, there is no significant amount of Zn found on the surface of the sample. This could be due to one of two reasons: (a) No ZnO was incorporated into PANI; (b) ZnO particles are somehow encased by PANI and thus the presence of ZnO could not be detected on the surface. Adding SDS in the polymerization of PANI-5% ZnO seemed to improve the incorporation of the dopant to 0.97 wt.%. However, the experimental error for zinc detection is greater than the measured value, thus it is uncertain whether a significant amount of zinc oxide was incorporated into PANI. The same behaviour is observed with PANI 2.5% ZnO, which suggests that ZnO is a poor dopant for PANI, as alluded to earlier as well. This can explain the negligible change in sorption for PANI-5% ZnO (see Table 11).

Table 12. EDX analysis of PANI with different dopants in mass %

Sample name	Carbon	Nitrogen	Oxygen	Sulfur	Tin	Titanium
PANI	65.78 ±6.67	10.54 ±18.35	17.46 ±11.83	6.22 ±8.48	-	-
PANI-5% SnO_2	62.82 ±6.97	8.20 ±19.86	17.26 ±11.71	6.86 ±7.15	4.86 ±37.62	-
PANI-5% TiO_2	60.76 ±7.14	11.55 ±17.44	16.01 ±12.14	7.10 ±5.45	-	4.59 ±19.96
Sample name	**Carbon**	**Nitrogen**	**Oxygen**	**Sulfur**	**Chlorine**	**Zinc**
PANI-2.5% ZnO	61.74 ±7.10	11.20 ±15.74	19.46 ±10.97	7.13 ±5.02	-	0.46 ± 21.32
PANI-2.5% ZnO-SDS	62.15 ±6.19	9.99 ±15.36	22.55 ±10.75	4.60 ±6.43	-	0.70 ± 24.71
PANI-5% ZnO	62.26 ±6.56	12.80 ±14.71	18.61 ±10.77	6.23 ±5.47	-	0.10 ±67.99
PANI-5% ZnO-SDS	60.65 ±7.29	11.78 ±14.91	18.56 ±10.75	8.05 ±4.82	-	0.97 ± 22.46
PANI-HCl	62.12 ±7.95	13.24 ±14.88	14.21 ±11.81	6.05 ±5.58	4.38 ±9.36	-
PANI-SDS	61.55 ±6.30	13.58 ±14.07	19.15 ±10.52	5.72 ±4.84	-	-

Table 13. EDX analysis of PANI with different dopants in mole %

Sample name	Carbon	Nitrogen	Oxygen	Sulfur	Tin	Titanium
PANI	72.88	10.02	14.52	2.58	-	-
PANI-5% SnO_2	73.16	8.19	15.09	2.99	0.57	-
PANI-5% TiO_2	70.25	11.45	13.90	3.07	-	1.33
Sample name	**Carbon**	**Nitrogen**	**Oxygen**	**Sulfur**	**Chlorine**	**Zinc**
PANI-2.5% ZnO	69.60	10.82	16.47	3.01	-	0.10
PANI-2.5% ZnO-SDS	69.44	9.57	18.92	1.93	-	0.14
PANI-5% ZnO	69.52	12.26	15.60	2.60	-	0.02
PANI-5% ZnO-SDS	69.02	11.50	15.85	3.43	-	0.20
PANI-HCl	70.68	12.92	12.14	2.58	1.69	-
PANI-SDS	68.60	12.98	16.02	2.39	-	-

Table 14. Elemental ratios of PANI with different dopants

Sample name	C/N	O/S	Cl/N
PANI	7.27	5.63	-
PANI-5% SnO_2	8.93	5.05	-
PANI-5% TiO_2	6.14	4.53	-
PANI-2.5% ZnO	6.43	5.47	-
PANI-2.5% ZnO-SDS	7.26	9.80	-
PANI-5% ZnO	5.67	6.00	-
PANI-5% ZnO-SDS	6.00	4.62	-
PANI-HCl	5.47	4.71	0.13
PANI-SDS	5.29	6.70	-

4.2.3 Crystallinity

As described in Section 3.4.2, the crystallinity of polymer samples is analyzed using XRD. The intensity of diffracted X-rays at angle of diffraction, 2θ, is plotted in Figure 41 and Figure 43. The plots show a combination of sharp peaks (crystalline) and hills (amorphous) The peaks represent a different crystal lattice and atomic arrangement in the material and each peak angle corresponds to one Miller index. Miller index is a notation system used in crystallography for describing lattice planes in a crystal. While this is not exactly in the scope of this research, it is worth comparing the index (peaks) with reference data.

Comparing with experimental results from the literature [69] in Figure 42, the synthesized PANI shows a similar pattern of three peaks with the middle being the highest and right-most peak being the shortest. In Figure 41, the peaks do not occur at the same angle as in the literature, likely due to misalignment of the sample. However, the plot can be shifted by the same fixed distance in the x-axis direction to match the experimental data for comparison. For instance, the spectrum data points from the literature in Figure 42 were shifted by 8 degrees to the left (typical error due to slight misalignments) and the intensity scale was multiplied by a factor of 100 for this purpose (as intensity scales are arbitrary). Comparing with previously reported cases [70], the synthesized PANI matches the crystalline lattice of emeraldine base which is the expected product based on the synthesis method used [68].

PANI and PANI-HCl have identical peaks with both incident angle and signal intensity, indicating similarity in both crystal lattices and crystallinity. PANI-SDS also shows peaks at the same angle (crystalline structure) but at a slightly lower intensity. This could be due to the different ratio of crystal lattices and overall lower crystallinity of the sample.

In Figure 41, all three samples showed nearly identical incident angle at around 14.1°, 17.0°, 18.6°, and 25.6°. The crystallinity index is calculated based on the peak intensity compared to the amorphous region signal [71] (see Appendix F for details). The crystallinity index of PANI and PANI-HCl is 72%, which is higher than typical semi-crystalline PANI of ~40% [16]. This is due to a lower polymerization temperature used during synthesis; a slower temperature results in higher crystallinity [72].

The crystallinity index decreased to 67% for PANI-SDS, which indicates that addition of the emulsifier influenced the structure of the polymer as seen in SEM images (Section 4.2.1). However, PANI-SDS

is also semi-crystalline with peaks at the same angles as the other samples. The overall reduction of filament dimensions (see Figure 32) and XRD results imply that SDS led to better emulsification of aniline; this would have improved the initial rate of conversion of monomer but lowered the molecular weight while increasing the rate of monomer consumption. This is observed in the PANI yield (see Table 15), where addition of SDS increased the % yield or conversion of monomer to polymer by 1.5~3.1%. While this is not the most accurate indicator of monomer conversion, the trend is significant, as it supports the experimental observations.

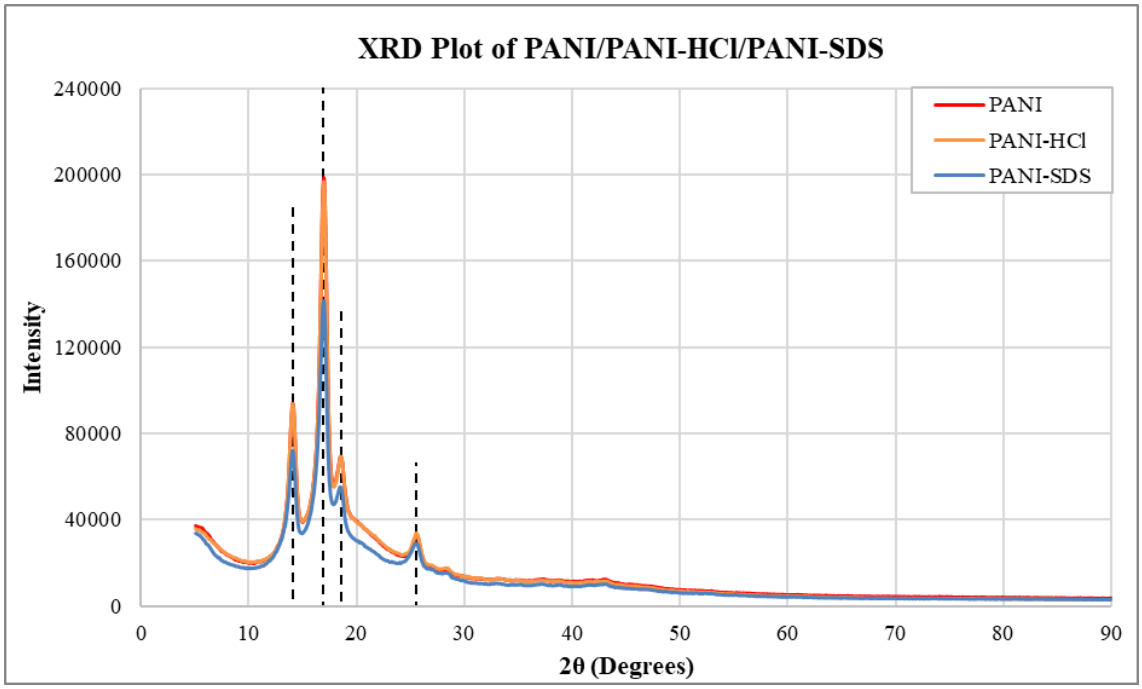

Figure 41. XRD plot of PANI, PANI-HCl, PANI-SDS; the numbers around the peaks are corresponding peak angles (the vertical dashed lines are indicative of the peaks, for easier visual identification)

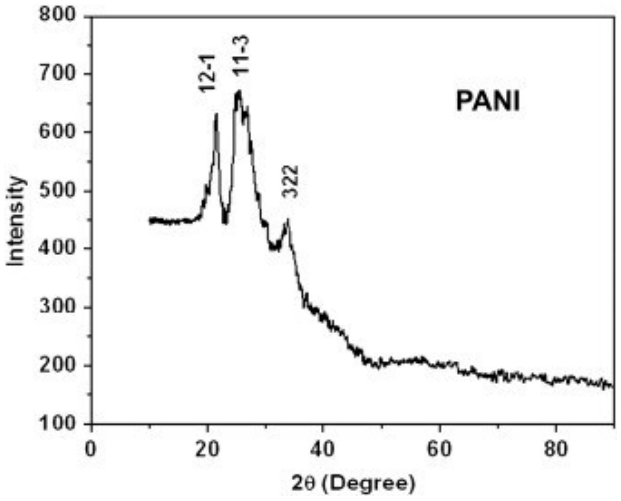

Figure 42. X-ray diffraction plot of polyaniline (PANI); the numbers around the peaks indicate hkl values or crystal planes (Miller index) corresponding to the peaks (reproduced with permission from [69])

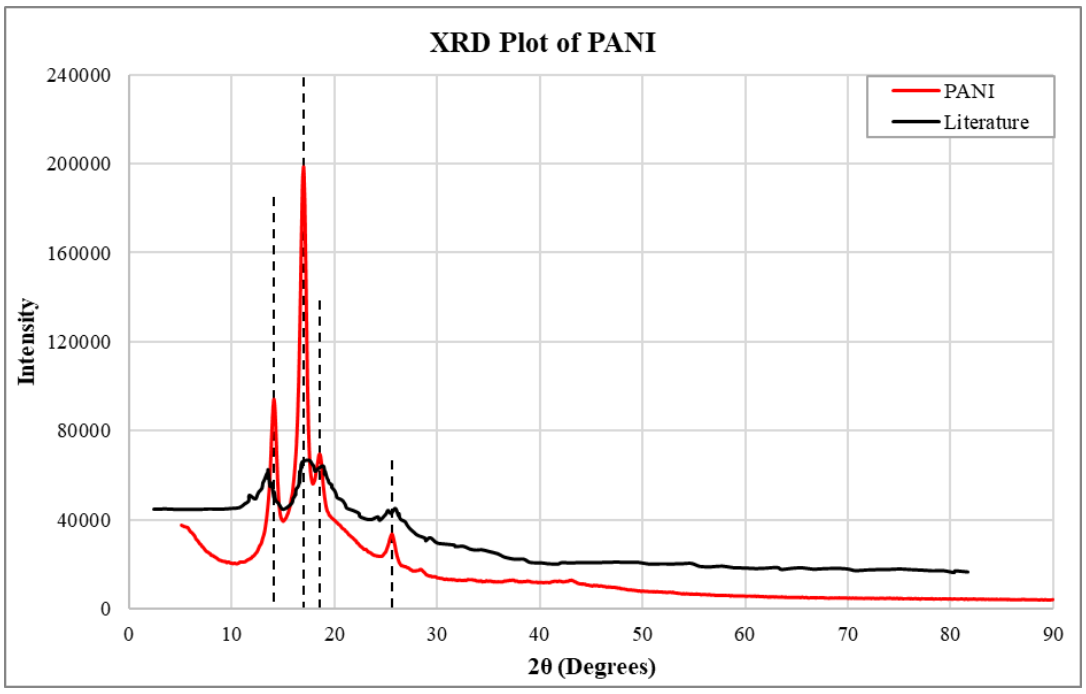

Figure 43. XRD plot comparison of literature values (reproduced with permission from [69]) and experimental data (the vertical dashed lines indicate the peaks, for easier visual identification)

Table 15. Table of PANI with SDS synthesis yield (monomer conversion basis)

Sample	Yield%	Sample	Yield%
PANI-5%ZnO	86%	PANI-2.5% ZnO	89.0%
PANI-5% ZnO-SDS	90.9%	PANI-2.5% ZnO-SDS	90.5%
PANI	81%	PANI-HCl	95.1% (90.9%[1])
PANI-SDS	83.5%	PANI-HCl-SDS	96.2% (92.0%[1])

[1] Assuming theoretical maximum incorporation of Cl into PANI, Cl takes up 4.38w/w% of the total material mass; when this is excluded, the yield is lower

4.2.4 Oxidation States of PANI

The UV-Vis absorbance spectra of PANI synthesized in DI water, 1.0M HCl and 0.05mM SDS are compared in Figure 44 (see also [63]). Each sample underwent independent replication with identical results. All the samples show one peak in the range of 300 nm-425 nm and another in the range 500 nm-725 nm with small variations in the local maxima and intensity. The peak wavelengths are summarized in Table 16.

According to Albuquerque et al. [61], both oxidized and reduced PANI show a peak around 350 nm (due to π-π* transition) due to the C=C bond present in the benzene ring. When PANI is oxidized, the n-π* transition shows as the peak around 600 nm. If the sample is further reduced, the intensity of the 620 nm peak is diminished, while oxidation causes a shift of the corresponding peak towards 550 nm. Comparing the peaks in Figure 45 shows that the samples are emeraldine PANI of varying y. PANI and PANI-SDS have two peaks with similar intensity and wavelengths. This confirms that addition of SDS does not affect the oxidation state of PANI.

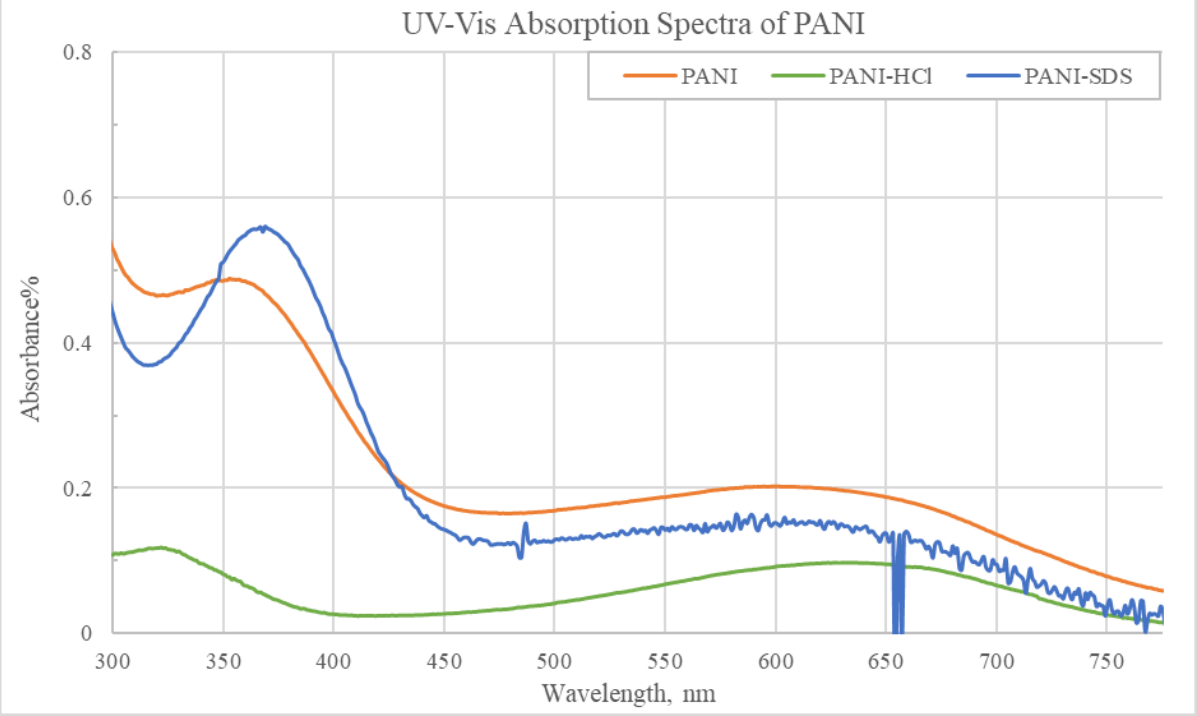

Figure 44. UV-Vis absorption spectra of PANI and doped PANIs (see [63])

Table 16. UV-Vis spectra peaks for PANI samples

Sample	Peak 1 wavelength (nm)	Peak 2 wavelength (nm)
PANI	350	600
PANI-HCl	325	625
PANI-SDS	370	600

In order to identify oxidation states, the PANI sample intensity was amplified for comparison with the literature data [61] for y=0.5, 0.55 and 0.9 (see Figure 45). This comparison is possible as the intensity of the signal is dependent on the concentration of sample solution. Compared to y=0.5 (EB), the PANI sample has a slight left shift of peak 2 and higher absorbance for peak 1. Since peak 2 shifts to the left as EB is oxidized and considering the absorbance difference in peak 1 and peak 2, the PANI sample oxidation state is estimated to be between 0.5 and 0.55. Similar data shifting and comparison were done with PANI-HCl and plotted with the literature data in Figure 46. The peaks overlap at identical wavelengths with y=0.5. This confirms that PANI-HCl is emeraldine, as expected.

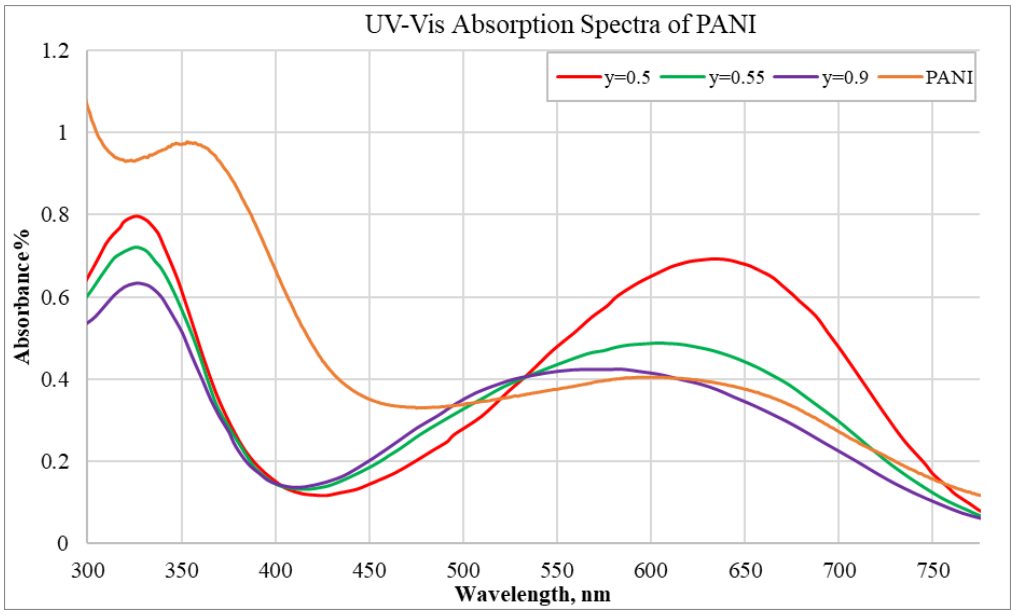

Figure 45. UV-Vis absorption spectra comparison between experimental PANI and literature data for PANI [61]

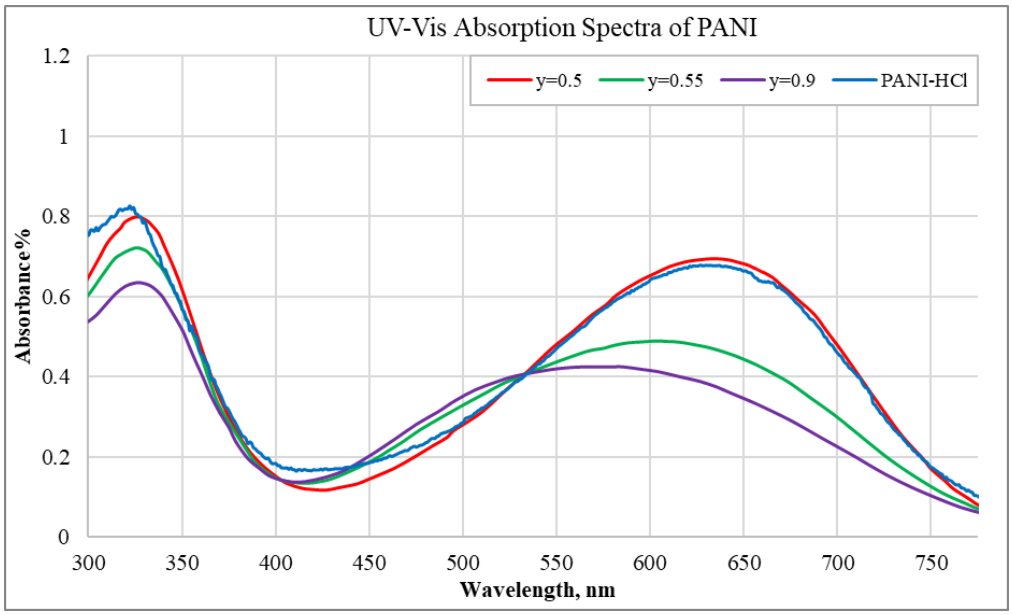

Figure 46. UV-Vis absorption spectra comparison between experimental PANI-HCl and literature data for PANI [61]

4.3 MEMS Sensor Testing for Methane

The most promising synthesized sensing materials for methane were made available to our MEMS sensor collaborators in Systems Design Engineering for the final testing of the actual MEMS sensor. The testing for methane took place successfully (as described below) but the setup developed issues after methane testing, and hence there were delays that made the reporting of the ammonia testing not possible in the time frames of this thesis. Some of the suggested materials failed to stay adhered to the sensor surface. For PDMS, the liquid state lacked surface tension to remain on the sensor. For the powder materials, those with a lower amount of metal oxide had enough physical integrity for testing. The list of sensing materials deposited and tested can be found in Table 17.

When the functionalized sensor was exposed to 50 ppm methane, a significant frequency shift was observed (see Table 18). A larger shift indicates higher sorption of gas and a larger sensor signal. Therefore, when exposed to the identical concentration of target gas, PANI 5% ZnO sorbed the most gas out of the three samples. This represents a very successful evaluation of possible sensing materials and ultimate confirmation with the actual MEMS platform.

Table 17. List of gas sensing materials for MEMS sensor application

Methane Test	
Sample	Adhesion to sensor
PANI 5% SnO_2	yes
PANI 5% ZnO	yes
PANI 5% ZnO-SDS	yes
PANI 10% SnO_2	X
PANI-HCl	X
PDMS M	X
PDMS T	X

Table 18. MEMS sensor response to 50 ppm methane for different sensing materials

Sample	Frequency shift (Hz)
PANI 5% SnO_2	48
PANI 5% ZnO	100
PANI 5% ZnO-SDS	77

4.4 Mechanistic Explanations

The paper by Stewart and Penlidis [73] gives a detailed overview of possible mechanisms that govern the interactions between sensing materials and analytes.

With respect to methane sorption, a typical non-polar hydrocarbon, a possible mechanism for sorption is as follows. Firstly, due to its lack of polarity, the molecular attraction between sensing material and analyte occurs by weak van der Waals forces. The porosity of PANI material promotes gas sorption via increasing surface area, which enhances the diffusion rate of analyte.

In addition, the interaction between PANI and analyte arises from the conjugated polymer's unique behaviour. PANI is a p-type semiconductor where the electron holes drive conduction. The MO dopants used for PANI are n-type semiconductors, which have excess electrons. When the two types of semiconductors are in contact, the charge carriers (electron holes and electrons) diffuse out and form a charge gradient (depletion region) at the boundary. It is suggested that reduces the activation energy for physisorption of methane [21]. Also, sensors utilizing p-n junction have shown higher sensitivity and selectivity than sensors that utilize only one type of semiconductor [74].

The reader can also consult reference [75] for the mechanism of methane detection by MO, which is also possible when MO is embedded into PANI.

Chapter 5 Concluding Remarks, Contributions, and Future Recommendations

5.1 Concluding Remarks

PANI 2.5% ZnO-SDS was the best sensing material for 10ppm F sorption with slightly higher average sorption than its undoped counterpart. The addition of SDS seemed to make the zinc oxide incorporation more homogeneous (although it did not affect sorption much).

When tested with MEMS sensor for sensitivity towards 50ppm methane, PANI-5% ZnO had the largest shift in frequency (largest signal). It is worth noting that doping with ZnO and SDS improved sorption for both formaldehyde and methane (despite the small level of dopant incorporation).

Overall, this thesis represents a successful sensing material evaluation, from polymer synthesis all the way to actual MEMS sensor testing.

5.2 Contributions

The thesis main contributions are:

1) Successful use of literature information, synthesis, and characterization of possible sensing materials; sorption properties evaluated in ppm of actual analyte sorption (instead of resistance values, which are not calibrated versus actual ppm levels); more testing of sensing materials (and hence, more data collection) for formaldehyde sorption.

2) Successful testing and demonstration of the actual MEMS sensor for methane, a typical GHG, at 50 ppm and room temperature (roughly in the 22-25℃ range, as opposed to the currently used 300-400℃).

5.3 Future Recommendations

5.3.1 Short-term Recommendations

From Section 4.1.4, further investigation of ZnO-SDS interaction effects on PANI sorption is in order. Reduction of SDS concentration from 5mM to 2mM could improve sensing material performance.

Testing the MEMS sensor with the most promising sensing materials (Section 2.4.2) for ammonia detection will be an immediate extension. In fact, ammonia testing with the MEMS sensor (Department of Systems Design Engineering) was ongoing during this MASc thesis' exam. Initial results with PPy, PANI with 5% tin oxide and PANI with 5% titanium oxide showed promise. PANI with 5% zinc oxide did not sorb. One can now compare with the suggested sensing materials from Table 2.

5.3.2 Long-term Recommendations

Expanding on the interaction of dopants in Section 4.1, the interaction of MO dopants with SDS could be investigated further.

References

[1] D. L. Pfost, C. D. Fulhage and D. Rastorfer, "Anaerobic lagoons for storage/treatment of livestock manure," *MU Extention, University of Missouri-Columbia,* 2000.

[2] G. N. Tiwari and R. K. Mishra, "4.9.3 Factors Influencing Biogas Yield," in *Advanced Renewable Energy Sources*, Royal Society of Chemistry (RSC), 2012, p. 197.

[3] Q. Niu and Y.-Y. Li, "Recycling of livestock manure into bioenergy," in *Recycling of solid waste for biofuels and bio-chemicals*, Springer, 2016, p. 165–186.

[4] R. Sinnott and G. Towler, "9.2.3 Materials Incompatibility," in *Chemical Engineering Design (6th Edition)*, Elsevier, 2020, p. 461.

[5] T. Hong, J. T. Culp, K.-J. Kim, J. Devkota, C. Sun and P. R. Ohodnicki, "State-of-the-art of methane sensing materials: A review and perspectives," *TrAC, Trends in analytical chemistry (Regular ed.),* vol. 125, p. 115820, 2020.

[6] Occupational Safety and Health Administration, "OSHA Occupational Chemical Database - Ammonia," Occupational Safety and Health Administration, 17 December 2020. [Online]. Available: https://www.osha.gov/chemicaldata/623. [Accessed 4 April 2023].

[7] M. A. M. Smeets, P. J. Bulsing, S. van Rooden, R. Steinmann, J. A. de Ru, N. W. M. Ogink, C. van Thriel and P. H. Dalton, "Odor and Irritation Thresholds for Ammonia: A Comparison between Static and Dynamic Olfactometry," *Chemical Senses,* vol. 32, p. 11–20, January 2007.

[8] J. R. Holton, J. A. Curry and J. A. Pyle, "Key Atmospheric Nitrogen Compounds," in *Encyclopedia of Atmospheric Sciences, Volumes 1-6*, Oxford, Elsevier, 2003, pp. 206-207.

[9] Occupational Safety and Health Administration, "OSHA Occupational Chemical Database - Hydrogen Sulfide," Occupational Safety and Health Administration, 10 February 2023. [Online]. Available: https://www.osha.gov/chemicaldata/652. [Accessed 20 July 2023].

[10] M. Arabi, M. Alghamdi, K. Kabel, A. Labena, W. S. Gado, B. Mavani, A. J. Scott, A. Penlidis, M. Yavuz and E. Abdel-Rahman, "Detection of volatile organic compounds by using MEMS sensors," *Sensors (Basel, Switzerland),* vol. 22, p. 4102, 2022.

[11] G. J. Monteny, C. M. Groenestein and M. A. Hilhorst, "Interactions and coupling between emissions of methane and nitrous oxide from animal husbandry," *Nutrient Cycling in Agroecosystems,* vol. 60, p. 123–132, 2001.

[12] M. Almaraz, E. Bai, C. Wang, J. Trousdell, S. Conley, I. Faloona and B. Z. Houlton, "Agriculture is a major source of NOx pollution in California," *Science Advances,* vol. 4, pp. 34-77, 2018.

[13] I. C. Anderson and J. S. Levine, "Simultaneous field measurements of biogenic emissions of nitric oxide and nitrous oxide," *Journal of Geophysical Research: Atmospheres,* vol. 92, pp. 965-976, 1987.

[14] I. Fives North American Combustion, North American Combustion Handbook - A Practical Basic Reference on the Art and Science of Industrial Heating with Gaseous and Liquid Fuels, Volume II, 3 ed., Fives North American Combustion, Inc, 2001.

[15] K. M. E. Stewart, "Design of Polymeric Sensing Materials for Volatile Organic Compounds: Optimized Material Selection for Ethanol with Mechanistic Explanations," Ph.D. Thesis, Department of Chemical Engineering, University of Waterloo, 2016.

[16] B. H. Mavani, "Polymeric Materials for Detection of Chemical Warfare Agents," *M.ASc. thesis, Chemical Engineering, University of Waterloo, Waterloo,* 2021. [Online]. Available: http://hdl.handle.net/10012/17744.

[17] P. Sun, Y. Jiang, G. Xie, X. Du and J. Hu, "A room temperature supramolecular-based quartz crystal microbalance (QCM) methane gas sensor," *Sensors and Actuators B: Chemical,* vol. 141, p. 104–108, 2009.

[18] M. Dosi, "Design of a Solid-State Electrochemical Methane Sensor Based on Laser-Induced Graphene," M.ASc thesis., Chemical Engineering, University of Waterloo, Waterloo, 2018.

[19] P. Bhattacharyya, P. K. Basu, H. Saha and S. Basu, "Fast response methane sensor using nanocrystalline zinc oxide thin films derived by sol–gel method," *Sensors and Actuators B: Chemical,* vol. 124, p. 62–67, 2007.

[20] F. Quaranta, R. Rella, P. Siciliano, S. Capone, M. Epifani, L. Vasanelli, A. Licciulli and A. Zocco, "A novel gas sensor based on SnO2/Os thin film for the detection of methane at low temperature," *Sensors and Actuators B: Chemical,* vol. 58, p. 350–355, 1999.

[21] S. Navazani, A. Shokuhfar, M. Hassanisadi, A. Di Carlo and N. Shahcheraghi, "Fabrication and characterization of a sensitive, room temperature methane sensor based on SnO2@ reduced graphene oxide-polyaniline ternary nanohybrid," *Materials Science in Semiconductor Processing,* vol. 88, p. 139–147, 2018.

[22] T. C. Merkel, V. I. Bondar, K. Nagai, B. D. Freeman and I. Pinnau, "Gas sorption, diffusion, and permeation in poly (dimethylsiloxane)," *Journal of Polymer Science Part B: Polymer Physics,* vol. 38, p. 415–434, 2000.

[23] A. H. Khoshaman, P. C. H. Li, N. Merbouh and B. Bahreyni, "Highly sensitive supra-molecular thin films for gravimetric detection of methane," *Sensors and Actuators B: Chemical,* vol. 161, p. 954–960, 2012.

[24] A. Hannon, Y. Lu, J. Li and M. Meyyappan, "A sensor array for the detection and discrimination of methane and other environmental pollutant gases," *MDPI: Sensors,* vol. 16, p. 1163, 2016.

[25] T. Sen, S. Mishra, S. S. Sonawane and N. G. Shimpi, "Polyaniline/zinc oxide nanocomposite as room-temperature sensing layer for methane," *Polymer Engineering and Science,* vol. 58, no. 8, p. 1438–1445, 2018.

[26] R. Rego, N. Caetano and A. Mendes, "Hydrogen/methane and hydrogen/nitrogen sensor based on the permselectivity of polymeric membranes," *Sensors and Actuators. B: Chemical,* vol. 111, p. 150–159, 2005.

[27] A. L. Kukla, Y. M. Shirshov and S. A. Piletsky, "Ammonia sensors based on sensitive polyaniline films," *Sensors and Actuators B: Chemical,* vol. 37, p. 135–140, 1996.

[28] X. Wang, L. Gong, D. Zhang, X. Fan, Y. Jin and L. Guo, "Room temperature ammonia gas sensor based on polyaniline/copper ferrite binary nanocomposites," *Sensors and Actuators B: Chemical,* vol. 322, p. 128615, 2020.

[29] Y. Zhang, J. Zhang, Y. Jiang, Z. Duan, B. Liu, Q. Zhao, S. Wang, Z. Yuan and H. Tai, "Ultrasensitive flexible NH3 gas sensor based on polyaniline/SrGe4O9 nanocomposite with ppt-level detection ability at room temperature," *Sensors and Actuators B: Chemical,* vol. 319, p. 128293, 2020.

[30] S. B. Kulkarni, Y. H. Navale, S. T. Navale, F. J. Stadler, N. S. Ramgir and V. B. Patil, "Hybrid polyaniline-WO3 flexible sensor: a room temperature competence towards NH3 gas," *Sensors and Actuators B: Chemical,* vol. 288, p. 279–288, 2019.

[31] M. E. Nicho, M. Trejo, A. Garcıa-Valenzuela, J. M. Saniger, J. Palacios and H. Hu, "Polyaniline composite coatings interrogated by a nulling optical-transmittance bridge for sensing low concentrations of ammonia gas," *Sensors and Actuators B: Chemical,* vol. 76, p. 18–24, 2001.

[32] Y. Jiang, T. Wang, Z. Wu, D. Li, X. Chen and D. Xie, "Study on the NH3-gas sensitive properties and sensitive mechanism of polypyrrole," *Sensors and Actuators B: Chemical,* vol. 66, pp. 280-282, 2000.

[33] R. Gangopadhyay and A. De, "Conducting polymer composites: novel materials for gas sensing," *Sensors and Actuators B: Chemical,* vol. 77, no. 1-2, p. 326–329, 2001.

[34] L. Hong, Y. Li and M. Yang, "Fabrication and ammonia gas sensing of palladium/polypyrrole nanocomposite," *Sensors and Actuators. B: Chemical,* vol. 145, p. 25–31, 2010.

[35] S. Ahmad, I. Khan, A. Husain, A. Khan and A. M. Asiri, "Electrical Conductivity Based Ammonia Sensing Properties of Polypyrrole/MoS2 Nanocomposite," *MDPI: Polymers,* vol. 12, p. 3047, 2020.

[36] V. V. Chabukswar, S. Pethkar and A. A. Athawale, "Acrylic acid doped polyaniline as an ammonia sensor," *Sensors and Actuators B: Chemical,* vol. 77, p. 657–663, 2001.

[37] K. K. Khun, Kamalpreet, A. Mahajan and R. K. Bedi, "SnO2 thick films for room temperature gas sensing applications," *Journal of Applied Physics,* vol. 106, p. 124509, 2009.

[38] S. Dacrory, A. M. Saeed and R. E. Abouzeid, "A novel ammonia sensor based on cellulose/graphene oxide functionalized with ethylenediamine," *Express Polymer Letters,* vol. 16, p. 786–797, 2022.

[39] M. Matsuguchi, J. Io, G. Sugiyama and Y. Sakai, "Effect of NH3 gas on the electrical conductivity of polyaniline blend films," *Synthetic Metals,* vol. 128, p. 15–19, 2002.

[40] J. Gong, Y. Li, Z. Hu, Z. Zhou and Y. Deng, "Ultrasensitive NH3 gas sensor from polyaniline nanograin enchased TiO2 fibers," *The Journal of Physical Chemistry C,* vol. 114, p. 9970–9974, 2010.

[41] A. Tripathi, K. P. Misra and R. K. Shukla, "Enhancement in ammonia sensitivity with fast response by doping Al2O3 in polyaniline," *Journal of Applied Polymer Science,* vol. 130, p. 1941–1948, 2013.

[42] G. D. Khuspe, S. T. Navale, M. A. Chougule and V. B. Patil, "Ammonia gas sensing properties of CSA doped PANi-SnO2 nanohybrid thin films," *Synthetic Metals,* Vols. 185-186, p. 1–8, 2013.

[43] G. Liu, Y. Zhou, X. Zhu, Y. Wang, H. Ren, Y. Wang, C. Gao and Y. Guo, "Humidity enhanced ammonia sensing of porous polyaniline/tungsten disulfide nanocomposite film," *Sensors and Actuators B: Chemical,* vol. 323, p. 128699, 2020.

[44] V. A. T. Dam, D. Wouters, W. Knoben, S. H. Brongersma and R. van Schaijk, "Polymer coated MEMS resonator for room temperature NH3 sensing," *IEEE Sensors,* p. 194–197, 2014.

[45] S.-W. Lee, N. Takahara, S. Korposh, D.-H. Yang, K. Toko and T. Kunitake, "Nanoassembled thin film gas sensors. III. Sensitive detection of amine odors using TiO2/poly (acrylic acid) ultrathin film quartz crystal microbalance sensors," *Analytical chemistry,* vol. 82, p. 2228–2236, 2010.

[46] A. Mirmohseni and A. Oladegaragoze, "Construction of a sensor for determination of ammonia and aliphatic amines using polyvinylpyrrolidone coated quartz crystal microbalance," *Sensors and Actuators B: Chemical,* vol. 89, pp. 164-172, 2003.

[47] H. Tai, Y. Jiang, G. Xie and J. Yu, "Preparation, Characterization and Comparative NH3-sensing Characteristic Studies of PANI/inorganic Oxides Nanocomposite Thin Films," *Journal of Materials Science & Technology,* vol. 26, p. 605–613, 2010.

[48] Q. Nie, Z. Pang, H. Lu, Y. Cai and Q. Wei, "Ammonia gas sensors based on In2O3/PANI hetero-nanofibers operating at room temperature," *Beilstein Journal of Nanotechnology,* vol. 7, p. 1312–1321, 2016.

[49] V. V. Plashnitsa, V. Gupta and N. Miura, "Mechanochemical approach for fabrication of a nano-structured NiO-sensing electrode used in a zirconia-based NO2 sensor," *Electrochimica Acta,* vol. 55, p. 6941–6945, 2010.

[50] P. K. Sekhar, E. L. Brosha, R. Mukundan, W. Li, M. A. Nelson, P. Palanisamy and F. H. Garzon, "Application of commercial automotive sensor manufacturing methods for NOx/NH3 mixed potential sensors for on-board emissions control," *Sensors and Actuators B: Chemical,* vol. 144, p. 112–119, 2010.

[51] Y. Chen and J.-Z. Xiao, "Synthesis of composite La1. 67Sr0. 33NiO4–YSZ for a potentiometric NOx sensor by microwave-assisted complex-gel auto-combustion," *Ceramics International,* vol. 39, p. 9599–9603, 2013.

[52] J.-C. Yang, J. V. Spirig, D. Karweik, J. L. Routbort, D. Singh and P. K. Dutta, "Compact electrochemical bifunctional NOx/O2 sensor with metal/metal oxide internal reference electrode for high temperature applications," *Sensors and Actuators B: Chemical,* vol. 131, p. 448–454, 2008.

[53] O. L. Figueroa, C. Lee, S. A. Akbar, N. F. Szabo, J. A. Trimboli, P. K. Dutta, N. Sawaki, A. A. Soliman and H. Verweij, "Temperature-controlled CO, CO2 and NOx sensing in a diesel engine exhaust stream," *Sensors and Actuators B: Chemical,* vol. 107, p. 839–848, 2005.

[54] B.-J. Kim, I.-G. Song and J.-S. Kim, "In2O3-based micro gas sensor for detecting NO x gases," *Electronic Materials Letters,* vol. 10, p. 509–513, 2014.

[55] P. Jha, M. Sharma, A. Chouksey, P. Chaturvedi, D. Kumar, G. Upadhyaya, J. S. B. S. Rawat and P. K. Chaudhury, "Functionalization of carbon nanotubes with metal phthalocyanine for selective gas sensing application," *Synthesis and Reactivity in Inorganic, Metal-Organic, and Nano-Metal Chemistry,* vol. 44, p. 1551–1557, 2014.

[56] A. Ray, A. F. Richter, A. G. MacDiarmid and A. J. Epstein, "Polyaniline: protonation/deprotonation of amine and imine sites," *Synthetic Metals,* vol. 29, pp. 151-156, 1989.

[57] P. Kong, P. Liu, Z. Ge, H. Tan, L. Pei, J. Wang, P. Zhu, X. Gu, Z. Zheng and Z. Li, "Conjugated HCl-doped polyaniline for photocatalytic oxidative coupling of amines under visible light," *Catalysis Science & Technology,* vol. 9, p. 753–761, 2019.

[58] A. J. Heeger, "Semiconducting and Metallic Polymers: The Fourth Generation of Polymeric Materials (Nobel Lecture)," *Angewandte Chemie (International ed.),* vol. 40, p. 2591–2611, 2001.

[59] W.-S. Huang, B. D. Humphrey and A. G. MacDiarmid, "Polyaniline, a Novel Conducting Polymer. Morphology and Chemistry of Its Oxidation and Reduction in Aqueous Electrolytes," *Journal of the Chemical Society, Faraday Transactions 1,* vol. 82, no. 8, pp. 2385-2400, 1986.

[60] J. Stejskal and R. G. Gilbert, "Polyaniline. Preparation of a conducting polymer(IUPAC Technical Report)," *Pure and Applied Chemistry,* vol. 74, p. 857–867, 2002.

[61] J. E. Albuquerque, L. H. C. Mattoso, D. T. Balogh, R. M. Faria, J. G. Masters and A. G. MacDiarmid, "A simple method to estimate the oxidation state of polyanilines," *Synthetic Metals,* vol. 113, pp. 19-22, 2000.

[62] K. M. E. Stewart, N. T. M. McManus, E. Abdel-Rahman and A. Penlidis, "Doped Polyaniline for the Detection of Formaldehyde," *Journal of Macromolecular Science, Part A: Pure and Applied Chemistry,* vol. 49, p. 1–6, January 2012.

[63] B. H. Mavani, "Polymeric Gas Sensing Materials for Detection of Toxic Analytes," Ph.D. Comprehensive Exam Report, Department of Chemical Engineering, University of Waterloo, Waterloo, March 15, 2023.

[64] Y. Shama, "MEMS Sensors For Aqueous Media," Ph.D. Thesis Proposal, System Design Engineering, University of Waterloo, Waterloo, 2022.

[65] E. Tang, G. Cheng and X. Ma, "Preparation of nano-ZnO/PMMA composite particles via grafting of the copolymer onto the surface of zinc oxide nanoparticles," *Powder Technology,* vol. 161, pp. 209-214, 2006.

[66] J. Huang and R. B. Kaner, "Nanofiber Formation in the Chemical Polymerization of Aniline: A Mechanistic Study," *Angewandte Chemie International Edition,* no. 43, p. 5817 –5821, 2004.

[67] K. M. Krishnan, "10.3 Image Contrast in a Scanning Electron Microscope," in *Principles of Materials Characterization and Metrology*, Oxford University Press, 2021, pp. 710-715.

[68] A. G. MacDiarmid, J. C. Chiang, A. F. Richter, N. L. D. Somasiri and A. J. Epstein, "Polyaniline: synthesis and characterization of the emeraldine oxidation state by elemental analysis," in *Conducting Polymers*, Springer, 1987, p. 105–120.

[69] S. Bhadra and D. Khastgir, "Determination of crystal structure of polyaniline and substituted polyanilines through powder X-ray diffraction analysis," *Polymer Testing,* vol. 27, p. 851–857, 2008.

[70] W. Łużny, M. Śniechowski and J. Laska, "Structural properties of emeraldine base and the role of water contents: X-ray diffraction and computer modelling study," *Synthetic Metals,* vol. 126, no. 1, pp. 27-35, 2002.

[71] J. Khouri, "Chitosan Edible Films Crosslinked by Citric Acid," *Ph.D thesis, Chemical Engineering, Univ. of Waterloo, Waterloo,* 2019. [Online]. Available: http://hdl.handle.net/10012/14877.

[72] J. Stejskal, A. Riede, D. Hlavatá, J. Prokeš, M. Helmstedt and P. Holler, "The effect of polymerization temperature on molecular weight, crystallinity, and electrical conductivity of polyaniline," *Synthetic Metals,* vol. 96, pp. 55-61, 1998.

[73] K. M. E. Stewart and A. Penlidis, "Designing polymeric sensing materials: what are we doing wrong?," *Polymers for Advanced Technologies,* vol. 28, p. 319–344, 2017.

[74] H. Kwon, J.-S. Yoon, Y. Lee, D. Y. Kim, C.-K. Baek and J. K. Kim, "An array of metal oxides nanoscale hetero p-n junctions toward designable and highly-selective gas sensors," *Sensors and Actuators B: Chemical,* vol. 255, pp. 1663-1670, 2018.

[75] Q. Zhang, Q. Zhou, Z. Lu, Z. Wei, L. Xu and Y. Gui, "Recent Advances of SnO2-Based Sensors for Detecting Fault Characteristic Gases Extracted From Power Transformer Oil," *Frontiers in Chemistry,* vol. 6, 2018.

[76] S. Navazani, A. Shokuhfar, M. Hassanisadi, M. Askarieh, A. Di Carlo and A. Agresti, "Facile synthesis of a SnO2@ rGO nanohybrid and optimization of its methane-sensing parameters," *Talanta,* vol. 181, p. 422–430, 2018.

[77] Z. Lou, L. Wang, T. Fei and T. Zhang, "Enhanced ethanol sensing properties of NiO-doped SnO 2 polyhedra," *New Journal of Chemistry,* vol. 36, p. 1003–1007, 2012.

[78] G. Xie, P. Sun, X. Yan, X. Du and Y. Jiang, "Fabrication of methane gas sensor by layer-by-layer self-assembly of polyaniline/PdO ultra thin films on quartz crystal microbalance," *Sensors and Actuators B: Chemical,* vol. 145, p. 373–377, 2010.

[79] M. Benounis, N. Jaffrezic-Renault, J.-P. Dutasta, K. Cherif and A. Abdelghani, "Study of a new evanescent wave optical fibre sensor for methane detection based on cryptophane molecules," *Sensors and Actuators B: Chemical,* vol. 107, p. 32–39, 2005.

[80] E. C. M. Hermans, "CO, CO2, CH4 and H2O sensing by polymer covered interdigitated electrode structures," *Sensors and Actuators,* vol. 5, p. 181–186, 1984.

[81] Y. Sakurai, H.-S. Jung, T. Shimanouchi, T. Inoguchi, S. Morita, R. Kuboi and K. Natsukawa, "Novel array-type gas sensors using conducting polymers, and their performance for gas identification," *Sensors and Actuators B: Chemical,* vol. 83, p. 270–275, 2002.

[82] C. Zhu, X. Cheng, X. Dong and Y. m. Xu, "Enhanced Sub-ppm NH3 Gas Sensing Performance of PANI/TiO2 Nanocomposites at Room Temperature," *Frontiers in Chemistry,* vol. 6, 2018.

[83] T. Patois, J.-B. Sanchez, F. Berger, P. Fievet, O. Segut, V. Moutarlier, M. Bouvet and B. Lakard, "Elaboration of ammonia gas sensors based on electrodeposited polypyrrole–Cobalt phthalocyanine hybrid films," *Talanta,* vol. 117, p. 45–54, 2013.

[84] S. Palaniappan and C. Saravanan, "Polyaniline–maleicacid–dodecylhydrogensulfate salt as sensor material for toxic gases," *Journal of applied polymer science,* vol. 118, p. 518–524, 2010.

[85] S. G. Pawar, M. A. Chougule, S. L. Patil, B. T. Raut, P. R. Godse, S. Sen and V. B. Patil, "Room Temperature Ammonia Gas Sensor Based on Polyaniline-TiO Nanocomposite," *IEEE Sensors Journal,* vol. 11, no. 12, p. 3417–3423, 2011.

[86] I. Venditti, I. Fratoddi, M. V. Russo and A. Bearzotti, "A nanostructured composite based on polyaniline and gold nanoparticles: synthesis and gas sensing properties," *Nanotechnology,* vol. 24, p. 155503, 2013.

[87] N. V. Bhat, A. P. Gadre and V. A. Bambole, "Structural, mechanical, and electrical properties of electropolymerized polypyrrole composite films," *Journal of Applied Polymer Science,* vol. 80, p. 2511–2517, 2001.

[88] J. L. Wojkiewicz, V. N. Bliznyuk, S. Carquigny, N. Elkamchi, N. Redon, T. Lasri, A. A. Pud and S. Reynaud, "Nanostructured polyaniline-based composites for ppb range ammonia sensing," *Sensors and Actuators B: Chemical,* vol. 160, p. 1394–1403, 2011.

[89] P. P. Sengupta, P. Kar and B. Adhikari, "Influence of dopant in the synthesis, characteristics and ammonia sensing behavior of processable polyaniline," *Thin Solid Films,* vol. 517, p. 3770–3775, 2009.

[90] L. He, Y. Jia, F. Meng, M. Li and J. Liu, "Gas sensors for ammonia detection based on polyaniline-coated multi-wall carbon nanotubes," *Materials Science and Engineering: B,* vol. 163, p. 76–81, 2009.

[91] E. Dickey, O. Varghese, K. Ong, D. Gong, M. Paulose and C. Grimes, "Room Temperature Ammonia and Humidity Sensing Using Highly Ordered Nanoporous Alumina Films," *Sensors (Basel, Switzerland),* vol. 2, p. 91–110, 2002.

[92] H. U. Khan, M. Tariq, M. Shah, M. Iqbal and M. T. Jan, "Inquest of highly sensitive, selective and stable ammonia (NH3) gas sensor: structural, morphological and gas sensing properties of polyvinylpyrrolidone (PVP)/CuO nanocomposite," *Synthetic Metals,* vol. 268, p. 116482, 2020.

[93] V. Guidi, M. C. Carotta, B. Fabbri, S. Gherardi, A. Giberti and C. Malagù, "Array of sensors for detection of gaseous malodors in organic decomposition products," *Sensors and Actuators B: Chemical,* vol. 174, p. 349–354, 2012.

Appendices

Appendix A. Summary of Sensing Materials

Appendix A.1. Sensing Materials for Methane

Sensing Material	Dopant	Detection Limit	Selectivity	Operational Temperature	Sensing Time	Recovery Time	Mechanism	Reference
Laser-induced graphene + ionic liquid/polyvinylidene fluoride coating	Pd nanoparticle	5 ppm		RT	50s	16~20min	Electrochemical	[18]
ZnO	-	0.1~1%		250	22s	27s	Resistive gas sensor (oxidation of sensor)	[19]
SnO_2	Osmium ($OsCl_3$)	200~2000 ppm		270			Resistive gas sensor (oxidation of analyte)	[20]
SnO_2@rGO-PANI	-	100ppm	Highly selective against NH3, $CO2^{(1)}$	RT	360s	1150s	Resistive gas sensor (oxidation of analyte)	[21]
SnO_2@rGO	-	1000ppm	Highly selective against NH3, CO2	150	61s	330s	Resistive gas sensor (oxidation of analyte)	[76]
PDMS	-	-	Higher affinity towards $CO_2^{(2)}$	35	-	-	Diffusion/ Sorption	[22]
Cryptophane A	-	3ppm	-	RT	20s	-	Sorption/ Gravimetric	[23]
SnO_2	NiO	6.7 ppm	Formaldehyde; Carbon dioxide; Methane	280 ℃			Resistive gas sensor (oxidation of analyte)	[77]
Polyaniline (PANI)	PdO (17%) Camphor sulfonic acid (CSA)	3000 ppm	-	RT			Resistive gas sensor (oxidation of analyte)	[78]
Cryptophane-A	-	5000 ppm	-					[79]
Cryptophane-A	-	20 000 ppm	Ammonia (1.4) Nitrogen Dioxide (3.2) Carbon Monoxide (51.5) Hydrogen Gas (9.4)					[17]
Protonated polyaniline (salt)	(protonated using HCl)	2ppm	Possibly low	RT	120	300		[24]

Sensing Material	Dopant	Detection Limit	Selectivity	Operational Temperature	Sensing Time	Recovery Time	Mechanism	Reference
Polyphenylacetylene	-	10mmHg	Selective towards CO (more sensitive to CO than CH4 and CO2) (more sensitive towards humidity	RT	-	-	-	[80]
poly(etherimide)		NA	H2/CH4: 22.67	RT				[26]
poly(dimethylsiloxane)		NA	H2/CH4: 1.20	RT				[26]
Polyaniline	HCl+sodium dodecyl sulfate-ZnO nanoparticle	100ppm	Low effect of humidity(3)	RT	20s			[25]
poly(3-n-dodecylthiophene)	-	300ppm	NH_3 and $CHCl_3$ competes; less sensitive to CH_4	60	600s	-	Resistive gas sensor	[81]

(1): The material showed higher sensor response with CO_2 and NH_3 than methane

(2): The literature compares permeability of methane and carbon dioxide in water

(3): High relative humidity had minimal to negligible effect on sensor performance

Appendix A.2. Sensing Materials for Ammonia

Sensing Material	Dopant	Detection Limit	Selectivity	Operational Temperature	Sensing Time	Recovery Time	Mechanism	Reference
Titanium dioxide (TiO_2)	Polyaniline (PANI) Hydro-chloric Acid (HCl)	50ppt					Resistive gas sensor	[40]
PANI	TiO_2	0.5ppm	CH_3OH, C_2H_5OH, NO H_2O (1)	RT	100s		Resistive gas sensor	[82]
PANI	TiO_2 (2)	1ppm	Water increased sensor response (3)	RT	3s	60s	Resistive gas sensor	[47]
PANI	SnO_2	1ppm	"	RT	3s	60s	Resistive gas sensor	[47]
PANI	In_2O_3	1ppm	"	RT	10s	60s	Resistive gas sensor	[47]
Protonated polyaniline (salt)	(protonated using HCl)	2ppm	-	RT	120	300		[24]
PANI	HCl+WS_2	10ppm	Humidity (RH 68%)	RT			Resistive gas sensor/Sorption	[43]
Titanium dioxide/ poly(acrylic acid) (TiO2/PAA)	-	0.11ppm	Butyl amine (1.9) Pyridine (3.8) Ethanol (13.8) Toluene (20.4) Chloroform (43.6)	RT	-		Quartz crystal microbalance (Sorption)	[45]
PANI	WO_3	1ppm	NO_2, H_2S, CH_3OH, C_2H_5OH	RT	32s	40s	Resistive gas sensor/Sorption	[30]
Polypyrrole (PPy)	Bu_4NClO_4	10ppm		-	20s	60s	Resistive gas sensor/Sorption	[32]
Polyaniline	$CuFe_2O_4$	5ppm		RT	84s	54s	Resistive gas sensor/Sorption	[28]
PANI	Acrylic Acid	1ppm		RT	150s	360s	Resistive gas sensor/Sorption	[36]
PPy	Cobalt phthalocyanine+ $LiClO_4$	1ppm		RT	300s		Resistive gas sensor/Sorption	[83]
Polyaniline (PANI)	$HClO_4$	5ppm		20	90s	4 min	$PAH^+ + NH_3$ -> PA + NH_4^+	[27]
Polyaniline	Dodecyl-hydrogen sulfate salt and maleic acid	10ppm		RT	5 min	2 min	Resistive gas sensor/Sorption	[84]
PANI	TiO_2	20ppm	CH_3OH, C_2H_5OH, NO_2, H_2S(4)	RT			Resistive gas sensor	[85]

Sensing Material	Dopant	Detection Limit	Selectivity	Operational Temperature	Sensing Time	Recovery Time	Mechanism	Reference
Cellulose	Graphene oxide+ ethylenediamine	5ppm		RT	490s	620s	Resistive gas sensor/Sorption	[38]
SnO_2	-	50ppm		RT			Resistive gas sensor/Sorption	[37]
PANI	In_2O_3	50ppm		RT			Resistive gas sensor/Sorption	[48]
Polyaniline (PANI)	3-mercapto-1-propane sulfonic acid (3MPS)	10.8ppm	Ethanol Toluene Acetonitrile	RT			Resistive gas sensor/Sorption	[86]
PANI	Al_2O_3	300ppm		RT			Resistive gas sensor/Sorption	[41]
PANI	SnO_2-Camphor sulfonic acid	100ppm		30	46s		Resistive gas sensor/Sorption	[42]
PPy	MoS_2	300ppm	Ethanol, Propanol, Acetaldehyde	RT	60~70s	50~60s	Resistive gas sensor/Sorption	[35]
PPy	Palladium (Nanoparticle)	50ppm		RT	14s	148s	Resistive gas sensor/Sorption	[34]
PANI	$SrGe_4O_9$	0.250 ppm		RT	62s	223s		[29]
Poly (methyl methacrylate)-Polyaniline (PMMA-PANI)	bis(2-ethyl hexyl) hydrogen phosphate (DiOHP)	500ppm		30	11 min		Resistive gas sensor/Sorption	[39]
PANI-PMMA	-	10ppm		RT	-	-	Optical Transmittance	[31]
PPy-PVA	-	1%		-	-	-	Electrochemical	[33]
Polythiophene	-	300ppm		RT	600s			[81]
Polypyrrole (PPy)	Poly (vinyl alcohol) PVA (5 w/v %)	1000 ppm						[87]
PANI-embedded PU	Camphor sulfonic acid	20ppb		RT	5min (1ppm)		Resistive gas sensor/Sorption	[88]
PANI	para-toluene sulfonic acid (PTSA)+HCl	100ppm		RT	4min	4min	Resistive gas sensor/Sorption	[89]
PANI-coated multi-wall carbon nanotubes	-	200ppb		RT	10~120s	100~500s	Resistive gas sensor/Sorption	[90]

Sensing Material	Dopant	Detection Limit	Selectivity	Operational Temperature	Sensing Time	Recovery Time	Mechanism	Reference
Nanoporous Alumina Al_2O_3	-	$1.5x10^7$ppm 0.15		RT	95s		Resistive gas sensor/Sorption	[91]
Polyvinylpyrrolidone (PVP)	CuO	10ppm		RT	15s		Capacitive gas sensor/Sorption	[92]
Poly(acrylic acid)	-	100ppb	40% RH	RT	5min		Mass-based (Change in resonance)	[44]
ZnO	-	10ppm	ethyl-mercaptan, hydrogen sulfide, n-butanol [1]	400			Resistive gas sensor/Sorption	[93]
WO_3 70% SnO_2 30%	-	0.5ppm	"	550			Resistive gas sensor/Sorption	[93]
SnO_2 70% TiO_2 30%	-	0.5ppm	"	600			Resistive gas sensor/Sorption	[93]
SnO_2 10% TiO_2 90%	-	1ppm	"	550			Resistive gas sensor/Sorption	[93]

(1): Compared response of sensor to different compounds in separate trials; not in mixture.

(2): PANI doped with TiO_2 had the largest response than PANI doped with SnO_2 or In_2O_3, and pure PANI.

(3): Increased relative humidity increased the sensor response towards NH_3; Saturation observed at >80.2% RH; suggests water sorption to the PANI film.

(4): Comparing sensitivities of NH_3 at 20 ppm and other gases at 100 ppm. Greater change in resistance in presence of 20ppm NH_3.

Appendix A.3. Sensing Materials for Nitrogen Oxide (NO_X)

Sensing Material	Dopant	Detection Limit	Selectivity	Operational Temperature	Sensing Time	Recovery Time	Mechanism	Reference
NiO		50ppm	Poor with Methane	800				[49]
$La_{0.8}Sr_{0.2}CrO_3$		100ppm		600				[50]
$La_{1.67}Sr_{0.33}NiO_4$	yttria-stabilized-zirconia (YSZ)	700ppm		400-550	4s	6s		[51]
Pt electrode+ YSZ electrolye		1ppm	Good for CO, propane, NH3	500				[52]
Pt-loaded Zeolite Y		100 ppm	High	300-500				[53]
In_2O_3		0.5ppm		200-350	60s	60s		[54]
Functionalized carbon nanotube with copper phthalocyanine		0.5ppm	Good for CO,SO2, NH3	RT	180s	360s		[55]

Appendix B. Raw Data Trends during Sorption Tests

Polyaniline (PANI), doped PANI, polypyrrole (Ppy), and polydimethylsiloxane (PDMS) with different end groups were tested for formaldehyde (F) sorption (formaldehyde source at 10 ppm). All sorption tests were performed with 0.1g of each sample at ambient temperature (23~25˚C). Table 4 and Table 19 show the samples tested and the sequence of tests performed.

Table 4. List of trials with PANI, doped PANI (repeated for reference)

Sample #	Name	Test	Purpose
1	PANI	F 10ppm	Sensitivity of F
2	PANI-5% SnO_2	F 10ppm	Sensitivity of F
3	PANI-10% SnO_2	F 10ppm	Sensitivity of F
4	PANI-5% ZnO	F 10ppm	Sensitivity of F
5	PANI-5% ZnO-SDS	F 10ppm	Sensitivity of F
6	PANI-2.5% ZnO	F 10ppm	Sensitivity of F
7	PANI-2.5% ZnO-SDS	F 10ppm	Sensitivity of F
8	PDMS-T (trimethylsilyl terminated)[(1)]	F 10ppm	Sensitivity of F
9	PDMS-M (monohydroxy terminated)[(2)]	F 10ppm	Sensitivity of F
10	PANI-HCl	F 10ppm	Sensitivity of F
11	PANI-SDS	F 10ppm	Sensitivity of F
12	PANI-HCl-SDS	F 10ppm	Sensitivity of F
13	PANI-20% ZnO	F 10ppm	Sensitivity of F
14	PANI-5% TiO_2	F 10ppm	Sensitivity of F
15	PANI-20% TiO_2	F 10ppm	Sensitivity of F
16	Polypyrrole[(1)]	F 10ppm	Sensitivity of F
17	PANI-2.5% ZnO-SDS B	F 10ppm	Sensitivity of F

[(1)] Purchased from Sigma Aldrich
[(2)] Purchased from Alfa Aesar

Table 19. Sequence of GC tests performed

Date	Sample No.	Sequence No.	Note
April 11, 2022[(1)]	1	1	
April 11, 2022	2	2	
April 12, 2022	3	3	
April 12, 2022	4	4	
April 13, 2022	5	5	
April 13, 2022	2 repl.	6	
April 13, 2022	8	7	Increased humidity in the afternoon
April 14, 2022	9	8	Loose connection in set-up during the blank run; corrected for subsequent runs.
May 12, 2022	4	9	Lower blank value than previous trials
May 12, 2022	1	10	
Aug 23, 2022	11	11	Lower blank value than previous trials (low for the whole week); Selected samples were corrected (see Appendix E.2 for details)
Aug 23, 2022	1	12	
Aug 24, 2022	7	13	
Aug 24, 2022	4	14	
Aug 24, 2022	10[(2)]	15	
Aug 25, 2022	5	16	
Aug 25, 2022	2	17	
Aug 25, 2022	6[(3)]	18	Readjusted baseline for this sample to minimize effect of water peak shift
Aug 26, 2022	3	19	
Aug 26, 2022	10 repl.	20	
Nov 1, 2022	6	21	
Nov 1, 2022	3[(3)]	22	
Nov 1, 2022	1	23	
Nov 2, 2022	10[(3)]	24	Readjusted baseline for this sample to minimize effect of water peak shift; did not stabilize (for t >132 min)
Nov 3, 2022	7	25	

Nov 3, 2022	11	26	
Nov 3, 2022	5[(3)]	27	Readjusted baseline for this sample to minimize effect of water peak shift
Dec 6, 2022	5	28	
Dec 6, 2022	7	29	
Dec 6, 2022	2	30	
Dec 7, 2022	10	31	
Dec 7, 2022	6	32	
Dec 8, 2022	7 repl.	33	
Dec 8, 2022	13	34	
Dec 8, 2022	12	35	
Dec 9, 2022	11	36	
Jan 31, 2023	1	37	
Jan 31, 2023	15	38	
Feb 1, 2023	10	39	
Feb 1, 2023	16	40	
Feb 1, 2023	5	41	
Feb 2, 2023	14	42	
Feb 2, 2023	13	43	
Mar 21, 2023	16	44	Recalibration of baseline (blank) concentration signal was done
Mar 21, 2023	7	45	
Mar 22, 2023	10	46	
Mar 22, 2023	17	47	
Mar 22, 2023	14	48	
Mar 23, 2023	13	49	
Mar 23, 2023	15	50	
Mar 23, 2023	16 repl.	51	
Mar 23, 2023	2	52	

[(1)] Ventilation of building/lab/fume hood fluctuated throughout the week of April 11th, 2022; it seemed that Plant Ops was doing some work on the 6th floor, unfortunately without informing the department.

[2] The sample did not stabilize. Another sorption test was done in the same week.
[3] Water peak for this sample shifted to the left, affecting the F concentration. To compensate, the blank measurement was adjusted accordingly.

A typical trial day involved a baseline concentration measured before the sample testing. Occasionally, baseline drifts occurred due to environment changes in the building beyond our control. On those days, the blank values were measured again at the end of the trial for confirmation.

The concentration of analyte F is measured with a flask without any sensing material (blank) to account for any possible loss within the testing system. To ensure stability of the test system, the concentration was measured until two consecutive values differ by 0.02 ppm, and the average of the last two values was used as the representative blank value for the day.

Comparing the behavior of blank runs across different dates (sequence 1 to10, see Table 19), the blanks had similar concentration and convergence behaviour, with an average of 9.18 ppm and a standard deviation of 0.189 ppm. In Figure 47, there is a noticeable difference for blank 4 due to an inadvertently inappropriately secured sealing of the main flask. However, even in this case, the concentration quickly stabilized to 9.36 ppm.

To test the consistency of the blanks, the Bonferroni t-test was performed. The blanks measured on four days were not significantly different (threshold value, α=0.05) from each other, thus the blanks from four consecutive days yield a reliable baseline for determining the amount of gas sorption. Blank 5 was significantly lower than the other four baselines, thus trials corresponding to that specific date (blanks) were repeated at a later date.

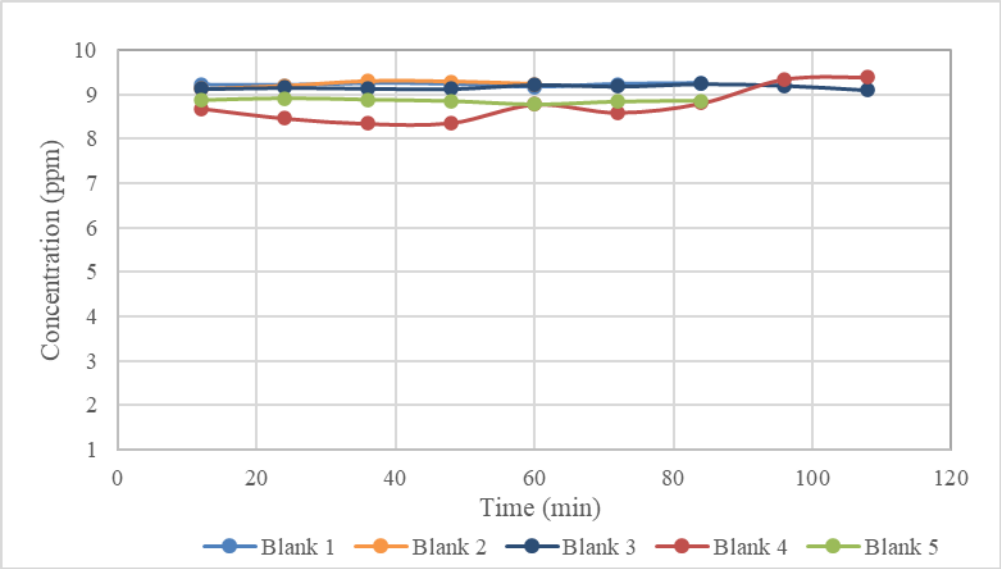

Figure 47. Plot of blanks concentrations for sequence 1 to 10 measured before each trial (exposed to F 10 ppm source)

As seen in Figure 48, the blank values decreased significantly for later trials (sequence 11-20) due to a faulty F cylinder. The trials completed in the same week showed fluctuations with average blank concentration of 8.05 ppm with standard deviation of 0.30. With lower input (blank) concentration, the absolute change in concentration also decreased for all samples (see Figure 49). This shows that the F sorption of PANI is proportional to the analyte concentration. Therefore, the data collected that specific week required corrections in the sorption value. The detailed analysis for this correction can be found in Appendix E.2.

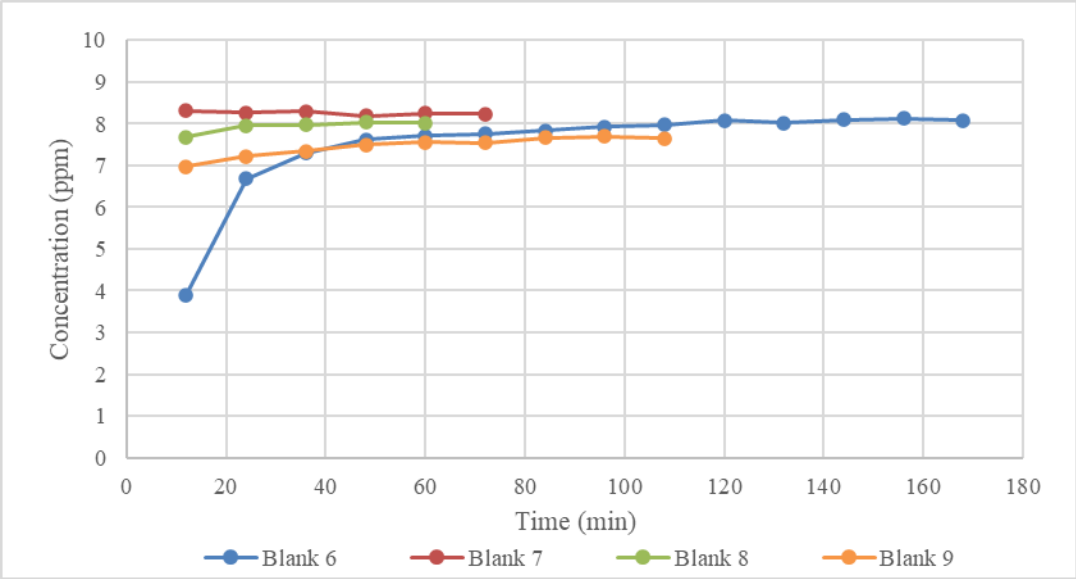

Figure 48. Plot of blanks concentrations for sequence 11 to 20 measured before each trial (exposed to F 10 ppm source)

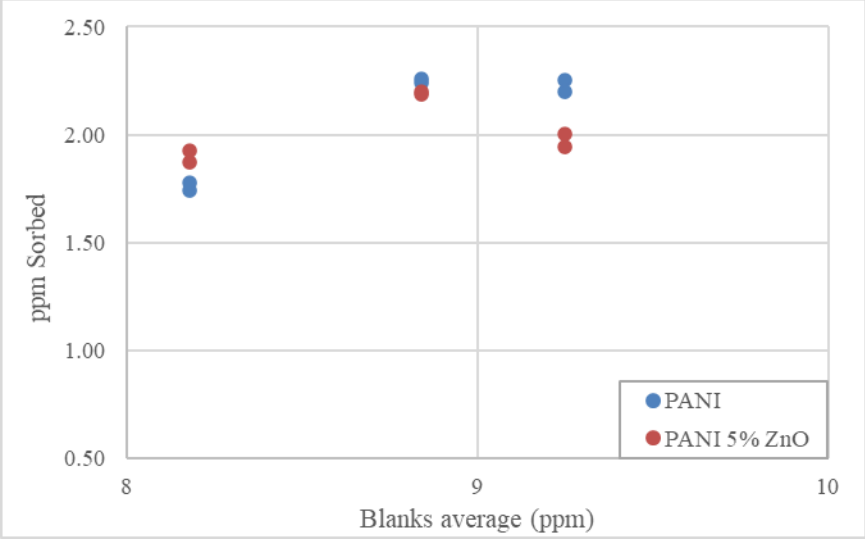

Figure 49. Comparison of ppm sorbed between GC trial runs for PANI and PANI 5% ZnO

For sequence 21 to 36, the blank values were within the expected range (10.0±0.50 ppm) with the fresh analyte cylinder (see Figure 50 and Figure 51). The variation in the concentration is minimal with expected blank concentration of 9.89±0.13 ppm.

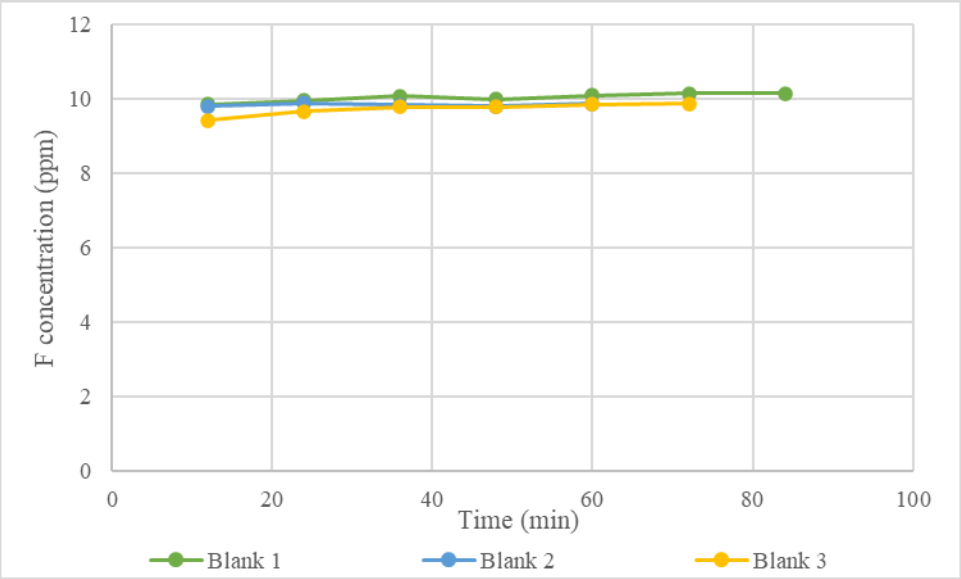

Figure 50. Comparison of blanks for sequence 21 to 27 measured before each trial (exposed to F 10 ppm source)

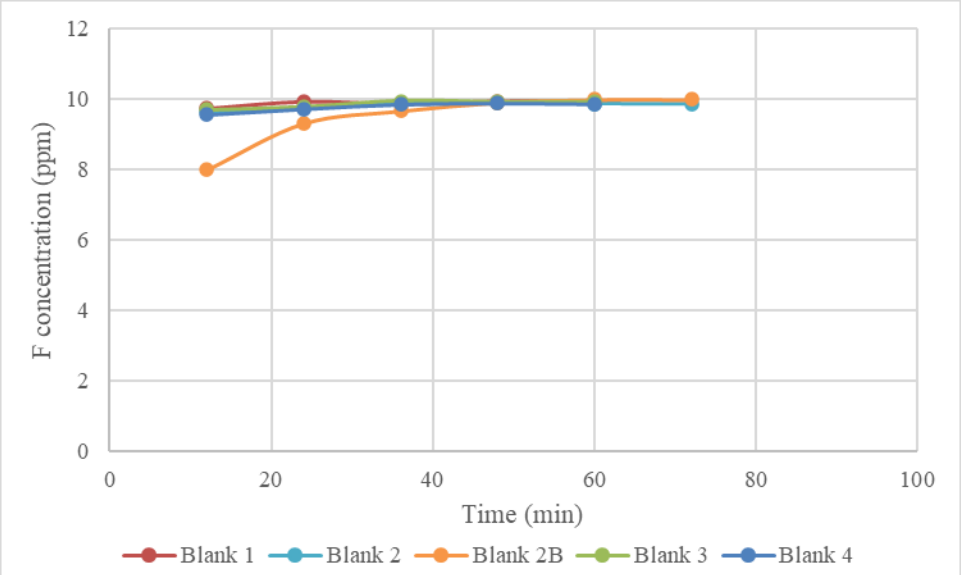

Figure 51. Comparison of blanks for sequence 28 to 36 measured before each trial (exposed to F 10 ppm source)

If a blank run taken as the first step early in the morning of an experimentation day showed some issue, e.g., fluctuations and concentration lower than expected (e.g., 9.24 ppm), then to confirm the baseline concentration, the same procedure was done at the end of the day; see Figure 52 and Figure 53.

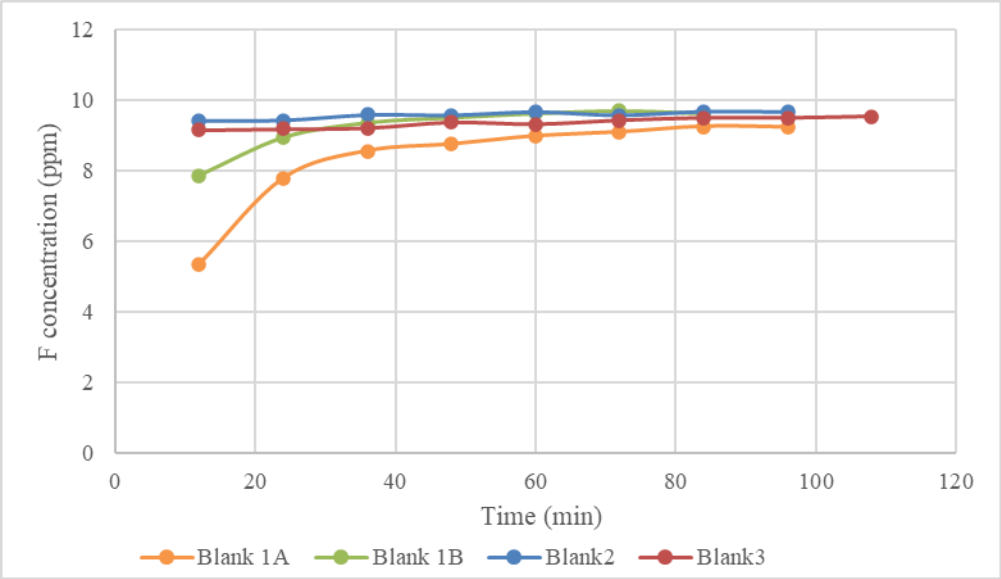

Figure 52. Comparison of blanks for sequence 37 to 43 measured before each trial (exposed to F 10 ppm source)

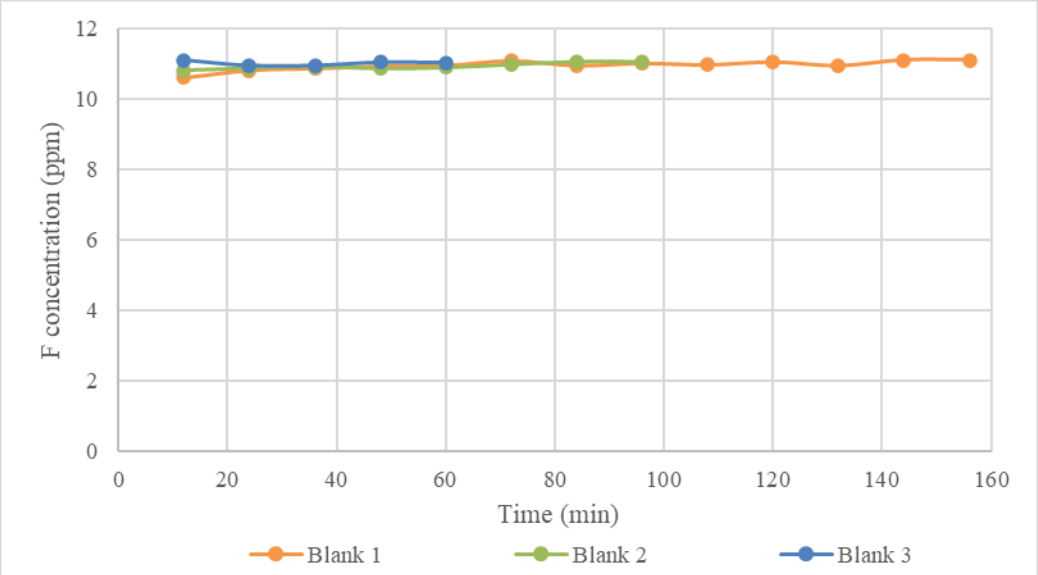

Figure 53. Comparison of blanks for sequence 44 to 52 measured before each trial (exposed to F 10 ppm source)

Appendix C. Statistical Analysis for Blanks (Baseline Sorption) Formaldehyde Tests

Typical GC sorption experimentation tests are conducted over 4 days with blank (baseline) concentration measured before any sensing material is tested. Sorption analysis starts with the assumption that the baseline is stable within the week of the GC tests. For that assumption to be true, the blank concentrations need to be checked if they are identical to each other. This section will show typical analysis of variance (ANOVA) tables/calculations, thus confirming the consistency of blanks using the least significant difference (LSD) approach.

ANOVA is a common method for determining the significance of error and spread of data in the face of independent variable variation. In this case, the variable is the blank value measured on different dates.

Given blank data for sequence 1-10 (see Table 19 for full sequence):

	Concentration (ppm)				
t (min)	Blank 1	Blank 2	Blank 3	Blank 4*	Blank 5
24	9.20	9.19	9.15	8.46	8.90
36	9.25	9.29	9.13	8.34	8.87
48	9.23	9.28	9.12	8.36	8.84
60	9.16	9.23	9.22	8.77	8.77
72	9.23		9.18	8.59	8.83
84	9.25		9.24	8.80	8.85
96			9.20	9.34	
108				9.38	

*The data points highlighted in red are lower than the expected range (9.20-10.00 ppm) due to experimental error (see Table 19 for explanation). The Blank 4 string of data is included to confirm that ANOVA and LSD can detect the odd baseline from the rest.

In this case, sum of squares of blanks is defined as:

$$SS_b = \sum_{b=1}^{p} \left(\frac{x_b^2}{n_b}\right) - \frac{GT^2}{n_t}$$

where

- b designates the column number in the data table (i.e. Blank b)
- x_b is sum of Blank b values
- n_b is number of data points in Blank b
- p is the number of blanks ($p = 5$)
- GT is sum of all concentrations
- n_t is the total number of data points

For the total and n:

$GT = 9.20 + 9.25 + \cdots + 8.83 + 8.85 = 279.65$ and $n = 31$

For each x_i the calculation will be like the following:

$x_1 = 9.20 + 9.25 + \cdots + 9.23 + 9.25 = 55.32$ with $n_b = 6$

Substituting respective values for SS_b:

$$SS_b = \sum_{b=1}^{p}\left(\frac{x_b^2}{n_b}\right) - \frac{GT^2}{n_t} = \left(\frac{55.32^2}{6} + \frac{36.99^2}{4} + \frac{64.24^2}{7} + \frac{70.04^2}{8} + \frac{53.06^2}{6}\right) - \frac{279.65^2}{32} = 1.37$$

with degrees of freedom (df) of blank is: $df_b = p - 1 = 5 - 1 = 4$

Similarly, the sum of squares total is:

$$SS_T = \sum_{i=1}^{n_t}\left(x_i^2\right) - \frac{GT^2}{n_t}$$

where x_i is i[th] data point when $\mathrm{i} = 1,2,3,\ldots,\mathrm{n_t}$

Thus,

$$SS_T = (9.20^2 + 9.25^2 + \cdots + 8.83^2 + 8.85^2) - \frac{279.65^2}{31} = 2.58$$

with degrees of freedom (df) for total: $df_T = n_t - 1 = 31 - 1 = 30$

Finally, the sum of squares for error is:

$SS_e = SS_T - SS_b = 2.58 - 1.37 = 1.21$

with degrees of freedom (df) for error: $df_e = df_T - df_b = 30 - 4 = 26$

The results are summarized in the table below.

Table 20. ANOVA table for blanks from sequence 1-10 (see Table 19)

	SS	df	MS	F
Blanks	1.37	4	0.342	7.34
Error	1.21	26	0.047	
Total	2.58	30		

(MS: mean squared value, SS/df)

To determine if there is significant difference between blanks, differences between the average of each blank ($\bar{x}_b$) and the overall average (average of all data points, $\bar{x}$) is tested with the following hypothesis:

$$\text{Given } \tau_b = \bar{x}_b - \bar{x} \text{ and } b: 1,2,3,4,5$$

$$H_0: \tau_b = 0$$

$$H_1: \tau_b \neq 0 \text{ for at least one } b$$

To reject the null hypothesis (H_0), the mean squared value for blanks (represents the inherent difference between blanks, without random error) should be significantly larger than MS_e (difference due to random error, i.e. data variance). This can be done using the ratio of the two MS as following:

$$F_0 = \frac{MS_b}{MS_e} = \frac{SS_b/df_b}{SS_e/df_e} = \frac{1.37/4}{1.21/26} = 7.34$$

Compare this to the F-distribution value with corresponding degrees of freedoms and significance level, α = 0.05 (95% confidence):

$$F_c = F_{df_1, df_2, \alpha} = F_{4,26,0.05} = 2.74$$

Since $F_0 > F_c$, the null H_0 is rejected. Thus, at least one of the blanks is significantly different from the rest.

While this is a simple method of checking uniformity of blanks, it cannot discern which blank is different. For this reason, the least significant difference (LSD) method is used. LSD defines the maximum difference that the two values can have until they are statistically significantly different. Essentially, for any two blanks to be considered identical, the difference between the two values should be smaller than the LSD.

For LSD, α of individual tests (comparisonwise) needs to be adjusted to keep the overall error rate (α') (experimentwise) below 0.05. Given α as error rate of 1 test, the overall probability of making at least one incorrect rejection of H_0 (in all the combination of tests) will be larger than α and it is unknown.

Thus, a reduced α_b is calculated based on the total number of possible tests (c). For the case of five blanks,

$$c = \frac{p(p-1)}{2} = \frac{5(5-1)}{2} = 10$$

$$\alpha_b = \frac{\alpha}{c} = \frac{0.05}{10} = 0.005$$

The standard error (SE) of the difference between two blanks is:

$$SE = \sqrt{\frac{2\,MS_e}{\bar{n}}}$$

$$\bar{n} = \frac{1}{p}\sum_{b=1}^{p} n_b = \frac{6+4+7+8+6}{5} = 6.2$$

Thus,

$$SE = \sqrt{\frac{2(0.045)}{6.2}} = 0.0265$$

Degrees of freedom for error ($df_e = 26$) is used for calculation of t value from student t distribution:

$$t_{\frac{\alpha}{2},df} = t_{\frac{0.005}{2},26} = 3.346$$

SE and t value are used to calculate LSD:

$$LSD = t_{0.005,27}(SE) = 3.346(0.0265) = 0.0886$$

LSD is now used for comparing Blank 1 and Blank 2 and show that two blanks are identical:

$$H_0: \bar{x}_1 = \bar{x}_2$$

$$H_1: \bar{x}_1 \neq \bar{x}_2$$

$|\bar{x}_1 - \bar{x}_2| = |9.22 - 9.25| = 0.03$

Since $|\bar{x}_1 - \bar{x}_2| < LSD$, blank 1 and blank 2 do not differ significantly, i.e. they are considered identical.

The LSD tests were completed for all the blank values and the results are summarized in order from Table 21 to Table 26.

In Table 22, the blanks were compared in groups of trials done within the same week, except for blank 5, which was done a month later. Blank 4 is different from blank 1, 2 and 3 because it had a loose sample flask during GC trials, which led to lower analyte concentration (but the final concentration after securing the flask was close enough to blanks average, so it was not a major issue). Blank 5 is different from other blank values as it was done later than others. However, it was close to blank 4 with $|\bar{x}_4 - \bar{x}_5|$ proved nearly identical to LSD, and the sorption results were consistent within the expected range for blank 5 to also be considered as an acceptable baseline.

Sequence 11-20 had distinctly lower and fluctuating baseline values (average of 8.01 ppm) compared to previous trials. As shown in Table 22, there was a significant difference in blank 2 and 4. Based on the analysis, it was discovered that there was a contamination of analyte source. Thus, a correction factor (see Appendix E.2) was applied.

In Table 23, blank 2 and 3 were proven to be identical, while blank 1 was slightly higher than the average. However, the absolute difference was relatively small (0.213~0.271) compared to difference values (0.463~0.726) observed in Table 22. The variation was due to the recalibration of GC with an analyte gas cylinder change prior to the experiment.

For sequence 28-36 (Table 24), all five blanks were statistically the same relative to the typical error/noise, thus all sorption data taken on different dates can be reliably compared.

For sequence 37-43 (Table 25), blank 1A showed a significant difference from blank values, including the blank concentration measured again later the same day. The value will be considered erroneous and blank 1B value was used for further analysis of sorption data.

No notable difference was found in sequence 44-52 (Table 26) with baseline concentrations remaining stable throughout the week.

Table 21. LSD comparison for 1-10 sequence blanks

Blank # Compared	Absolute Difference	LSD Test (0.0886)
1 and 2	0.027	Not different
1 and 3	0.043	Not different
1 and 4	0.465	Different
1 and 5	0.377	Different
4 and 5	0.088	Not different

Table 22. LSD comparison for 11-20 sequence blanks

Blank # Compared	Absolute Difference	LSD Test (0.471)
1 and 2	0.463	Not different
1 and 3	0.213	Not different
1 and 4	0.262	Not different
2 and 4	0.726	Different

Table 23. LSD comparison for 21-27 sequence blanks

Blank # Compared	Absolute Difference	LSD Test (0.142)
1 and 2	0.213	Different
1 and 3	0.271	Different
2 and 3	0.059	Not different

Table 24. LSD comparison for 28-36 sequence blanks

Blank # Compared	Absolute Difference	LSD Test (0.323)
1 and 2A*	0.060	Not different
1 and 2B*	0.132	Not different
2A and 2B*	0.072	Not different
1 and 3	0.013	Not different
1 and 4	0.080	Not different

*Two blank trials were done on the same day (day 2 of the trial week) to test the stability of GC test system

Table 25. LSD comparison for 37-43 sequence blanks

Blank # Compared	Absolute Difference	LSD Test (0.494)
1A and 1B*	0.648	Different
1A and 2*	0.784	Different
1B and 2*	0.136	Not different
2 and 3	0.210	Not different

*Two blank trials were done on the same day (day 1 of the trial week) to test the stability of GC test system.

Table 26. LSD comparison for 44-52 sequence blanks

Blank # Compared	Absolute Difference	LSD Test (0.156)
1 and 2	0.014	Not different
1 and 3	0.069	Not different
2 and 3	0.083	Not different

Appendix D. Standard Error and Confidence Interval Calculations

This appendix contains sample calculations for typical data analysis applied throughout the thesis.

The standard error for sorption of sensing materials is calculated as per following procedure.

Given the data set for pristine PANI sorption for 10ppm formaldehyde source:

PANI sorption (ppm)	2.23	2.25	2.82	2.75	2.19

The standard deviation is calculated using the following equation:

$$SE = \sqrt{S^2} = \sqrt{\frac{\sum_{i=1}^{n}(x_i - \bar{x})^2}{n-1}}$$

Average ($\bar{x}$) of the data is 2.45ppm.

Variance (S^2) is $\frac{\sum_{i=1}^{n}(x_i-\bar{x})^2}{n-1}$ which equals to 0.0962.

Thus, the standard deviation (SE) of pristine PANI sorption is 0.310.

Given five data points, 95% confidence interval can be calculated using student t distribution:

$$\bar{x} \pm t_{\frac{\alpha}{2},df}\frac{SE}{\sqrt{n}}$$

For α=0.05 and d.f. of 4, t-value is 2.77. Therefore, 95% CI of pristine PANI is 2.45 ± 0.385.

All the samples for GC sorption tests were analyzed and their results are summarized in Table 27. The confidence interval of sorption should not include negative values. PPy and PANI-TiO_2 do not meet this constraint due to low trial replication, however the standard deviation is low enough to consider the measurements as consistent.

Table 27. Confidence intervals (on a 95% confidence level) for formaldehyde sorption (ppm) for PANI and PANI with dopants (exposed to F=10ppm)

Material	Average sorption values with CI
PANI	2.45 $\pm$ 0.385 ppm of F
PANI 5% SnO_2	2.49 $\pm$ 0.528 ppm of F
PANI 10% SnO_2	2.28 $\pm$ 0.632 ppm of F
PANI 2.5% ZnO	2.47 $\pm$ 0.494 ppm of F
PANI 2.5% ZnO-SDS	2.81 $\pm$ 0.982 ppm of F
PANI 5% ZnO	2.02 $\pm$ 0.381 ppm of F
PANI 5% ZnO-SDS	2.70 $\pm$ 0.793 ppm of F
PANI 20% ZnO	2.25 $\pm$ 0.882 ppm of F
PANI 5% TiO_2	1.84 $\pm$ 2.668 ppm of F
PANI 20% TiO_2	1.76 $\pm$ 3.145 ppm of F
PANI-HCl	2.14 $\pm$ 0.842 ppm of F
PANI-HCl-SDS	2.11 $\pm$ 0.032 ppm of F
PANI-SDS	2.08 $\pm$ 0.331 ppm of F
PPy	0.94 $\pm$ 1.077 ppm of F

Note: CI for PDMS-M and PDMS-T were not analyzed for lack of replication in testing.

Appendix E. Statistical Analysis for Formaldehyde Sorption Tests

Appendix E.1. Hypothesis Testing of Expected Sorption Values

Null hypothesis (H_0) test on sorption values of PANI and doped PANI

For a representative case of null hypothesis testing of two sensing material samples, pristine PANI and PPy will be compared. For one to say that sorption of PANI and PPy are different, one must prove that the two values are significantly (95% confidence, α=0.05) different. The t-distribution is used, since the sample size (number of sorption test replications) is small (3-5 replications for each material) and the true standard deviation is unknown.

First, the standard deviations of two data sets need to be similar. For this, the F-test is performed on the sorption variances between the two materials. The null hypothesis is:

$$H_0: \sigma_1^2 = \sigma_2^2$$

$$H_1: \sigma_1^2 \neq \sigma_2^2$$

$$F_0 = \frac{\sigma_1^2}{\sigma_2^2} \approx \frac{S_1^2}{S_2^2} \ \ and\ S_1^2 > S_2^2$$

With SE of 0.310 and 0.433 for PANI and PPy, respectively:

$$F_0 = \frac{0.433^2}{0.310^2} = 1.954$$

The F_0 needs to be larger than the critical F value (F_c) to reject the null hypothesis:

$$F_c = F_{\alpha, df_1, df_2}$$

where $df = (number\ of\ replicated\ sorption\ test) - 1$

$df_1(for\ PPy) = 2$ and $df_2(for\ PANI) = 4$

Thus,

$F_{0.05,2,4} = 6.94 > F_0 = 1.954$

Since F_0 is lower than F_c, the null hypothesis cannot be rejected and the standard deviation of the two samples are the same. Thus, the pooled variance (S_p) of the two materials can be used for the following calculation.

$$S_p^2 = \frac{df_1 S_1^2 + df_2 S_2^2}{df_1 + df_2}$$

$$S_p^2 = \frac{2(0.433^2) + 4(0.310^2)}{2 + 4} = 0.1268$$

Comparing the two sorption values using t-test with same but unknown standard deviation (95% confidence, α=0.05):

$$H_0: \mu_1 = \mu_2$$

$$H_1: \mu_1 \neq \mu_2$$

$$t_0 = \left| \frac{y_1 - y_2}{S_p \sqrt{\frac{1}{n_1} + \frac{1}{n_2}}} \right|$$

Given that

$$y_1(PPy\ average) = 0.94, \qquad y_2(PANI\ average) = 2.45$$

$$n_1(number\ of\ PPy\ tests) = 3, \qquad n_2(number\ of\ PANI\ tests) = 5$$

$$t_0 = \frac{2.45 - 0.94}{\sqrt{0.1268}\sqrt{\frac{1}{5} + \frac{1}{3}}} = 5.80$$

The t_0 needs to be larger than the critical t value (t_c) to reject the null hypothesis:

$$t_c = t_{\frac{\alpha}{2}, df_t}$$

where $\alpha = 0.05$ and $df_t = df_1 + df_2 = 2 + 4 = 6$

$t_{\frac{0.05}{2},6} = 2.447$

Since $t_0 = 5.80 > 2.447$, reject the null hypothesis. PANI and PPy are different with 95% confidence.

Same calculations are done for pairs of other materials of interest. The results of hypothesis tests can be found in Table 28.

Table 28. Summary of mean hypothesis tests for sensing materials

Comparison	Standard deviation F-test (rejection of null hypothesis $\sigma_1^2 = \sigma_2^2$)	Mean t-test (rejection of null hypothesis $\mu_1 = \mu_2$)
PANI, PANI-5% SnO_2	Fail; not different	Fail; not different
PANI, PANI-10% SnO_2	Fail; not different	Fail; not different
PANI, PANI-2.5% ZnO	Fail; not different	Fail; not different
PANI, PANI-2.5% ZnO-SDS	Fail; not different	Fail; not different
PANI, PANI-5% ZnO	Fail; not different	Fail; not different
PANI, PANI-5% ZnO-SDS	Fail; not different	Fail; not different
PANI, PANI-20% ZnO	Fail; not different	Fail; not different
PANI, PANI-5% TiO_2	Fail; not different	Fail; not different
PANI, PANI-20% TiO_2	Fail; not different	Fail; not different
PANI-5% SnO_2, PANI-5% ZnO	Fail; not different	Fail; not different
PANI-2.5% ZnO, PANI-2.5% ZnO-SDS	Fail; not different	Fail; not different
PANI-5% ZnO, PANI-5% ZnO-SDS	Fail; not different	Fail; not different
PANI, PANI-HCl	Fail; not different	Fail; not different
PANI, PANI-SDS	Fail; not different	Rejected; two are different
PANI, PDMS-T	Fail; not different	Rejected; two are different
PANI, PDMS-M[1]	N/A	Rejected; two are different
PDMS-T, PDMS-M[1]	N/A	Rejected; two are different

[1]The standard deviation of PDMS-M was 0.00 ppm.

Appendix E.2. Recalibration of Sorption Values

The analyte gas cylinder used for sequences 11-20 was contaminated with other aldehydes due to ageing of F.

When 95% confidence intervals (CI) of sorption are plotted with experimental data (see Figure 54), PANI-ZnO and PANI-HCl were unrealistically wide and included values lower than 0, which is impossible. Compared to the GC trials in the past and the trials done with the faulty cylinder, the sorption is 1.6 times smaller than for the pure F cylinder, leading to sorption data shifting and a wider spread. To mitigate this error, recalibration for sequence 11-20 was done by multiplying erroneous data points by factor of 1.6 (see Figure 55). When the sensing material sorption with an uncharacteristically wide spread was corrected, consistent sorption values were observed.

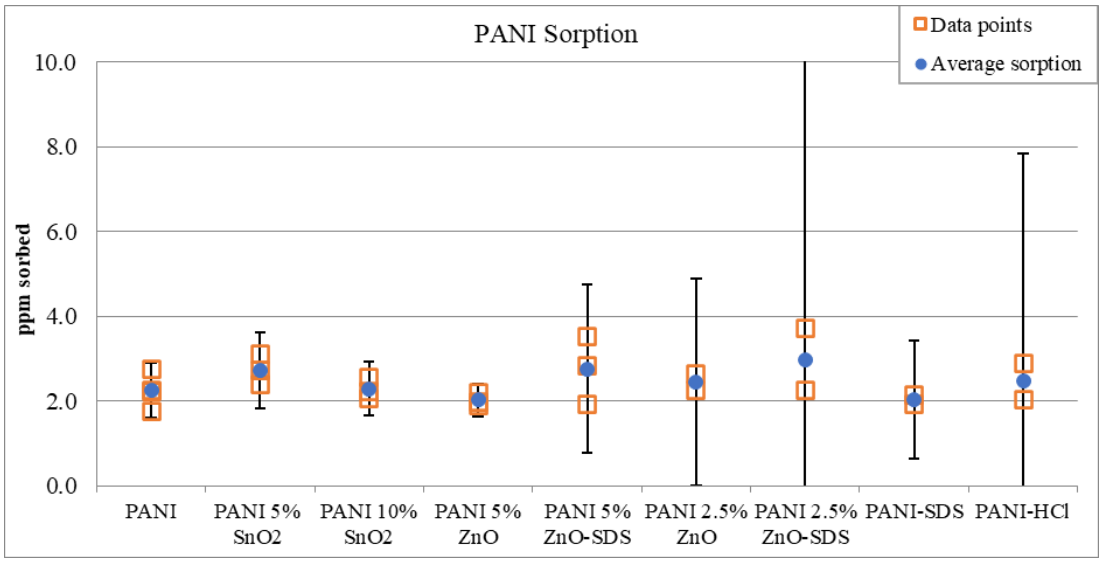

Figure 54. Plot of sorption concentration, average, and 95% CI of different PANI samples (sequence 1-20)

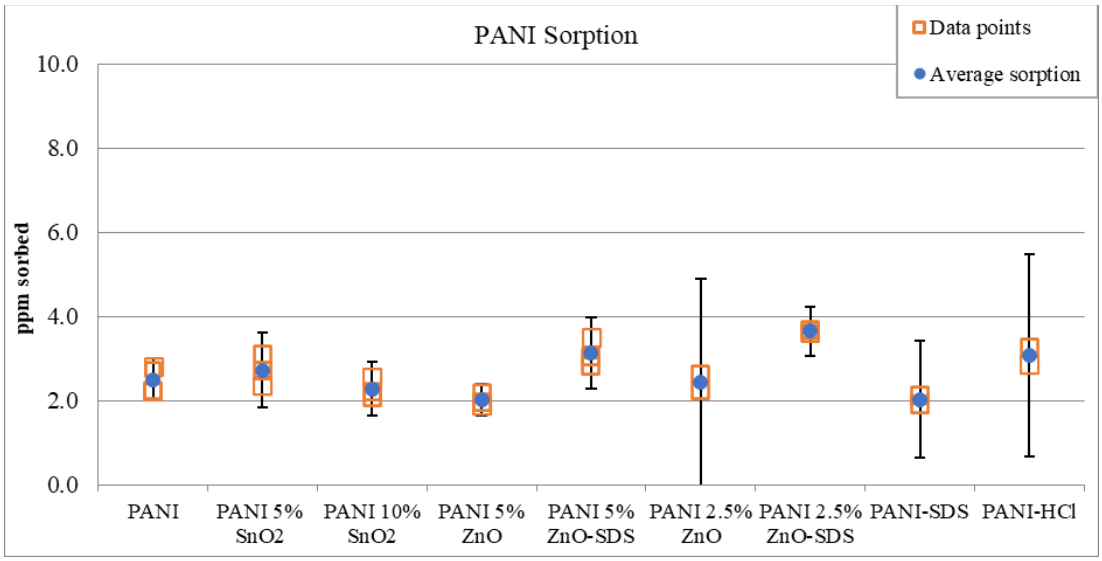

Figure 55. Plot of sorption concentration data, average, and 95% CI of different PANI samples (same as Figure 54) with data from sequence 11-20 adjusted with a factor of 1.6

Appendix F. XRD Data and Crystallinity Analysis

The crystallinity of PANI was determined using XRD. The peaks represent organized lattice entities in the structure; hence, they define the degree of crystallinity in the material. The location of the crystalline peaks can be shifted based on the orientation of the sample. However, the relative distance between the peaks is characteristic of the material and remains the same regardless of intensity of signal (See Figure 43). Utilizing the 'intensity method' for analysis, an approximate degree of crystallization for semi-crystalline polymers can be calculated [71]:

$$Cr = \frac{I_{Cr} - I_{Am}}{I_{Cr}} \times 100\%$$

I_{Am} is the highest intensity of the amorphous region (valley between peaks) and I_{Cr} is the intensity of the highest crystalline peak.

The tallest peak was chosen for comparisons between samples as the peak is at least double the intensity of the others. The intensity of the peak is compared to the intensity of the estimated intensity for each sample. As seen in Table 29, pristine PANI and PANI with HCl showed no difference in crystallinity while PANI-SDS had lower crystallinity. This is a rough estimate of the material structure, yet it supports the observations from SEM.

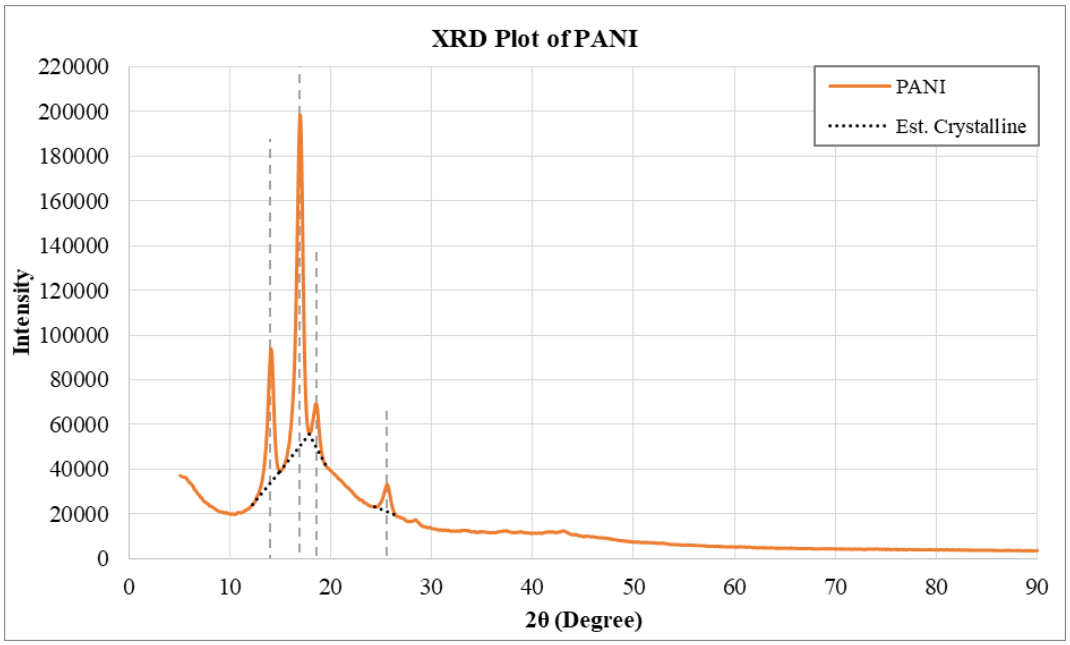

Figure 56. XRD plot of pristine PANI with estimated amorphous signals

Table 29. Estimated crystallinity index of PANI and doped PANI

Sample	I_c	I_a	Crystallinity index
PANI	198483	55876	72%
PANI-HCl	196706	55444	72%
PANI-SDS	141105	47016	67%

Appendix G. Certificates for Copyright Material

This appendix contains license agreements for Figure 1, Figure 2, Figure 3, Figure 4, Figure 5, Figure 6, Figure 7, Figure 8, Figure 9, Figure 10, Figure 11, Figure 15, Figure 16, Figure 17, Figure 42.

License agreements for Figure 1

MI

MU Extension IMC <imc@missouri.edu>

To: Gina Kim

Wed 2023-08-02 2:43 PM

Kayoung,

Per your request, you may use Figure 5 from University of Missouri Extension publication EQ387, Anaerobic Lagoons for Storage/Treatment of Livestock Manure, in your master's thesis as long as you credit University of Missouri Extension and the publication title.

Best wishes,

Victoria Stokes
Senior Business Operations Associate
MU Extension Integrated Marketing Communications
O: 573-882-6845 | **E:** [stokesv@missouri.edu]stokesv@missouri.edu
Help desk: imc@missouri.edu

License agreements for Figure 2

ELSEVIER LICENSE TERMS AND CONDITIONS

Sep 06, 2023

This Agreement between University of Waterloo -- Kayoung Kim ("You") and Elsevier ("Elsevier") consists of your license details and the terms and conditions provided by Elsevier and Copyright Clearance Center.

License Number	5623211005369
License date	Sep 06, 2023
Licensed Content Publisher	Elsevier
Licensed Content Publication	Sensors and Actuators B: Chemical
Licensed Content Title	Fast response methane sensor using nanocrystalline zinc oxide thin films derived by sol–gel method
Licensed Content Author	P. Bhattacharyya,P.K. Basu,H. Saha,S. Basu
Licensed Content Date	Jun 10, 2007
Licensed Content Volume	124
Licensed Content Issue	1
Licensed Content Pages	6
Start Page	62
End Page	67
Type of Use	reuse in a thesis/dissertation
Portion	figures/tables/illustrations
Number of figures/tables/illustrations	1
Format	both print and electronic
Are you the author of this Elsevier article?	No
Will you be translating?	No
Title	Synthesis and Characterization of Polymeric Gas Sensing Materials for Detection of Agriculture Lagoon Off-Gas
Institution name	University of Waterloo
Expected presentation date	Sep 2023
Portions	Figure 1
Requestor Location	University of Waterloo 95 Selwyn Road Richmond Hill, ON L4E 5E1 Canada Attn: University of Waterloo
Publisher Tax ID	GB 494 6272 12
Total	**0.00 CAD**
Terms and Conditions	

INTRODUCTION

1. The publisher for this copyrighted material is Elsevier. By clicking "accept" in connection with completing this licensing transaction, you agree that the following terms and conditions apply to this transaction (along with the Billing and Payment terms and conditions established by Copyright Clearance Center, Inc. ("CCC"), at the time that you opened your RightsLink account and that are available at any time at https://myaccount.copyright.com).

GENERAL TERMS

2. Elsevier hereby grants you permission to reproduce the aforementioned material subject to the terms and conditions indicated.

License agreements for Figure 3 and Figure 4

ELSEVIER LICENSE TERMS AND CONDITIONS

Sep 06, 2023

This Agreement between University of Waterloo -- Kayoung Kim ("You") and Elsevier ("Elsevier") consists of your license details and the terms and conditions provided by Elsevier and Copyright Clearance Center.

License Number	5623221063451
License date	Sep 06, 2023
Licensed Content Publisher	Elsevier
Licensed Content Publication	Materials Science in Semiconductor Processing
Licensed Content Title	Fabrication and characterization of a sensitive, room temperature methane sensor based on SnO2@reduced graphene oxide-polyaniline ternary nanohybrid
Licensed Content Author	Shiva Navazani,Ali Shokuhfar,Mostafa Hassanisadi,Aldo Di Carlo,Nikta Shahcheraghi
Licensed Content Date	Dec 1, 2018
Licensed Content Volume	88
Licensed Content Issue	n/a
Licensed Content Pages	9
Start Page	139
End Page	147
Type of Use	reuse in a thesis/dissertation
Portion	figures/tables/illustrations
Number of figures/tables/illustrations	2
Format	both print and electronic
Are you the author of this Elsevier article?	No
Will you be translating?	No
Title	Synthesis and Characterization of Polymeric Gas Sensing Materials for Detection of Agriculture Lagoon Off-Gas
Institution name	University of Waterloo
Expected presentation date	Sep 2023
Portions	Figure 7, Figure 12
Requestor Location	University of Waterloo 95 Selwyn Road Richmond Hill, ON L4E 5E1 Canada Attn: University of Waterloo
Publisher Tax ID	GB 494 6272 12
Total	**0.00 CAD**
Terms and Conditions	

INTRODUCTION

1. The publisher for this copyrighted material is Elsevier. By clicking "accept" in connection with completing this licensing transaction, you agree that the following terms and conditions apply to this transaction (along with the Billing and Payment terms and conditions established by Copyright Clearance Center, Inc. ("CCC"), at the time that you opened your RightsLink account and that are available at any time at https://myaccount.copyright.com).

GENERAL TERMS

License agreements for Figure 5

JOHN WILEY AND SONS LICENSE TERMS AND CONDITIONS

Aug 16, 2023

This Agreement between University of Waterloo -- Kayoung Kim ("You") and John Wiley and Sons ("John Wiley and Sons") consists of your license details and the terms and conditions provided by John Wiley and Sons and Copyright Clearance Center.

License Number	5610920384591
License date	Aug 16, 2023
Licensed Content Publisher	John Wiley and Sons
Licensed Content Publication	Journal of Polymer Science Part B: Polymer Physics
Licensed Content Title	Gas sorption, diffusion, and permeation in poly(dimethylsiloxane)
Licensed Content Author	T. C. Merkel, V. I. Bondar, K. Nagai, et al
Licensed Content Date	Jan 4, 2000
Licensed Content Volume	38
Licensed Content Issue	3
Licensed Content Pages	20
Type of Use	Dissertation/Thesis
Requestor type	University/Academic
Format	Print and electronic
Portion	Figure/table
Number of figures/tables	1
Will you be translating?	No
Title	Synthesis and Characterization of Polymeric Gas Sensing Materials for Detection of Agriculture Lagoon Off-Gas
Institution name	University of Waterloo
Expected presentation date	Sep 2023
Portions	Figure 4
Requestor Location	University of Waterloo 95 Selwyn Road Richmond Hill, ON L4E 5E1 Canada Attn: University of Waterloo
Publisher Tax ID	EU826007151
Total	**0.00 CAD**
Terms and Conditions	

TERMS AND CONDITIONS

This copyrighted material is owned by or exclusively licensed to John Wiley & Sons, Inc. or one of its group companies (each a"Wiley Company") or handled on behalf of a society with which a Wiley Company has exclusive publishing rights in relation to a particular work (collectively "WILEY"). By clicking "accept" in connection with completing this licensing transaction, you agree that the following terms and conditions apply to this transaction (along with the billing and payment terms and conditions established by the Copyright Clearance Center Inc., ("CCC's Billing and Payment terms and conditions"), at the time that you opened your RightsLink account (these are available at any time at http://myaccount.copyright.com).

Terms and Conditions

License agreements for Figure 6 and Figure 7

ELSEVIER LICENSE TERMS AND CONDITIONS

Sep 06, 2023

This Agreement between University of Waterloo -- Kayoung Kim ("You") and Elsevier ("Elsevier") consists of your license details and the terms and conditions provided by Elsevier and Copyright Clearance Center.

License Number	5623230193347
License date	Sep 06, 2023
Licensed Content Publisher	Elsevier
Licensed Content Publication	Sensors and Actuators B: Chemical
Licensed Content Title	Room temperature ammonia gas sensor based on polyaniline/copper ferrite binary nanocomposites
Licensed Content Author	Xingwei Wang,Likun Gong,Dongzhi Zhang,Xiaoxi Fan,Yingbo Jin,Liang Guo
Licensed Content Date	Nov 1, 2020
Licensed Content Volume	322
Licensed Content Issue	n/a
Licensed Content Pages	1
Start Page	128615
End Page	0
Type of Use	reuse in a thesis/dissertation
Portion	figures/tables/illustrations
Number of figures/tables/illustrations	2
Format	both print and electronic
Are you the author of this Elsevier article?	No
Will you be translating?	No
Title	Synthesis and Characterization of Polymeric Gas Sensing Materials for Detection of Agriculture Lagoon Off-Gas
Institution name	University of Waterloo
Expected presentation date	Sep 2023
Portions	Figure 9, Figure 10
Requestor Location	University of Waterloo 95 Selwyn Road Richmond Hill, ON L4E 5E1 Canada Attn: University of Waterloo
Publisher Tax ID	GB 494 6272 12
Total	**0.00 CAD**
Terms and Conditions	

INTRODUCTION

1. The publisher for this copyrighted material is Elsevier. By clicking "accept" in connection with completing this licensing transaction, you agree that the following terms and conditions apply to this transaction (along with the Billing and Payment terms and conditions established by Copyright Clearance Center, Inc. ("CCC"), at the time that you opened your RightsLink account and that are available at any time at https://myaccount.copyright.com).

GENERAL TERMS

2. Elsevier hereby grants you permission to reproduce the aforementioned material subject to the terms and conditions indicated.

License agreements for Figure 8 and Figure 9

ELSEVIER LICENSE TERMS AND CONDITIONS

Sep 06, 2023

This Agreement between University of Waterloo -- Kayoung Kim ("You") and Elsevier ("Elsevier") consists of your license details and the terms and conditions provided by Elsevier and Copyright Clearance Center.

License Number	5623230948356
License date	Sep 06, 2023
Licensed Content Publisher	Elsevier
Licensed Content Publication	Sensors and Actuators B: Chemical
Licensed Content Title	Ultrasensitive flexible NH3 gas sensor based on polyaniline/SrGe4O9 nanocomposite with ppt-level detection ability at room temperature
Licensed Content Author	Yajie Zhang,Junxin Zhang,Yadong Jiang,Zaihua Duan,Bohao Liu,Qiuni Zhao,Si Wang,Zhen Yuan,Huiling Tai
Licensed Content Date	Sep 15, 2020
Licensed Content Volume	319
Licensed Content Issue	n/a
Licensed Content Pages	1
Start Page	128293
End Page	0
Type of Use	reuse in a thesis/dissertation
Portion	figures/tables/illustrations
Number of figures/tables/illustrations	2
Format	both print and electronic
Are you the author of this Elsevier article?	No
Will you be translating?	No
Title	Synthesis and Characterization of Polymeric Gas Sensing Materials for Detection of Agriculture Lagoon Off-Gas
Institution name	University of Waterloo
Expected presentation date	Sep 2023
Portions	Figure 6, Figure 8
Requestor Location	University of Waterloo 95 Selwyn Road Richmond Hill, ON L4E 5E1 Canada Attn: University of Waterloo
Publisher Tax ID	GB 494 6272 12
Total	**0.00 CAD**
Terms and Conditions	

INTRODUCTION

1. The publisher for this copyrighted material is Elsevier. By clicking "accept" in connection with completing this licensing transaction, you agree that the following terms and conditions apply to this transaction (along with the Billing and Payment terms and conditions established by Copyright Clearance Center, Inc. ("CCC"), at the time that you opened your RightsLink account and that are available at any time at https://myaccount.copyright.com).

License agreements for Figure 10

ELSEVIER LICENSE TERMS AND CONDITIONS

Sep 06, 2023

This Agreement between University of Waterloo -- Kayoung Kim ("You") and Elsevier ("Elsevier") consists of your license details and the terms and conditions provided by Elsevier and Copyright Clearance Center.

License Number	5623231183046
License date	Sep 06, 2023
Licensed Content Publisher	Elsevier
Licensed Content Publication	Sensors and Actuators B: Chemical
Licensed Content Title	Hybrid polyaniline-WO3 flexible sensor: A room temperature competence towards NH3 gas
Licensed Content Author	S.B. Kulkarni,Y.H. Navale,S.T. Navale,F.J. Stadler,N.S. Ramgir,V.B. Patil
Licensed Content Date	Jun 1, 2019
Licensed Content Volume	288
Licensed Content Issue	n/a
Licensed Content Pages	10
Start Page	279
End Page	288
Type of Use	reuse in a thesis/dissertation
Portion	figures/tables/illustrations
Number of figures/tables/illustrations	1
Format	both print and electronic
Are you the author of this Elsevier article?	No
Will you be translating?	No
Title	Synthesis and Characterization of Polymeric Gas Sensing Materials for Detection of Agriculture Lagoon Off-Gas
Institution name	University of Waterloo
Expected presentation date	Sep 2023
Portions	Figure 7
Requestor Location	University of Waterloo 95 Selwyn Road Richmond Hill, ON L4E 5E1 Canada Attn: University of Waterloo
Publisher Tax ID	GB 494 6272 12
Total	**0.00 CAD**
Terms and Conditions	

INTRODUCTION

1. The publisher for this copyrighted material is Elsevier. By clicking "accept" in connection with completing this licensing transaction, you agree that the following terms and conditions apply to this transaction (along with the Billing and Payment terms and conditions established by Copyright Clearance Center, Inc. ("CCC"), at the time that you opened your RightsLink account and that are available at any time at https://myaccount.copyright.com).

GENERAL TERMS

2. Elsevier hereby grants you permission to reproduce the aforementioned material subject to the terms and conditions indicated.

License agreements for Figure 11

CCC Marketplace

This is a License Agreement between Kayoung Kim ("User") and Copyright Clearance Center, Inc. ("CCC") on behalf of the Rightsholder identified in the order details below. The license consists of the order details, the Marketplace Permissions General Terms and Conditions below, and any Rightsholder Terms and Conditions which are included below.

All payments must be made in full to CCC in accordance with the Marketplace Permissions General Terms and Conditions below.

Order Date	06-Sep-2023	Type of Use	Republish in a thesis/dissertation
Order License ID	1394130-1		
ISSN	2044-4761	Publisher	Royal Society of Chemistry
		Portion	Image/photo/illustration

LICENSED CONTENT

Publication Title	Catalysis Science & Technology	Rightsholder	Royal Society of Chemistry
		Publication Type	e-Journal
Article Title	Conjugated HCl-doped Polyaniline for Photocatalytic Oxidative Coupling of Amines under Visible Light	Start Page	753
		End Page	761
		Issue	3
		Volume	9
Author/Editor	Royal Society of Chemistry (Great Britain)		
Date	01/01/2011		
Language	English		
Country	United Kingdom of Great Britain and Northern Ireland		

REQUEST DETAILS

Portion Type	Image/photo/illustration	Distribution	Worldwide
Number of Images / Photos / Illustrations	1	Translation	Original language of publication
Format (select all that apply)	Print, Electronic	Copies for the Disabled?	No
		Minor Editing Privileges?	No
Who Will Republish the Content?	Academic institution	Incidental Promotional Use?	No
Duration of Use	Life of current edition	Currency	CAD
Lifetime Unit Quantity	Up to 499		
Rights Requested	Main product		

NEW WORK DETAILS

Title	Synthesis and Characterization of Polymeric Gas Sensing Materials for Detection of Agriculture Lagoon Off-Gas	**Institution Name**	University of Waterloo
		Expected Presentation Date	2023-09-15
Instructor Name	Alexander Penlidis		

ADDITIONAL DETAILS

Order Reference Number	N/A	**The Requesting Person/Organization to Appear on the License**	Kayoung Kim

REQUESTED CONTENT DETAILS

Title, Description or Numeric Reference of the Portion(s)	Figure 1	**Title of the Article/Chapter the Portion Is From**	Conjugated HCl-doped Polyaniline for Photocatalytic Oxidative Coupling of Amines under Visible Light
Editor of Portion(s)	Ge, Zhenyu; Gu, Xianmo; Kong, Peng; Li, Zhong; Liu, Pei; Pei, Linjuan; Tan, Hao; Wang, Jie; Zheng, Zhanfeng; Zhu, Pengqi	**Author of Portion(s)**	Ge, Zhenyu; Gu, Xianmo; Kong, Peng; Li, Zhong; Liu, Pei; Pei, Linjuan; Tan, Hao; Wang, Jie; Zheng, Zhanfeng; Zhu, Pengqi
Volume / Edition	9		
Page or Page Range of Portion	753-761	**Issue, if Republishing an Article From a Serial**	3
		Publication Date of Portion	2019-01-01

Marketplace Permissions General Terms and Conditions

The following terms and conditions ("General Terms"), together with any applicable Publisher Terms and Conditions, govern User's use of Works pursuant to the Licenses granted by Copyright Clearance Center, Inc. ("CCC") on behalf of the applicable Rightsholders of such Works through CCC's applicable Marketplace transactional licensing services (each, a "Service").

1) **Definitions.** For purposes of these General Terms, the following definitions apply:

"License" is the licensed use the User obtains via the Marketplace platform in a particular licensing transaction, as set forth in the Order Confirmation.

"Order Confirmation" is the confirmation CCC provides to the User at the conclusion of each Marketplace transaction. "Order Confirmation Terms" are additional terms set forth on specific Order Confirmations not set forth in the General Terms that can include terms applicable to a particular CCC transactional licensing service and/or any Rightsholder-specific terms.

"Rightsholder(s)" are the holders of copyright rights in the Works for which a User obtains licenses via the Marketplace platform, which are displayed on specific Order Confirmations.

"Terms" means the terms and conditions set forth in these General Terms and any additional Order Confirmation Terms collectively.

"User" or "you" is the person or entity making the use granted under the relevant License. Where the person accepting the Terms on behalf of a User is a freelancer or other third party who the User authorized to accept the General Terms on the User's behalf, such person shall be deemed jointly a User for purposes of such Terms.

License agreements for Figure 15, Figure 16, and Figure 17

MDPI Open Access Information and Policy

All articles published by MDPI are made immediately available worldwide under an open access license. This means:

- everyone has free and unlimited access to the full-text of *all* articles published in MDPI journals;
- everyone is free to re-use the published material if proper accreditation/citation of the original publication is given;
- open access publication is supported by the authors' institutes or research funding agencies by payment of a comparatively low **Article Processing Charge (APC)** for accepted articles.

Permissions

No special permission is required to reuse all or part of article published by MDPI, including figures and tables. For articles published under an open access Creative Common CC BY license, any part of the article may be reused without permission provided that the original article is clearly cited. Reuse of an article does not imply endorsement by the authors or MDPI.

License agreements for Figure 42

ELSEVIER LICENSE TERMS AND CONDITIONS

Sep 06, 2023

This Agreement between University of Waterloo -- Kayoung Kim ("You") and Elsevier ("Elsevier") consists of your license details and the terms and conditions provided by Elsevier and Copyright Clearance Center.

License Number	5610940976726
License date	Aug 16, 2023
Licensed Content Publisher	Elsevier
Licensed Content Publication	Polymer Testing
Licensed Content Title	Determination of crystal structure of polyaniline and substituted polyanilines through powder X-ray diffraction analysis
Licensed Content Author	Sambhu Bhadra,Dipak Khastgir
Licensed Content Date	Oct 1, 2008
Licensed Content Volume	27
Licensed Content Issue	7
Licensed Content Pages	7
Start Page	851
End Page	857
Type of Use	reuse in a thesis/dissertation
Portion	figures/tables/illustrations
Number of figures/tables/illustrations	1
Format	both print and electronic
Are you the author of this Elsevier article?	No
Will you be translating?	No
Title	Synthesis and Characterization of Polymeric Gas Sensing Materials for Detection of Agriculture Lagoon Off-Gas
Institution name	University of Waterloo
Expected presentation date	Sep 2023
Portions	Figure 1
Requestor Location	University of Waterloo 95 Selwyn Road Richmond Hill, ON L4E 5E1 Canada Attn: University of Waterloo
Publisher Tax ID	GB 494 6272 12
Total	**0.00 CAD**
Terms and Conditions	

INTRODUCTION

1. The publisher for this copyrighted material is Elsevier. By clicking "accept" in connection with completing this licensing transaction, you agree that the following terms and conditions apply to this transaction (along with the Billing and Payment terms and conditions established by Copyright Clearance Center, Inc. ("CCC"), at the time that you opened your RightsLink account and that are available at any time at https://myaccount.copyright.com).

GENERAL TERMS